Evaluation of the Structural Performance of Shear Walls Built by Multi-layer Composite Laminated Panels

by

Lin Zheng

A thesis submitted in partial fulfillment of the requirements for the degree of

Master of Science

in

Civil (Cross-disciplinary)

Department of Civil and Environmental Engineering

University of Alberta

Abstract

Recently, the implementation of cross-laminated timber (CLT) in building systems has rapidly developed in many countries including Canada. Despite this, further improvement in the product performance of CLT is desirable. Composite Laminated Panels (CLP) have been developed due to the need to overcome one of the key weaknesses of traditional CLT, namely the rolling shear failure. CLP is made by combining traditional lumber with structural composite lumber (SCL). This thesis focuses on the structural performance of CLP shear walls and their connections. The aim of this project was to evaluate the mechanical properties of CLP connections as well as the lateral load performance of CLP shear walls, and the feasibility of using current mechanics-based models to predict the strength of connections and shear walls fabricated with CLP.

To study the structural performance of CLP connections together with CLP shear walls, this thesis presents experimental and analytical investigations. Monotonic and cyclic tests were carried out at both the fastener level and the wall level. Afterward, the predictions using current analytical models were compared with experimental results.

Full-scale coupled CLP shear wall panels were tested with different connection configurations to achieve target kinematic wall behaviours under lateral load. The structural performance of the tested shear wall tests was characterised by lateral strength, stiffness, ductility ratio, and energy dissipation, which are all significant parameters required for seismic design. Furthermore, the experimental results also served to validate existing analytical models to predict the strength and deflection of CLT shear walls in the elastic region. It was found that the analytical model for

predicting lateral strength of CLP shear walls generally gives good predictions, while the deflections of CLP shear walls were largely underestimated by the analytical deflection model.

Specimens for connection tests were obtained by cutting the CLP panels from the undamaged parts of the panels after the shear wall tests. This study showed that the structural performance of CLP connections is significantly influenced by the properties of timber material. Replacing lumber with Laminated Strand Lumber (LSL) in the core layer exhibited a remarkable increase in stiffness and strength, and tended to fail in a ductile manner. The utilisation of LSL in face layers enhanced stiffness and strength, but reduced ductility.

Overall, this investigation demonstrated that CLP connections and shear walls can provide similar or better performance compared with those fabricated with traditional CLT panels.

Preface

This thesis is an original work by Lin Zheng. No part of this thesis has been previously published.

Acknowledgements

Table of Contents

List of Tables

List of Figures

List of symbols and abbreviations

A_{eff} = *effective cross — section area of the panel*

a_m = *total thickness of the mply CLT panel*

b = *width of the wall*

b_1 = *width of the left panel in coupled wall*

b_2 = *width of the right panel in coupled wall*

CLT = *cross laminated timber*

CLP = *composite laminated panel*

CP = *Couple — panel behaviour*

COV = *COV coefficient of variation*

E_0 = *modulus of elasticity in parallel to grain directions*

E_{90} = *modulus of elasticity in perpendicular to grain directions*

$EEEP$ = *energy elastic — plastic*

EI_{eff} = *effective bending stiffness*

EYM = *European Yield Model*

F = *lateral force on the wall*

F_{r-sl} = *combined rocking — sliding resistance of the shear wall*

G_0 = *shear modulus parallel to grain*

G_{90} = *shear modulus perpendicular to grain*

h = *wall height*

k_i = *composition factors*

k_{AB} = *stiffness of angle brackets*

k_{HD} = *stiffness of hold — downs*

$LLRS$ = *lateral load resisting systems*

$LVDTs$ = *linear variable differential transformers*

LVL = *laminated veneer lumber*

LSL = *laminated Strand Lumber*

MTP	$=$	$mass\ timber\ panel$
SCL	$=$	$structural\ composite\ lumber$
SPF	$=$	$spruce-pine-fir$
STS	$=$	$self\ tapping\ screws$
SW	$=$	$Single-wall\ behaviour$
δ_b	$=$	$deformation\ of\ the\ panel\ due\ to\ bending$
δ_r	$=$	$deformation\ of\ the\ panel\ due\ to\ rocking$
δ_{sl}	$=$	$deformation\ of\ the\ panel\ due\ to\ sliding$
δ_{total}	$=$	$total\ wall\ deflection$

Chapter 1 Introduction

1.1 Background

Over the last decade, mass timber panels (MTP) have been increasingly implemented in construction as a sustainable and cost-effective building material. The most well-known MTP product is cross-laminated timber (CLT), which is made from sawn lumber planks that are orthogonally glued together. As a viable product in the mid- and high-rise construction market, CLT is increasingly replacing other traditional materials such as steel and concrete. Although CLT possesses both good shape stability and possible two-way force transfer ability due to its crosswise lamination, its transverse layers are prone to rolling shear failure under an out-of-plane load.

Recently, an innovative multi-layer composite laminated panel (CLP) has been developed by combining laminated strand lumber (LSL) and dimension lumber to overcome the rolling shear failure while maintaining the high mechanical performance and aesthetic appearance of natural wood. Research by Niederwestberg et al. (2018), showed that the shear resistance, bending stiffness, and moment resistance of CLP were higher by up to 143%, 43%, and 87%, respectively, than regular CLT. They also established that the use of LSL in transverse layers could eliminate the potential rolling shear failure in CLT.

Both mass timber panel shear wall systems and mass timber braced frame systems are viable structural systems to resist lateral loads. However, they possess distinct characteristics that may make one more appropriate for a certain project over the other, for example architectural requirements. In the present project, mass timber panel shear wall system made with CLP was investigated as a extension to a previously conducted project at the University of Alberta that developed the CLP product (Niederwestberg et al 2018). Wind and seismic forces are resisted by shear walls in MTP buildings. Properly designed shear walls transmit in-plane shear forces to the foundation. The shear walls

must have adequate strength and rigidity to prevent collapse and limit deformations. In general, there are two methods to quantify the lateral load behaviour of shear walls. The first is to perform racking tests and relate the results to construction details. The second is rationally or empirically correlating the lateral strength shear wall to the properties of the connections and shear wall panels. Hence, this research project contained two testing series: (1) connection tests and (2) shear wall tests. This project is an expansion of a previous project that developed three-layer and five-layer CLP for out-of-plane bending applications (Niederwestberg et al., 2018).

1.2 Research Objectives

The overall goal of this study was to verify the applicability of the commonly accepted mechanics-based analytical models of the CLT shear wall to CLP and also explore the application of European Yield Model (EYM) to the analysis and design of self-tapping screw connections in CLP with thin steel side plates. The emphasis was on the consistency between predicted values and experimental results, the constraints on the application of the models, and the material property inputs into the EYM.

The specific objectives of the experimental research presented in this dissertation are to:
> (1) Evaluate the lateral strength and stiffness of self-tapping screw connections with thin steel plates in different layups of CLP and compare test results to the predictions according to European Yield Model.
> (2) Compare the in-plane mechanical performance of shear walls built with CLP with that built with traditional CLT panels.
> (3) Compare the predicted values (load-carry capacity and deflection) of the CLP shear wall using existing CLT shear wall models with experimental results under lateral loading.

1.3 Methodology

This project aims to use the self-tapping screw connection tests to provide further insight into the measured load-deformation behaviour of the full-scale CLP shear walls, which is mainly governed by connection behaviour. This project is divided into two sections.

Section one deals with the connection behaviour while the second secion focuses on shear wall behaviour.

At the start, to provide the research foundation for this project, a review of theories and relevant prior research was conducted. It can be concluded that mass timber panels can be treated as a rigid body and the connection strength governs the load-carrying capacity, whereas lateral deflection could contain contributions from connection slip and panel deformation.

Following the literature review, testing of self-tapping screw joints and shear walls was conducted. Phase 1 consists of the testing of screwed joints with four types of CLP layups and traditional CLT. Three replications for each group were tested to ensure the variation in the experiment so that statistical tests could be applied to evaluate differences. The joints test matrix contained five different panel layups, two loading orientations (parallel and perpendicular to the grain), and two loading types (monotonic and reversed cyclic). The main purpose of this testing was to better understand the influence of replacing lumber with LSL laminates on connection behaviour and, in turn, to further assist in understanding the behaviour of full-scale CLP shear walls. The resistances and stiffness of hold-downs as well as inter-panel joints in addition to the base shear connections were determined. Subsequently, Phase II of this project included five and four full-scale shear wall tests using the same panel layups as the screwed joint tests subjected to monotonic and cyclic loads, respectively. It aimed to investigate if the lateral capacity of the CLP shear wall could be predicted based on screwed joint properties and the applicability of existing CLT shear wall analytical models for CLP.

The design approaches used in this thesis are in alignment with the current design provisions in Canada's wood design standard, CSA O86 (CSA 2019), and the shear wall models were based on recent research findings.

1.4 Outline of thesis

This thesis is organized in the following manner:

Chapter 1 provides the basic background knowledge of CLP with the research objectives and methods.

Chapter 2 reviews the past studies related to the development of hybrid CLT, the structural performance of CLT connections and shear walls as well as the modeling of CLT shear wall behaviours.

Chapter 3 presents an experimental investigation of CLP-steel plate self-tapping screw joints under monotonic and reversed cyclic loads. The joint performance was evaluated in terms of ultimate strength, stiffness, yield strength, and ductility. The results are compared with CLT joint test results. The chapter ends with a comparison of the predicted strengths obtained by CSA O86 EYM and test values of self-tapping screw joints.

Chapter 4 presents a discussion of the testing of full-sized CLP and CLT shear walls under monotonic and cyclic loading. The application of existing CLT shear wall models to predict the strength and load-deflection behaviours of CLP shear walls was evaluated. The differences between the test results and model predictions are examined.

Chapter 5 provides conclusions and recommendations for future research.

Chapter 2 Literature Review

2.1 Introduction

This research focuses on the structural performance of composite laminated panels (CLP), which is an innovative engineered wood product and an improved version of cross-laminated timber (CLT) in terms of its mechanical performance. The development and mechanical characteristics of CLT are introduced first. Then, the mechanics of screwed joints in CLT and the typical connection systems in CLT shear walls along with experimental investigations are presented, followed by the design approaches and analytical models of the CLT shear wall. This chapter reviews the relevant research that has been conducted in these fields. A summary of findings from the literature review is presented by the end of this chapter.

2.2 Cross Laminated Timber

Cross laminated timber, originally developed in Europe in the 1990s, is a mass timber panel with layers of lumber laminates orthogonally bonded with a structural adhesive. The cross-wise and laminar structure of CLT makes it capable of resisting loads both in-plane and out-of-plane, and provides high dimensional stability. The advantages of the high degree of prefabrication and fast erection with CLT make it a suitable and valuable alternative to concrete, masonry and steel. Additionally, CLT panels constitute a promising solution for a wide variety of structural applications in either all wood or wood-hybrid buildings, including roof, floor and wall assemblies. The panels can be easily connected to other members or structural materials by means of fasteners and connectors. The invention of CLT contributed to the advancement of panelised building technologies. CLT buildings are similar to a box structure as they are constituted by an assembly of prefabricated CLT panels to resist both gravity and lateral loads. Because the CLT panel behaves as a rigid body the behaviour of CLT lateral load resisting systems (LLRS) is governed largely by the connections in the systems (Brandner et al., 2016).

Apart from its structural benefits, the sustainable and low carbon footprint features of CLT allows CLT to appeal to builders worldwide and, consequently, is employed in residential and commercial mid-rise and high-rise construction. In order to keep pace with advancements in CLT, the majority of research in recent years has focused on the structural performance of CLT systems. The design properties of CLT are found in the European timber design code Eurocode 5 (EN 1995-1-1 2004). Efforts by FPinnovations and The Engineered Wood Association (APA) have been undertaken to adopt CLT in North American construction market. The first edition of the approved Standard for Performance-Rated Cross Laminated Timber 'ANSI/APA PRG 320' (APA 2012) was published in 2012, with the most recent version published in 2019. In Canada, CLT structures are designed according to the standard outlined by CSA O86 'Engineering design in wood' (CSA 2019).

2.2.1 In-plane stiffness of CLT panels

There are two basic forms of stress for panels: (1) loading perpendicular to the plane of the panel (out-of-plane bending); and (2) loading parallel to the plane of the panel (in-plane behaviour). Understanding the in-plane mechanical characteristics of CLT panels is essential in designing a CLT shear wall. Blass and Fellmoser (2004) proposed the composition factor to calculate the strength and stiffness of a CLT panel based on composite theory. The composition factor is defined as the ratio of the strength or stiffness of the considered cross section to the strength or stiffness of a hypothetical homogeneous cross section with all of the layers' grain direction placed parallel to the direction of the stress. The composition factors for different loading scenarios relative to the in-plane CLT layup are summarised in Table 2.1. Table 2.2 provides the equations for calculating the effective strength and stiffness properties of CLT panels under bending, tension, and compression.

Table 2.1 Composition factors k_i for CLT panels under in-plane load (Blass and Fellmoser (2004))
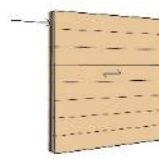
Load Configuration	Composition Factors, k_i
	$$k_3 = 1 - \left(1 - \frac{E_{90}}{E_0}\right) \times \frac{a_{m-2} - a_{m-4} + \cdots\cdots \pm a_1}{a_m}$$
	$$k_4 = \frac{E_{90}}{E_0} + \left(1 - \frac{E_{90}}{E_0}\right) \times \frac{a_{m-2} - a_{m-4} + \cdots\cdots \pm a_1}{a_m}$$

Table 2.2 Effective strength and stiffness for CLT panels (Blass and Fellmoser (2004))

Loading direction	Grain direction of face layers	Effective strength	Effective stiffness
Bending	Parallel	$f_{\mathrm{m,0.ef}} = f_{\mathrm{m,0}} \cdot k_3$	$E_{\mathrm{m,0.ef}} = E_0 \cdot k_3$
	Perpendicular	$f_{\mathrm{m,90.ef}} = f_{\mathrm{m,0}} \cdot k_4$	$E_{\mathrm{m,90.ef}} = E_0 \cdot k_4$
Tension	Parallel	$f_{t,0.ef} = f_{t,0} \cdot k_3$	$E_{t,0.ef} = E_0 \cdot k_3$
	Perpendicular	$f_{t,90.ef} = f_{t,0} \cdot k_4$	$E_{t,90.ef} = E_0 \cdot k_4$
Compression	Parallel	$f_{c,0.ef} = f_{c,0} \cdot k_3$	$E_{c,0.ef} = E_0 \cdot k_3$
	Perpendicular	$f_{c,90.ef} = f_{c,0} \cdot k_4$	$E_{c,90.ef} = E_0 \cdot k_4$
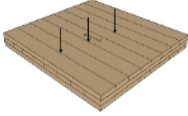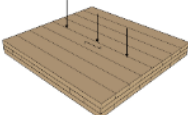
Note: $f_{0.ef}$ and $f_{90.ef}$ represent the effective strength parallel to grain and perpendicular to grain, respectively. $E_{0.ef}$ and $E_{90.ef}$ denote the effective modulus of elasticity (MOE) of the lumber parallel to grain and perpendicular to grain, respectively.

2.2.2 Out-of-plane bending stiffness of CLT panels

Layup combinations of CLT can bring significant differences in mechanical properties, both in-plane and out-of-plane. When the transverse layers of CLT under out-of-plane bending are exposed to shear perpendicular to the grain it can lead to rolling shear failure and relatively large shear deformation. Therefore rolling shear strength and stiffness are critical properties in the design of CLT systems under out-of-plane bending. The rolling

shear modulus (G_{90}) is generally assumed to be 1/10 of the shear modulus in the parallel direction (G_0), whereas the MOE perpendicular to the grain is assumed to be 1/30 of the MOE in the parallel direction in CSA O86 (2019). The Timoshenko Beam Theory and Shear Analogy Method are the two commonly used analytical approaches for determining CLT bending strength and stiffness properties. Niederwestberg et al. (2018) found that the shear stiffness values were sensitive to the ratio of major planar shear modulus to minor planar shear modulus in both methods. The composition factors for different loading scenarios relative to the out-of-plane CLT layup are summarised in Table 2.3.

Table 2.3 Composition factors k_i for CLT panels under out-of-plane load (Blass and Fellmoser (2004))

Load Configuration	Composition Factors, k_i
	$$k_1 = 1 - \left(1 - \frac{E_{90}}{E_0}\right) \times \frac{a_{m-2}^3 - a_{m-4}^3 + \cdots\cdots \pm a_1^3}{a_m^3}$$
	$$k_2 = \frac{E_{90}}{E_0} + \left(1 - \frac{E_{90}}{E_0}\right) \times \frac{a^3_{m-2} - a^3_{m-4} + \cdots\cdots \pm a_1^3}{a_m^3}$$

2.3 Development of Hybrid Cross Laminated Timber

The driving force of developing the hybrid CLT was the need to improve the traditional CLT product while allowing the CLT market to continue to grow. There are currently two directions for the development of hybrid CLT. One approach is to consider using different grades or wood densities in order to achieve economic efficiency and sustainability in the CLT industry without compromising the mechanical performance of CLT. The other approach is to utilise the superior mechanical properties of structural composite lumber (SCL) in panel layups to overcome the typical rolling shear failure of

CLT, as most SCL products have a high shear strength compared with dimension lumber. Also, the better dimensional stability of SCL helps to minimise the internal stresses due to moisture changes (FPInnovations, 2019).

Wang et al. (2015) evaluated the feasibility of using poplar in cross-layers in CLT. As the mechanical properties were found to be similar with those of traditional CLT made of spruce-pine-fir (SPF) lumber, the use of poplar in CLT manufacturing might be an effective way to expand the source of species for CLT manufacturing.

Another hybrid CLT product was developed at Oregon State University. It was manufactured with high-grade or high-density lumber as face layers and a core layer made of low-grade or low-density species. An evaluation of connection performance in the aforementioned hybrid layup panels was conducted, and an advanced model for predicting the strength of connections in hybrid CLT by considering the variation in density profile was proposed (Mahdavifar et al., 2018).

Ma et al. (2021) evaluated the mechanical characteristics of hybrid CLT panels made of low-value sugar maple (*Acer saccharum*) and white spruce (*Picea glauca*), which combined hardwood and softwood in panel layup design. In total, three types of layup combinations were developed: sugar maple-white spruce in combination with white spruce-sugar maple with two types of adhesives (melamine-formaldehyde and resorcinol-formaldehyde) and white spruce-sugar maple-white spruce glued with resorcinol formaldehyde. To examine the flexural and shear behaviour of each mixed-species hybrid CLT panel, third-point bending experiments were performed on both long and short spans. The test results showed that the bending modulus, bending strength, shear stiffness, and shear strength were all enhanced when sugar maple (hardwood) was used in the longitudinal layers in comparison with E1 grade CLT in APA/ANSI PRG-320. Similarly, the use of sugar maple in transverse layers also improved the bending modulus, bending strength, and shear strength, but the shear stiffness remained unchanged or was found to be even less than that of E1 grade CLT.

Niederwestberg et al. (2018) developed an innovative hybrid CLT, which was aimed at overcoming the rolling shear failure in the transverse layer of traditional CLT when loaded out-of-plane. In their study, five-ply panels made of structural composite lumber (SCL) and dimension lumber, known as composite laminated panel (CLP), were developed. The shear resistance, bending stiffness, and moment resistance of CLP were found to be higher than traditional CLT by up to 143%, 43%, and 87%, respectively.

Due to the promising performance of CLP compared with generic CLT (Niederwestberg et al., 2018), it is crucial to evaluate the performance of the connections utilised in these integrated new panel layups. Currently, limited information is known about the connection behaviour of hybrid CLT. Thus, further research is required to generate connection data to support the use of hybrid CLT in structural applications.

2.4 CLT connections

2.4.1 Panel-to-panel connections

The in-plane panel-to-panel connections are widely used in wall-to-wall and floor-to-floor applications, which is not only an effective way to resist in-plane shear forces, but can also resist out-of-plane bending. As the mass timber panels are rigid relative to the behaviour of the connection, the ductility of the system is mainly dependent on connections.

Currently, the most commonly used in-plane shear connections between panels are the spline joint, half-lap (step joint), and butt joint, as illustrated in Figure 2.1. Strips in spline joints are usually made from plywood, laminated veneer lumber (LVL), or other engineered wood products, which can be designed to resist both shear and moment. Furthermore, double surface spline connection or using structural composite lumber (SCL) as the strips are effective approaches to increase the stiffness and capacity. However, half-lap joints cannot be designed as a moment-resisting connection as they can only carry normal and shear loads (Augustin, 2008). The advantage of a butt joint

connection is that it is simple to install without any additional prefabrication requirements. The use of self-tapping screws (STS) in mass timber construction is very popular as it has a high withdrawal resistance and a continuous thread that allows tensile and compressive forces to be transferred along the embedded length. Long STS with high lateral and withdrawal capacity can resist both axial and lateral loads, this is in contrast to traditional dowel-type connectors such as nails or lag screws (Hossain et al., 2016).

(a)

(b)

(c)
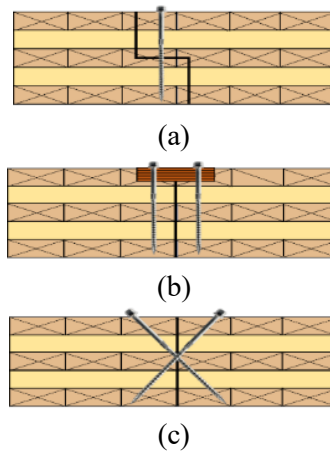
Figure 2.1 CLT panel-to-panel connection: (a) half-lap joint; (b) spline joint, (c) butt joint (Hossain et al., 2016)

Blass and Bejtka (2001) proposed empirical equations to calculate the load-carrying capacity of wood-to-wood connections with inclined STS loaded in axial and lateral directions in glulam beams, accounting for load-to-grain angle. The self-tapping screws used in their study were 7.5 mm in diameter and 182 mm in length. The test results showed that the maximum load-carrying capacity for a wood-to-wood connection occurs at around 60 degrees, and as the angle between the STS axis and the loading direction decreased, the stiffness of the connection gradually increased. Due to the inclined angle, the failure of the connection occurred when the withdrawal strength of STS, yield strength of STS, or the embedment strength of the wood member was reached. The angle of insertion of STS plays a large role in governing failure mode.

Joyce et al. (2011) evaluated two types of in-plane panel-to-panel CLT shear connections, namely, double spline and angled screws. The test results indicated that the double spline connection showed a better performance than the angled screw connection, however, the angled screw connections had a higher stiffness value.

Gavric et al. (2015a, 2015b) conducted comprehensive test series to evaluate the performance of typical CLT connections, including metal connectors such as hold-downs and angle brackets, together with screwed panel-to-panel CLT connections. In terms of screwed panel-to-panel CLT connections, component level tests were carried out on both parallel (wall-to-wall and floor-to-floor) and orthogonal (wall-to-wall, wall-to-floor) directions in shear and withdrawal under monotonic and cyclic loading. The wall panels were all five-layered CLT with a total thickness of 85 mm and all floor elements were 142 mm thick 6-layered CLT made with a double layer in the middle. Connection types of spline joints and half-lap joints were investigated. Through evaluating the mechanical properties (strength, stiffness, ductility, and energy dissipation) according to EN 12512 (2001), half-lap joints were found to have a higher initial stiffness while spline joints were able to resist loads at a larger ultimate displacement. Furthermore, the failure modes of the half-lap joint were primarily brittle, whereas the LVL spline joints were able to exhibit ductile behaviour. The capacity calculated by Eurocode 5 (EN 1995-1-1 2004) equations corresponded well with the test results. However, the Uibel and Blaß method (2001) provided a more accurate prediction based on more conservative embedment strength, which takes the location of the fastener in relation to gaps, grooves, and grain orientation into account.

Hossain et al. (2016) evaluated the performance of fully threaded (FT) self-tapping screws with double inclination in three-ply CLT panels. The STS used in their study was 8 mm in diameter and 180 mm in length. Seven groups were tested under monotonic loading and four groups were tested under cyclic loading. The wood-to-wood specimens had doubled inclination self-tapping screws at an angle of 45 degrees to the joint line as well as an insertion angle of 32.5 degrees to connect two shear planes. The test results

showed that double-angled butt joints under static and cyclic loading provided an average ductility ratio of 7.7 and 4.1, respectively. The ductility of these double-inclination butt joints can be classified as moderate-to-high, indicating that it was a viable connection method used in CLT lateral load resisting systems.

Hossain et al. (2019) evaluated the performance of STS-CLT joints under monotonic and reversed cyclic tests. They conducted surface spline joint with STS loaded in shear only and half-lap joint with STS loaded in either shear or withdrawal. The influence of the number of shear planes and the size of specimens were considered in their study. They found the ductility ratio of STS-CLT joint in shear was high but the stiffness was low. However, the STS-CLT joint exhibited high stiffness with low ductility in withdrawal. Another noteworthy point is the group effect for the strength of the joint under reversed cyclic loading was more apparent than that under monotonic loading.

2.4.2 Other connections

The calculation of lateral strength of a screwed connection in the Canadian timber design standard (CSA 2019) is based on the European Yield Model, which was developed from Johansen's work (Johansen, 1949). The lateral resistance of steel-to-wood connections depends on the thickness of the steel plate and wood member, screw diameter, and lumber density. The CSA O86-19 standard gives provisions for calculating the lateral resistance of steel-to-wood connections for all possible failure modes, including the crushing of wood and plastic hinge formation in the fastener.

Table 2.4 presents six possible failure modes and the corresponding design equations in CSA O86 (CSA 2019).

Table 2.4 Lateral resistance and failure modes of two-member connection in CSA O86 (CSA 2019)

Failure mode	Lateral strength resistance	Illustration of failure mode
(a)	$f_1 d_F t_1$	
(b)	$f_2 d_F t_2$	
(c)	$f_1 d_F{}^2 \left(\sqrt{\dfrac{1}{6} \dfrac{f_2}{(f_1 + f_2)} \dfrac{f_y}{f_1}} + \dfrac{1}{5} \dfrac{t_1}{d_F} \right)$	
(d)	$f_1 d_F{}^2 \left(\sqrt{\dfrac{1}{6} \dfrac{f_2}{(f_1 + f_2)} \dfrac{f_y}{f_1}} + \dfrac{1}{5} \dfrac{t_2}{d_F} \right)$	
(e)	$f_1 d_F{}^2 \dfrac{1}{5} \left(\dfrac{t_1}{d_F} + \dfrac{f_2}{f_1} \dfrac{t_2}{d_F} \right)$	
(f)	$f_1 d_F{}^2 \sqrt{\dfrac{2}{3} \dfrac{f_2}{(f_1 + f_2)} \dfrac{f_y}{f_1}}$	

where:
t_1 = head-side member thickness for two-member connections [mm]
t_2 = length of penetration into point-side member for two-member connections [mm]
f_1 = embedment strength of the side plate [MPa]
f_2 = embedment strength of the main member [MPa]
d_F = diameter of fastener [mm]
f_y = yield strength of fastener [MPa]

Eurocode 5 (2014) provides more categories for the load-carrying capacity of steel-to-timber connections, with steel plate thickness being a critical parameter. Steel plates of a thickness that is less than or equal to 0.5d are classified as thin plates, whereas steel plates of thickness greater than or equal to d, with a tolerance on hole diameters being less than 0.1d, are categorised as thick plates. In terms of thin-side steel plates, only two types of failure modes are presented (see Figure 2.2):

a) Crushing of wood member while the fastener remains straight in both members.

b) Crushing of wood member with one plastic hinge formed in the fastener.

For a thick steel plate, three possible failure modes are noted:

c) Crushing of wood member while the steel plate remains elastic.

d) Crushing of wood member with one plastic hinge formed in the fastener.

e) Crushing of wood member with two plastic hinges formed in the fastener.

<div align="center">

(a)   (b)   (c)   (d)   (f)

</div>
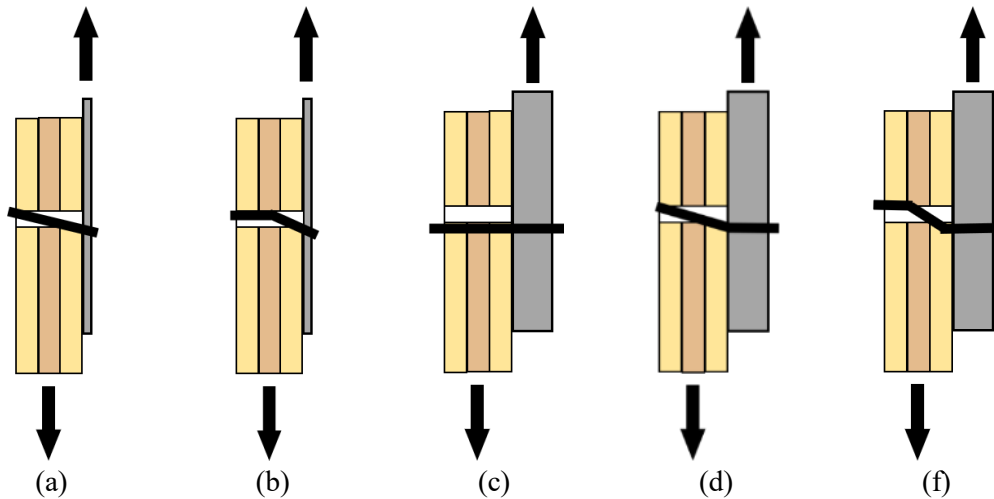
Figure 2.2 Failure modes of steel-to-wood connections (Source: Eurocode 5)

Furthermore, the design expressions in Eurocode 5 (2014) consider not only the load-carrying capacity based on Johansen's yield theory (1949), but also the contribution of rope effects.

Gavric et al. (2013) established that capacity-based design principles should be applied at the connection level for the seismic design to ensure the ductile failure modes precede the brittle modes of failure, to further ensure ductile responses of the wall systems. The basic principle of the capacity-based design at the connection level is to ensure that the plastic hinges formed on the fasteners instead of crushing failure in the wood member.

Gavric et al. (2013) put forward several suggestions in order to obtain a better mechanical performance of typical connectors used in CLT structures: (1) utilisation of screws with a larger diameter at the bottom of the angle brackets; (2) increasing the sections (thickness) of the metal sheet of the connector (to provide a higher yield moment capacity); (3) ensuring that the number and diameter of fasteners are sufficient to

guarantee that the fracture failure in the tension of the connector occurs after the failure of the nailed/screwed connection between the steel metal sheet and CLT panels; and (4) slender nails or screws in CLT connection can exhibit desired ductile performance.

Tomasi and Smith (2015) investigated the mechanical behaviour of commonly used and innovative angle brackets under both monotonic and cyclic loading protocols. The capacity of base shear connections is mainly influenced by the geometries of the bracket and also the types of fasteners used to connect to CLT panels and foundations. Additionally, they concluded that it is significant to consider the capacity of angle brackets to resist the reversed shear flow at the base of the shear wall and also that the design values cannot be estimated based on simplified models. The only reliable way to determine design capacity for certain types of angle bracket connections is through test-based investigations.

Fragiacomo et al. (2011) conducted the seismic analysis of massive timber panels connected to the foundation using different kinds of angle brackets with nails, screws, and self-tapping screws. They highlighted the capacity design principles and design over strength capacity of connections in order to avoid the brittle failure mechanism. The overstrength factor γ_{RD} is defined as the ratio between the 95th percentile of the connection strength distribution and the design strength F_d. Based on the test results, a value of 1.3 was determined as the shear and uplift overstrength factor for BMF 105 steel brackets (Simpson Strong-Tie[®]).

Gavric et al. (2015b) evaluated the mechanical properties of hold-downs and steel angle brackets that were used to connect the wall panels to the foundations under monotonic and cyclic loading. By comparing the test results with calculations based on the analytical models they found that the predicted stiffness values were much higher than the experimental values. It is suggested that currently only experimental strength and stiffness values of hold-downs and angle brackets should be utilised in seismic analyses. In terms of obtaining better mechanical performance of CLT metal connectors, they

recommended increasing the thickness or section of the angle bracket to prevent plasticisation of the metal part and using larger diameter screws that can provide a higher withdrawal capacity in the lower part of the angle brackets.

Mahdavifar et al. (2018) carried out a series of connection tests using two types of fasteners CAN 4 × 60 nails and SDS25300 wood screws, and a steel side plate on seven different species/grade combinations of hybrid CLT specimens under lateral loads. Douglas fir, western hemlock, and lodgepole pine were chosen for their study. The use of low-grade-density substrate in the core layers of hybrid CLT panels was found to have no significant effect on yield modes or fastener strength. Three adjusted European Yield Models for hybrid CLT panels, accounting for the effect of changing density, were proposed. However, these models still need to be investigated further.

Recent studies, such as Liu (2019), Masroor et al. (2020) and D'Arenzo et al. (2021), have highlighted that angle brackets are used to resist shear but they are also subjected to uplift loads. Innovative angle brackets with an increased thickness of the metal sheet together with using fully threaded screws were used to connect the angle bracket to the floor panels to achieve high mechanical performances in both the vertical-tensile and horizontal-shear directions. D'Arenzo et al. (2019) investigated behaviour of the novel angle brackets used in CLT structures under monotonic loading. The CLT panels were five-ply 150 mm thick and subjected to tensile and shear loads with full nailing and partial nailing configurations covered. The test results confirmed that the mechanical properties of innovative angle brackets were similar in vertical and horizontal directions. Group effects should be considered to evaluate the strength of angle brackets. A better approximation was found when the effective number of fasteners $n_{eff} = n^{0.9}$, was taken into account, where *n* is the number of fasteners.

Pozza et al. (2018) conducted an experimental investigation on the axial-shear interaction in WHT 540 hold-down (Rothoblaas®) used in CLT shear walls under seismic

action with the aim of examining the performance of hold-downs when subjected to certain levels of prescribed lateral displacements. The uplift resistance of hold-downs decreased almost linearly, accompanied by a significant increase in elastic stiffness when exposed to increasing levels of imposed lateral displacements. It can be concluded that the axial-shear interaction of hold-downs is fairly minor up to 7.5 mm lateral displacements when angle brackets resist the shear of a shear wall system and remain elastic.

2.5 CLT shear wall testing

The CLT shear wall systems constructed with mechanical connections can behave in a ductile manner when subjected to seismic load. Dujic et al. (2006) carried out shaking table tests on two full-scale CLT shear wall specimens, involving single-panel and coupled-panel walls using lumber strips stacked on the top. The test results indicated that the walls behaved linear-elastically while the non-linear behaviour was primarily caused by the mechanical anchoring systems.

Dujic et al. (2008) conducted one of the first comprehensive experimental studies on the lateral strength and stiffness of CLT shear walls with openings. Two wall configurations were tested under cyclic loading, one with openings and the other without. Tests were conducted to determine the in-plane modulus of elasticity and shear modulus as well as the behaviour of the component connector under combined tension-shear. They conducted a parametric study on 36 wall configurations to investigate the influence of openings on strength and stiffness. They concluded that the opening, with areas up to 30% of the wall surface, may not have a significant reduction on strength while the stiffness was reduced by about 50%.

Another comprehensive study on the seismic performance of CLT buildings, called the SOFIE project, began in 2006. The test specimens were full-size modular buildings made entirely of CLT panels. Under the SOFIE project, a three-storey and a seven-storey CLT building were tested in a shake table. Ceccotti (2008) suggested a value of 3 for the q-

factor based on the shake table test on the three-storey building. Based on this finding, the seven-storey building was designed and tested using a shake table. Both the three-storey and seven-storey buildings performed in a ductile manner that confirmed that it was feasible to use capacity-based design approaches with a reasonable q-factor to design CLT mid-rise or even high-rise buildings.

Upon completion of the SOFIE project, a couple of research studies were carried out globally to further evaluate and enhance the CLT shear wall systems. FPInnovations initiated a series of CLT shear wall tests to quantify the structural performance of the CLT shear wall as well as to develop design approaches for CLT systems in seismic regions.

Popovski et al. (2010) tested 12 different wall configurations under monotonic and cyclic loading. The CLT specimens were all three-ply panels with a thickness of 94 mm. In their testing program, various wall aspect ratios (1:1; 1:1.5, and 2.1:1), opening size and location, and connection layouts were investigated. The test results verified that the CLT can be used in lateral load resisting systems. In addition, using inter-panel joints can enhance the ductility of the entire shear wall. This CLT shear wall test program ultimately led to the recommended values for force modification factors of 2.0 for R_d and 1.5 for R_o.

Gavric et al. (2015c) conducted an experimental investigation on single and coupled CLT shear walls under cyclic loading to explore the influence of inter-panel joint and anchoring systems on CLT shear wall performance. The test results revealed that the design of inter-panel joints had a significant impact on kinematic wall behaviours, and that vertical loads can have a beneficial effect. In-plane deformations of CLT panels themselves were found to be less than 3% of total displacements. This confirmed that the CLT panels can be considered to be a rigid body and that rocking and sliding contributed to the majority of the deformability components of CLT shear walls. Furthermore, advanced analytical models, including non-linear responses, were

developed and confirmed by experimental results. The proposed advanced analytical models take into account the vertical contribution of angle brackets, the horizontal contribution of hold-downs, and the shear-uplift interaction of angle brackets in order to achieve a more accurate prediction.

Popovski and Gavric (2016) investigated the structural performance of a two-storey CLT house subjected to quasi-static monotonic and cyclic loads. The objective of this investigation was to assess the load-deformation response of 3D CLT walls with associated failure mechanisms and the level of storey drifts that the CLT buildings can reach without significant damage. The failure mechanism of most cases was the failure of nails in the brackets because of rocking and sliding. It was found that the damage in the second storey was lower than that of the first storey. The test results also indicated that the walls perpendicular to the loading direction contributed to the overall structure's stiffness and strength. The ductility of the CLT building can be achieved by a proper selection of fasteners and connectors along with the locations of the connectors. However, despite these precautions CLT buildings can reach relatively high storey drifts (Popovski and Gavric, 2016).

Numerous studies have highlighted the significance of angle bracket shear-uplift interactions. D'Arenzo et al. (2021), for example, evaluated the structural performance of full-scale CLT shear walls connected to a CLT floor by using only innovative Titan V angle brackets (Rothoblaas®), which were proven to have coupled shear-lift resistances (D'Arenzo et al., 2019). All CLT shear walls were made of three-ply panels with a 100 mm thickness. Six full-scale shear wall tests were performed to evaluate the influence of different wall aspect ratios, vertical loads, loading types, and the number of connections on the seismic performance of CLT shear walls. The majority of failure modes were connected to the failures of nails in the outmost angle brackets. Only one wall exhibited brittle failures. However, the deformation contribution results were not comparable to those of the earlier study conducted by Gavric et al. (2015c). A larger proportion of panel deformations along with a smaller proportion of rocking and sliding

were found due to the higher stiffness in the novel angle brackets rather than that of traditional connectors.

2.6 Development of analytical models of CLT shear walls

Despite the publication of design provisions for CLT lateral load resisting systems, researchers continue to investigate and make efforts to improve analytical models in order to provide designers and engineers with an accurate prediction of the lateral resistance and deformations of CLT shear walls. The majority of approaches (Gavric et al., 2013; Casagrande et al., 2016; Shahnewaz et al., 2019; Masroor et al., 2021) were developed based on static equilibrium and the assumption that the panels are rigid. The performance of the shear walls was governed by the behaviour of the connection systems.

The simplified analytical model of CLT shear walls was first proposed by Ceccotti et al. (2008), which only considered the uplift resistance of hold-downs and shear resistances of angle brackets. In recent years, the bi-axial behaviour of innovative angle brackets and hold-downs has caught the attention of researchers. The significance of considering the comprehensive contribution of angle brackets and hold-downs has been highlighted.

Gavric et al. (2014) summarised five different shear wall design models, as shown in Figure 2.3. Model D1 assumed that the lateral resistance of the shear wall was based on shear resistances of angle brackets. Model D2 assumed angle brackets resist shear only and that hold-downs resist uplift only. As well, model D3 considered the full shear and uplift resistance of all brackets and uplift resistance only of hold-downs. Models D4 and D5 considered two types of shear-uplift interactions (circular and linear). Gavric et al. (2014) noted that model D3, D4 and D5 produced more consistent results than models D1 and D2. Note that these models considered pure sliding or rocking behaviour only, although the combined sliding-rocking behaviour was the most realistic.
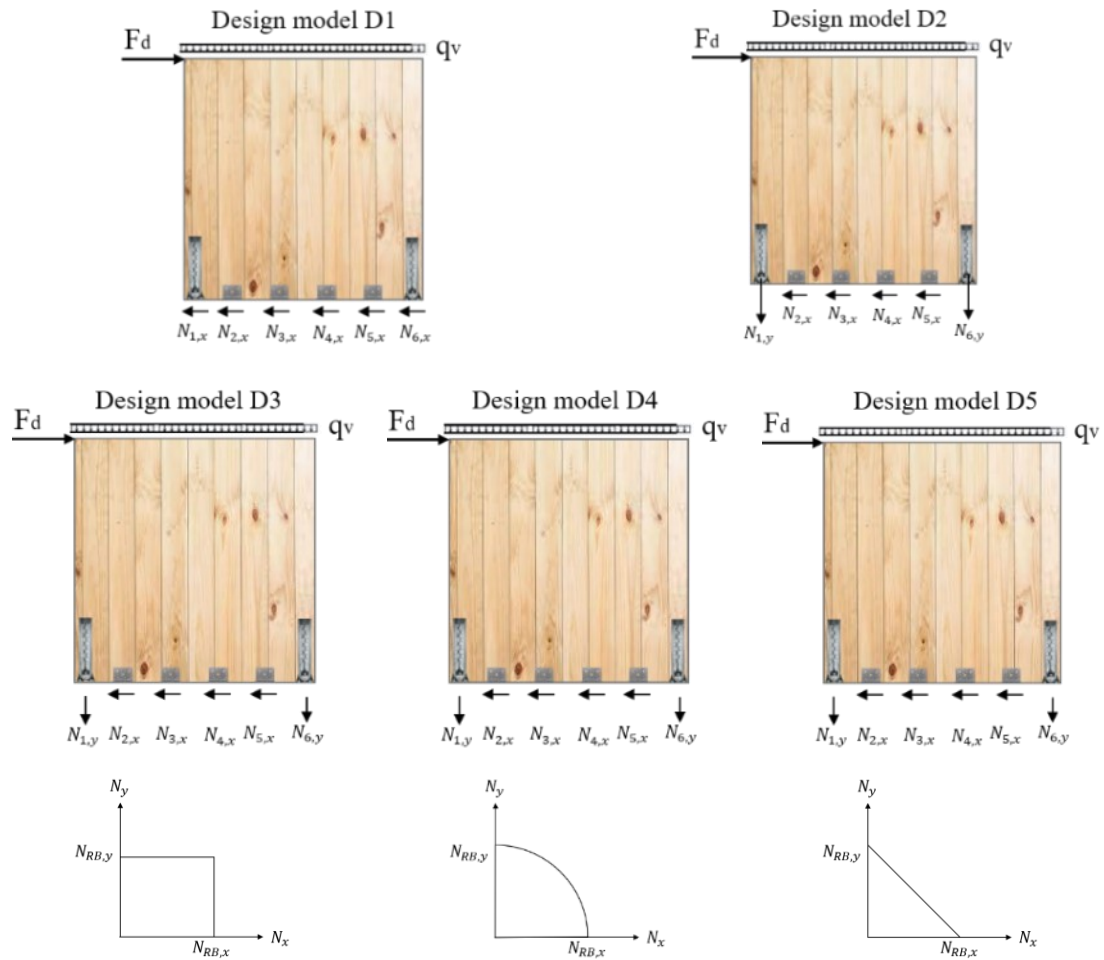
where:

F_d = factored lateral strength of the CLT wall

q_v = vertical load

$N_{RB,x}$ = horizontal reaction of the angle bracket

$N_{RB,y}$ = vertical reaction of the angle bracket

Figure 2.3 Lateral resistance of CLT shear walls based on connection properties

(Gavric et al. (2014))

Gavric et al. (2015c) proposed an advanced analytical model for the nonlinear behaviour of CLT shear wall systems in order to predict the complete load-displacement relationship of CLT wall systems. The model was a trilinear response based on connection properties, along with considerations of the coupled effect of two-directional loading of hold-downs and angle brackets (see Figure 2.4). The trilinear approximation can be generated by connecting the following points: the axis origin (0; 0); the yielding point (d_y; F_y); the peak point (d_{max}; F_{max}); and the ultimate point (d_u; F_u), together with

three stiffness values: k_{el} (elastic); $k_{pl,1}$ (post-elastic); and $k_{pl,2}$ (softening) to characterise the three segments.
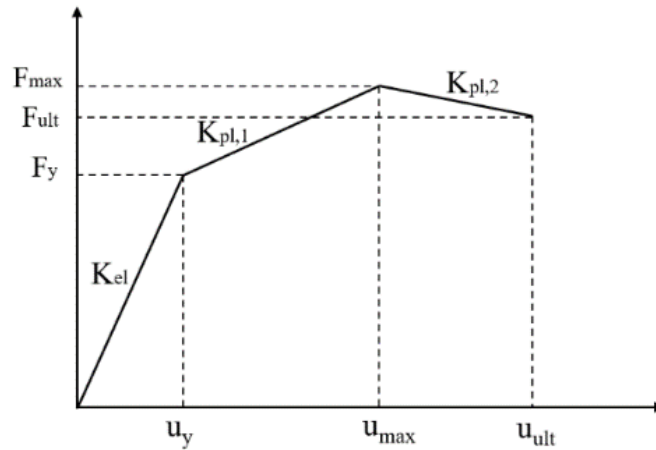
Figure 2.4 Trilinear load-displacement relationship adopted for CLT connections
(Gavric et al. (2015c))

Casagrande et al. (2016) proposed and validated an analytical model for the elastic behaviour of a multi-panel CLT shear wall based on a comparison of stiffness values between the hold-down, angle bracket, and panel joint connection. Three rocking mechanical behaviours were determined by comparing the corresponding stiffness ratios. When the hold-down stiffness is much higher than that of panel joints, each panel will have a centre of rotation that corresponds to couple-panel behaviour (CP). Single-wall behaviour (SW) denotes that the panel joint connection is much stiffer as well as having a progressive uplift of the panels. The intermediate behaviour lies between CP and SW with some panels in contact with the base.

Shahnewaz et al. (2019) put forward resistance equations of CLT shear walls for platform-type CLT buildings based on kinematic behaviours under a lateral load. The proposed equations cover different anchoring connector layouts and single or coupled wall segments. Equations for five types of walls were presented: (1) single walls with brackets only; (2) single walls with brackets and hold-downs; (3) coupled walls with

brackets only; (4) coupled walls with brackets and two hold-downs; and (5) coupled walls with brackets and four hold-downs. Through comparing the test results and predictions, it was noted that the proposed analytical models provide conservative predictions. However, models of sliding only were not recommended for design use. The models did not take perpendicular walls into consideration and the accuracy of the model needed to be further validated.

Masroor et al. (2021) pointed out several missing analytical expressions in the CLT shear wall design approaches and then presented improved analytical equations for CLT shear walls to ensure a coupled wall behaviour for multi-panel CLT shear walls. Their models considered the bi-directional contributions of the angle brackets and compression zone effect at the bottom of the shear wall. The model predictions were compared with those produced by finite element models. The desired coupled-panel behaviour in both elastic and plastic regions can be achieved by properly employing the overstrength factor associated with energy dissipative and non-energy dissipative elements to ensure a planned sequence of yielding of hold-downs, angle brackets, and panel joints. However, these models should be validated by comparing their predictions with test data.

2.7 Summary

The advancement of mass timber products such as CLT has gained momentum over the last ten years. Further improvement in the performance of these mass timber panels is necessary to maintain this momentum. Composite laminated panel (CLP) is an example of an improved mass timber panel product, which is the focus of this thesis project. Reviewing previous research on CLT, including the mechanical properties of CLT panels, the performance of CLT connections, CLT shear wall behaviours, and analytical models of CLT shear wall systems is useful for gaining a thorough understanding of mass timber shear wall systems before conducting experimental work and evaluating the associated properties of CLP.

In terms of commonly used shear wall models, ignoring the shear capacity of hold-downs

and the tension capacity of angle brackets undoubtedly underestimates the overall shear wall capacity. Recently proposed analytical models provide an improvement by taking the bi-directional resistance of hold-downs and angle brackets into account, along with the combined sliding-rocking kinematic motion of the wall systems. Additionally, analytical models for coupled-panel or even multi-panel shear walls with better ductility and energy dissipation capacity have been proposed.

There are currently no design guidelines for CLP due to the hybrid layup combinations. However, CLP shares some similarities with CLT such as being considered a rigid body under lateral design and it is dependent on mechanical connections as a source of energy dissipation in seismic design. Therefore, it is critical to understand and evaluate the actual behaviour of CLP connections as well as shear walls. It is, therefore, necessary to compare the experimental results with currently available approaches for CLT connections and CLT shear walls, which may contribute to the future development of the models for shear walls built with hybrid panels.

Chapter 3 Performance of Self-tapping Screwed Connections in CLP

3.1 Introduction

This chapter begins with a description of all of the specimens. This discussion is followed by the STS joint connection program that includes the test setup, procedure, and test results. Connection tests were conducted on different combinations of CLP layups, and the grain orientation of the top layer of the CLP, and loading types (monotonic and reversed cyclic). The results from screwed connection tests are analysed and used to predict the strength and elastic stiffness of CLP shear walls discussed in Chapter 4. This chapter provides a summary of the mechanical properties of connection specimens based on test results. This includes the lateral strength P_{peak}; yield strength P_{yield}; stiffness K_e; and ductility ratio μ based on test results. A comparison between the experimental results and predictions based on O86 EYM equations is presented. The applicability of EYM equations in predicting the lateral load capacities of CLP connections containing self-tapping screws is also discussed.
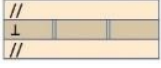
3.2 Materials and methods

3.2.1 Materials

The laminated strand lumber (LSL) panels and lumber were supplied by Tolko Industries Ltd. (Vernon, BC). The lumber was SPF No. 2 or a better grade. The adhesive used was a one-part polyurethane supplied by Henkle Canada Corporation (Mississauga, ON, Canada), which is commonly used in the commercial production of CLT. After evaluating the bond performance of the adhesive and optimising the bonding parameters, three-layered CLP panels (107 mm x 1220 mm x 2440 mm) were fabricated by InnoTech Alberta (Edmonton, AB). Three-layer CLT panels were also produced to provide the reference specimens in both connection and shear wall tests discussed in Chapter 4. Table 3.1 shows the different layer orientations and detailed information of the CLP and CLT panels. Six specimens were cut from each panel and a total of 60 specimens were

prepared for the connection test program.

Table 3.1 Layup information of CLP and CLT panels fabricated by InnoTech Alberta

Panel ID	Layup	Layer orientation	Quantity	Illustration
A1	L-LSL-L	//-//-//	5	
A2	L-LSL-L	//- ⊥ -//	5	
B	LSL-L-LSL	//-//-//	5	
C	LSL-LSL-LSL	//-//-//	4	

Notes: "L" is lumber; "LSL" is laminated strand lumber. "//" indicates that the major strength direction of the layer was orientated parallel to the long side of the panel. "⊥" indicates that the minor strength direction of the layer was orientated perpendicular to the long side of the panel.

As illustrated in Table 3.1, layup A1, B, and C have all three layers with their grain aligned in the same direction, while layup A2 has a similar layer structure as found in traditional CLT, i.e., the grain of the middle layer is oriented perpendicular to the grain of the two outside layers. Both A1 and A2 are hybrid specimens with lumber faces and an LSL core. The only difference between them is the orientation of the core layer. A1 and A2 have LSL core layers oriented parallel and perpendicular to the grain of the outer layers. Specimen B is also a type of hybrid specimen with LSL faces and a lumber core, and it has a reverse layer combination in contrast with group A. The last type of CLP specimen of C was entirely made of LSL laminates with the grain of all three layers parallel to each other.

Used in the test were SDS25300 self-tapping screws, 6.35 mm diameter and 63.5 mm length, as shown in Figure 3.1. They were made of SAE J403 low-carbon steel wire with a bending yield strength of 1130 MPa (164000 psi) according to the manufacturer (SAE 2014). The thread length was 60 mm. This self-tapping screw (STS) has high strength in structural application with no-predrilling installation requirements, which is

recommended for wood-to-wood and wood-to-steel connections.

Figure 3.1 SDS25300 wood screws (courtesy of Simpson Strong-Tie®)

The steel side plate (HRS416Z) was manufactured from galvanized steel complying with ASTM A653, SS Grade 33, with a minimum yield strength of 227 MPa (33,000 psi) and a minimum ultimate tensile strength of 310 MPa (45,000 psi) based on the data provided by the supplier, as shown in Figure 3.2.

Figure 3.2 Steel side plate-HRS416Z (courtesy of Simpson Strong-Tie®)

3.2.2 Test specimens

The screwed connection test program included 60 connection specimens. Half were for the monotonic and the other half for reversed cyclic loading. The CLP member dimensions are 200 mm × 120 mm × 107 mm for those in specimens with load applied parallel to the face layer grain and 200 mm × 200 mm × 107 mm for those in specimens with load applied perpendicular to the face layer grain. On each side of the CLP member, a 3mm thick steel plate was attached by use of two self-tapping screws (SDS HEAVY-DUTY SDS25300) leading to a total of four STS in two single-shear connections per specimen as shown in
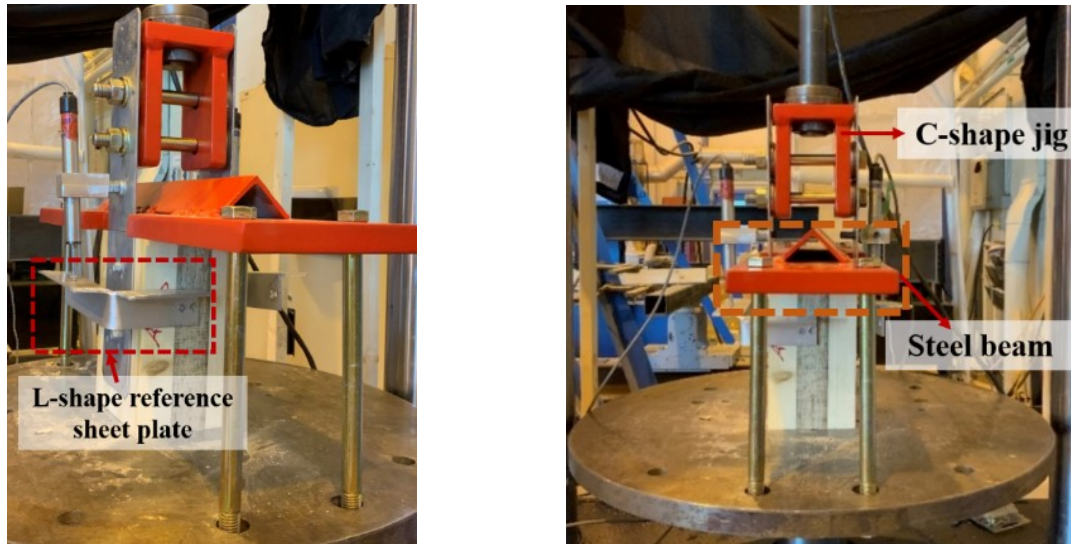
Figure 3.4 Connection test setup

Table 3.2 shows the connection specimen configurations. Three replicates were tested for each connection specimen configuration under monotonic or reversed cyclic load.

Table 3.2 Test matrix for CLP and CLT connection tests

Test series	CLP layup	Loading direction
A1-//	L-LSL (pa)-L	parallel
A2-//	L-LSL (perp)-L	parallel
B-//	LSL-L-LSL	parallel
C-//	LSL-LSL-LSL	parallel
CLT-//	L-L-L	parallel
A1-⊥	L-LSL (pa)-L	perpendicular
A2-⊥	L-LSL (perp)-L	perpendicular
B-⊥	LSL-L-LSL	perpendicular
C-⊥	LSL-LSL-LSL	perpendicular
CLT-⊥	L-L-L	perpendicular

Note: "//" represents the connection loaded parallel to the face layer grain.
"⊥" represents the connection loaded perpendicular to the face layer grain.

3.2.3 Test method

The specimens tested under monotonic loading were loaded at a rate of 5 mm/min. The monotonic test was carried out first to derive a reference displacement for the cyclic test. The reversed cyclic test protocol was based on Method B (displacement-controlled loading procedure) of ASTM E2126 (ASTM 2019). The loading schedule consisted of two displacement patterns in order to generate sufficient data in the elastic and inelastic regions. The first displacement pattern consisted of five reversed cycles with amplitudes of 1.25%, 2.5%, 5%, 7.5%, and 100% of the corresponding ultimate displacement (Δ_m) of each type of CLP. The ultimate displacement (Δ_m) is defined as the post-peak displacement at 80% of the mean peak load in the monotonic tests. In the second part of the protocol, 20%, 40%, 60%, 80%, and 100% of the ultimate displacement was successively applied to the specimen and each amplitude phase consists of three full cycles (see Figure 3.3).
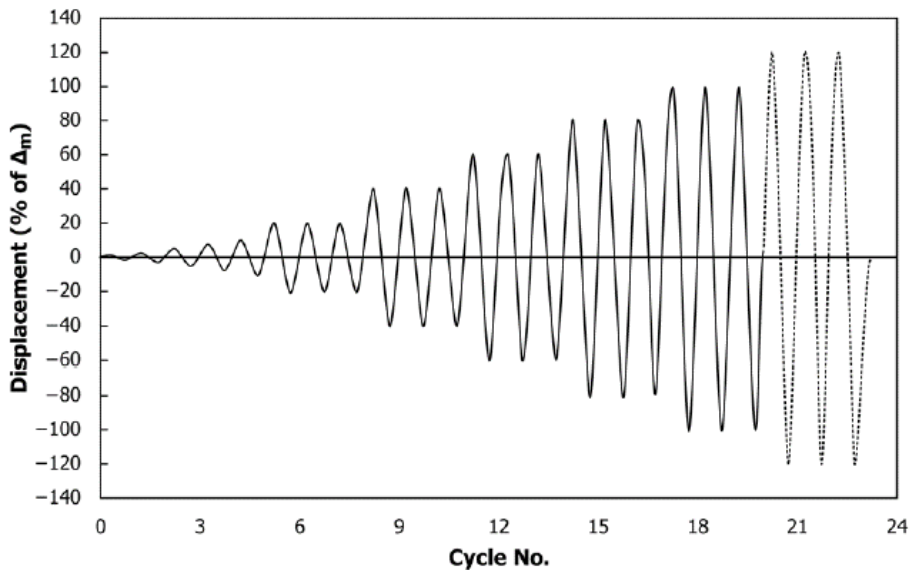
Figure 3.3 Displacement-controlled loading procedure (Method B) of ASTM E2126 (ASTM 2019)

The loading rate was adjusted as tabulated in Table 3.3. The tests were stopped when the load dropped by more than 20% of the peak load.

Table 3.3 Sequence of amplitudes for the reversed cyclic loading protocol

Pattern	Step	No. of cycles	Cycle no.	Amplitude - percent of Δ_m (%)	Loading rate (mm/s)
1	1	1	1	1.25	0.07
	2	1	2	2.5	0.07
	3	1	3	5	0.07
	4	1	4	7.5	0.07
	5	1	5	10	0.07
2	6	3	6–9	20	0.16
	7	3	10–12	40	0.16
	8	3	13–15	60	0.16
	9	3	16–18	80	0.16
	10	3	19–21	100	0.16
	11	3	22–24	120	0.16
	12	3	25–27	140	0.16

Figure 3.4 Connection test setup
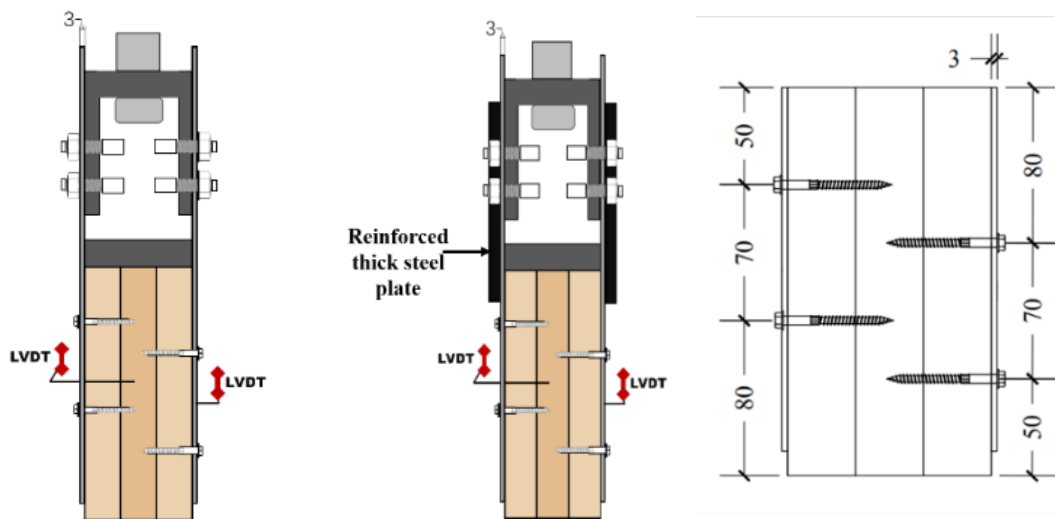
Figure 3.5 Sketch of joint connection test setup: monotonic test (left); cyclic test (middle); screw pattern (right) (dimensions in mm)

To investigate the monotonic and cyclic load behaviour of STS connections in CLP, two different setups were designed, as shown in Figure 3.5. The monotonic test setup was based on the apparatus developed by Wang (2009) and Plesnik et al. (2016). It was later adopted by Spasojevic (2019) and Zhang (2021). The lower portion of the test setup was joint to be tested, steel side plates were directly connected to the wood member with two

screws on each side with 70 mm spacing between them. While the upper segment was a rigid dummy joint made of steel side plates connected by two bolts to a C-shape jig. The tension load was applied through the steel plates attached to the specimen. A horizontal steel beam with a triangle hollow section was bolted to the reaction frame in order to avoid out-of-plane movement and rotation.

For the cyclic tests, two additional thick steel plates were installed at both sides of the specimen, as shown in Figure 3.5, to prevent the 3 mm steel side plates from buckling when the specimen was loaded in compression. The thick steel plates stopped at about 30 mm from the closest screw. The relative displacement between the wood middle member and steel side member was measured with two linear variable differential transformers (LVDTs) that were fastened to the steel side plate as well as L-shape reference sheet plates placed between two self-tapping screws (see Figure 3.4).

3.3 Test results

3.3.1 Monotonic tests

Analysis of the screw joint results was conducted in accordance with the equivalent energy elastic-plastic (EEEP) method given in ASTM E2126 (ASTM 2019), as illustrated in Figure 3.6. Stiffness, K_e, of a test specimen was determined by calculating the slope of the load-displacement response between 10% to 40% of the peak load. The units Δ_u and Δ_{yield} represent the displacement at capacity and displacement at yield load, respectively. E_d refers to the energy dissipated at the ultimate displacement. The yield load, P_{yield} can be calculated as expressed in (3.1).
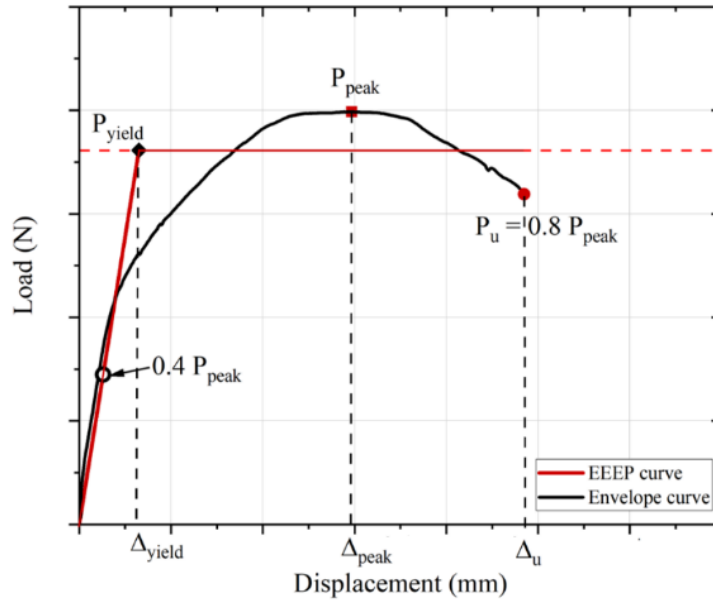
Figure 3.6 EEEP curve in ASTM E2126 (ASTM 2019)

$$P_{yield} = (\Delta_u - \sqrt{\Delta_u{}^2 - \frac{2A}{K_e}})K_e \qquad (3.1)$$

If $\Delta_u{}^2 < \frac{2A}{K_e}$, it is permitted to assume $P_{yield} = 0.85P_{peak}$

where A is the area under the envelope curve from zero to ultimate displacement (Δ_u).

To evaluate the capacity of one screw, the measured load values were divided by the number of screws in the specimen. This is justified based on a previous study by Murty et al. (2010) that demonstrated that for small diameter fasteners (6.4 mm), the applied load was fairly evenly shared between the fasteners in a connection specimen. The connection displacement was the average of the measurements from the two LVDTs. Load-displacement curves of specimens under the monotonic load was applied parallel to the grain and perpendicular to the grain. They are presented in Figure 3.7 and Figure 3.8, respectively.

These figures illustrate the differences in behaviour between test groups that can be

divided into two categories: Layup A and traditional CLT as one category and layups B and C as the second category. It can be observed that specimens A1, A2, and traditional CLT experienced similar ductile behaviour and exhibited comparable stiffness, yield point, and ductility. Their load-displacement responses demonstrated that they could be loaded continually beyond its yield point without considerable loss of strength.

In contrast, screws in specimens B and C displayed significantly higher strength and stiffness but relatively low ductility. The displacements at the yield load were approximately 6 mm for specimens B and C, while the displacements at the ultimate load were around 13 mm. This phenomenon can be attributed to the utilisation of LSL as the face layer of CLP, in other words, CLP with LSL on the face tended to exhibit higher strength and stiffness than lumber on the face. This is because LSL had a higher density than sawn lumber. However, despite specimens B and C having higher strengths, the displacements at failure were extremely low (around 13 mm) compared with specimens A1, A2, and the traditional CLT (22–25 mm). This observation becomes more obvious when the connection was loaded parallel to grain. For example, the ultimate displacement of traditional CLT (25 mm) was almost twice as much as those of specimen B (14 mm) and C (13 mm), which indicated that layups B and C may not be suitable for seismic applications.
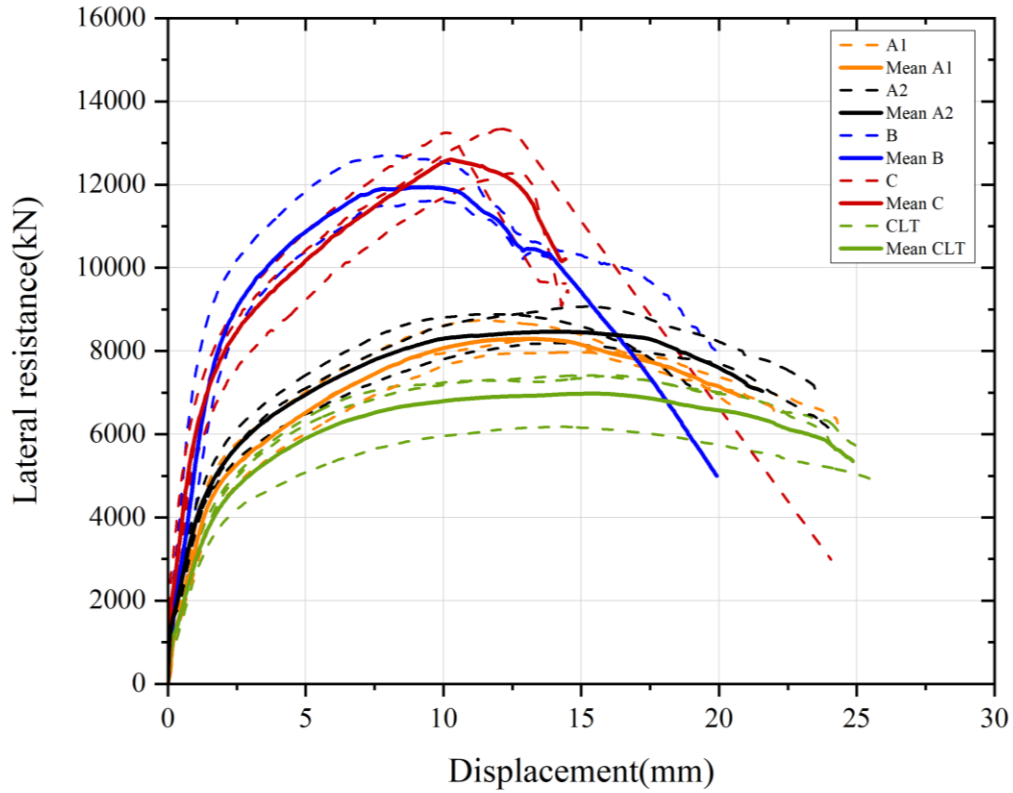
Figure 3.7 Load-displacement curves and their mean value curves under monotonic
load applied parallel to grain (Per screw)

Overall, CLP had higher strength and stiffness than CLT regardless of whether LSL was placed in the face or core layer. However, specimens with lumber as the face layer and LSL as the core, i.e., A1 and A2, exhibited better ductile behaviour and higher strength compared with CLT. This made them more suitable for seismic applications than traditional CLT and CLP with LSL as face layers (B and C).
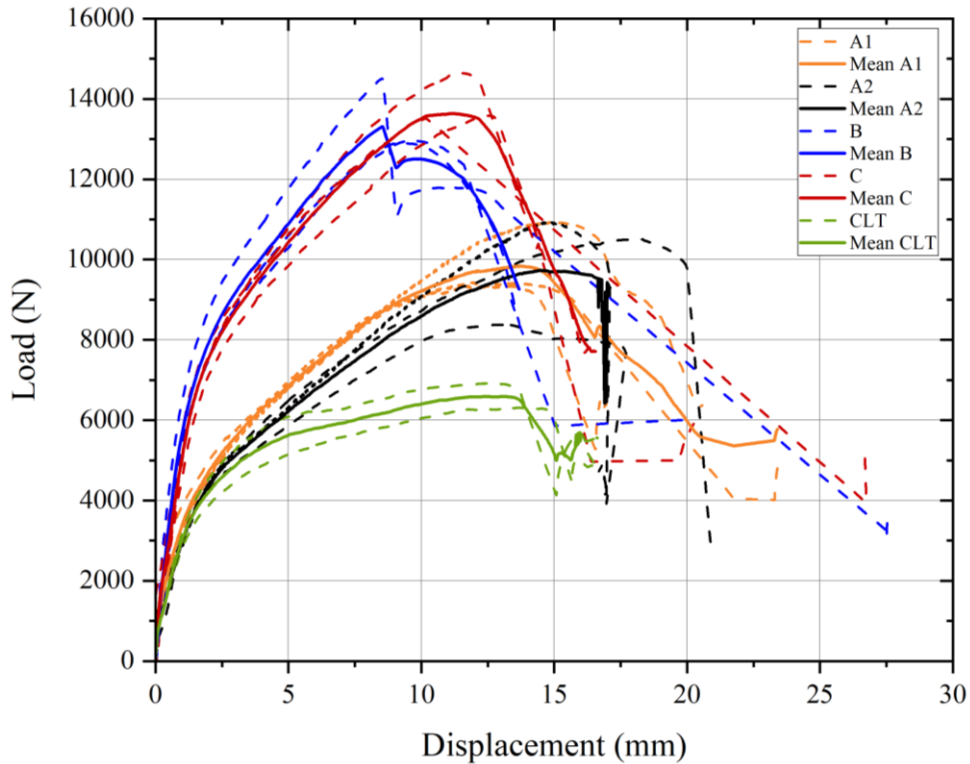
Figure 3.8 Load-displacement curves and mean value curves under monotonic load applied perpendicular to the grain (Per screw)

With regard to specimens loaded perpendicular to the grain of the face layer, similar to the trend in parallel cases, the load-displacement responses of specimens can be grouped into two categories (see Figure 3.8). Additionally, it is apparent from Figure 3.8 that the mode of failure under perpendicular to the grain loading was relatively brittle as is evident from the sudden drop in the load after the peak load was attained.

Table 3.4 presents the mean values of the mechanical properties of the test groups along with the range (minimum and maximum values). It can be observed that specimen C, made entirely of LSL, had the highest strength and stiffness values among all the test groups. Specimen B, with LSL in the face layers, had lower strength than specimen C but higher values than the remaining groups.

Table 3.4 Summary of screwed joint test results under monotonic loading

Specimen ID	K_e (kN/mm)	P_{yield} (kN)	Δ_{yield} (mm)	P_{peak} (kN)	Δ_u (mm)	E_d (kJ)	$\mu = \Delta_u/\Delta_{yield}$
A1-//-m	2.66	7.50	7.70	8.34	22.02	616.13	2.86
	(2.2 - 2. 9)	(7.2 - 7.8)	(7.3 - 8.5)	(8.0 - 8.7)	(19.9 - 24.2)	(584.8 - 654.1)	(2.7 - 3.0)
A2-//-m	3.16	7.92	7.84	8.72	21.83	650.11	2.79
	(2.6 - 3.4)	(7.4 - 8.2)	(7.0 - 8.5)	(8.2 - 9.1)	(19.2 - 23.3)	(585.1 - 715.0)	(2.7 - 2.8)
B-//-m	5.60	11.34	5.52	12.16	12.98	538.28	2.45
	(4.2 - 7.4)	(10.9 - 11.5)	(4.4 - 6.2)	(11.6 - 12.7)	(10.1 - 15.4)	(427.3 - 677.1)	(1.7 - 3.5)
C-//-m	5.86	11.00	6.55	12.95	13.51	551.12	2.08
	(4.9 - 7.1)	(10.4 - 11.3)	(5.7 - 7.2)	(12.3 - 13.3)	(12.8 - 14.2)	(533.2 - 570.6)	(1.9 - 2.4)
CLT-//-m	2.40	6.49	7.30	7.00	24.60	602.03	3.40
	(2.3 - 2.6)	(5.6 - 6.9)	(6.7 - 7.8)	(6.2 - 7.4)	(23.9 - 25.4)	(544.7 - 640.8)	(3.1 - 3.7)
A1-⊥-m	2.67	8.26	8.68	9.91	19.02	577.00	2.31
	(2.1 - 3.5)	(7.8 - 9.2)	(8.2 - 11.6)	(10.1 - 15.2)	(16.5 - 21.8)	(534.2 - 629.1)	(1.7 - 3.0)
A2-⊥-m	2.06	8.41	9.54	9.94	18.39	551.10	1.95
	(2.0 - 2.1)	(7.2 - 9.0)	(8.0 - 10.8)	(8.4 - 11.0)	(17.0 - 20.5)	(458.3 - 662.5)	(1.7 - 2.2)
B-⊥-m	5.58	11.50	5.88	13.45	13.52	599.99	2.39
	(5.1 - 6.3)	(10.7 - 12.4)	(4.6 - 7.9)	(12.9 - 14.5)	(12.6 - 15.0)	(533.3 - 716.1)	(1.9 - 2.8)
C-⊥-m	5.01	11.45	5.95	13.92	12.70	523.78	2.20
	(4.4 - 5.3)	(10.6 - 12.3)	(3.6 - 7.5)	(13.5 - 14.7)	(9.0 - 14.8)	(426.7 - 632.8)	(2.0 - 2.5)
CLT-⊥-m	2.67	5.88	6.35	6.53	16.14	353.75	3.46
	(2.2 - 3.0)	(5.6 - 6.1)	(5.3 - 7.5)	(6.3 - 6.9)	(11.2 - 16.5)	(233.7 - 378.3)	(2.7 - 4.2)

Note : Values in brackets are range of measured values.

For monotonic responses, compared with CLT (specimen D), the CLP specimens had up to 85% higher strength (A1: 19.1%; A2: 24.6%; B: 73.7%; and C: 85.0%) and up to 144% higher stiffness values (A1: 10.8%; A2: 31.7%; B: 133%; and C: 144%) in parallel direction, and up to 113.2% higher strength (A1: 51.7%; A2: 52.2%; B: 105.9%; and C: 113.2%) and up to 108.9% higher stiffness values (B: 108.9% and C: 55.8%) in the

perpendicular direction. The stiffness values of A1, A2, and traditional CLT are nearly the same. Of more interest is that all CLP groups loaded perpendicular to the grain had slightly higher ultimate strengths than the parallel to grain specimens (see Figure 3.9). Statistically, it can be concluded that there is no difference between the strengths in the two directions of the CLP groups. The possible reason is the STS employed in this study had a relatively small diameter (6.35 mm). It is known that for small diameter fasteners(less than 6.35 mm), timber design standards around the world such as CSA O86 (2019) in Canada and NDS (2018) in the United States, do not differentiate between parallel and perpendicular to the grain loading for lateral resistance design of timber connections.
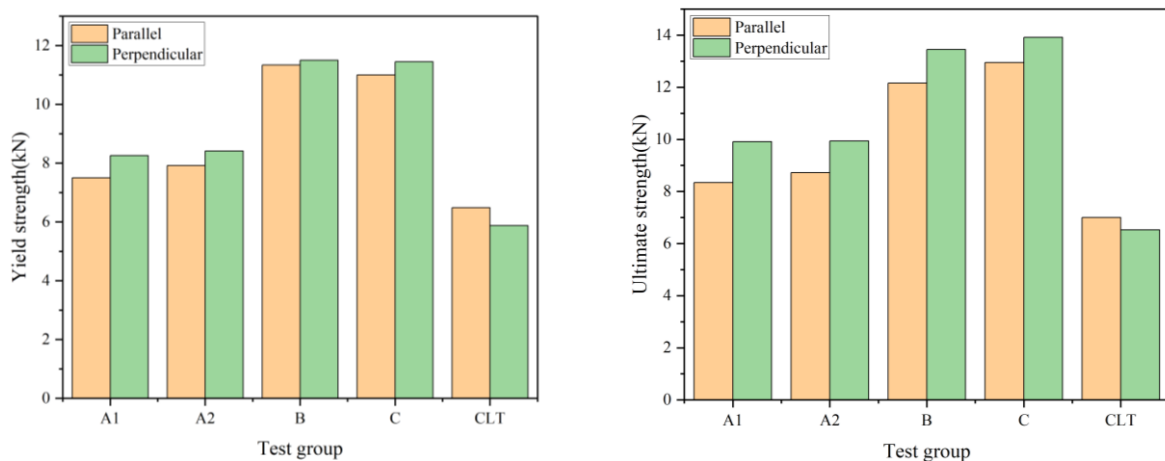
Figure 3.9 Comparison of average yield strength (left) and average ultimate strength (right) between two directions

The test results showed that all STS joints exhibited low to moderate ductility (average 2.56) irrespective of the specimen layups and loading directions. Typical failure modes were the formation of plastic hinges which are indicated by changes in the slope of the load-displacement curves (see Figure 3.7 and Figure 3.8), specifically mode (d) or (f) for a two-member joint defined in CSA O86-19 (CSA 2019) (See Figure 3.10).

| (a) A1-// | (b) B -// | (c) C-// | (d) CLT-// |

| (e) A2 -⊥ | (f) B -⊥ | (g) C -⊥ | (h) CLT-⊥ |
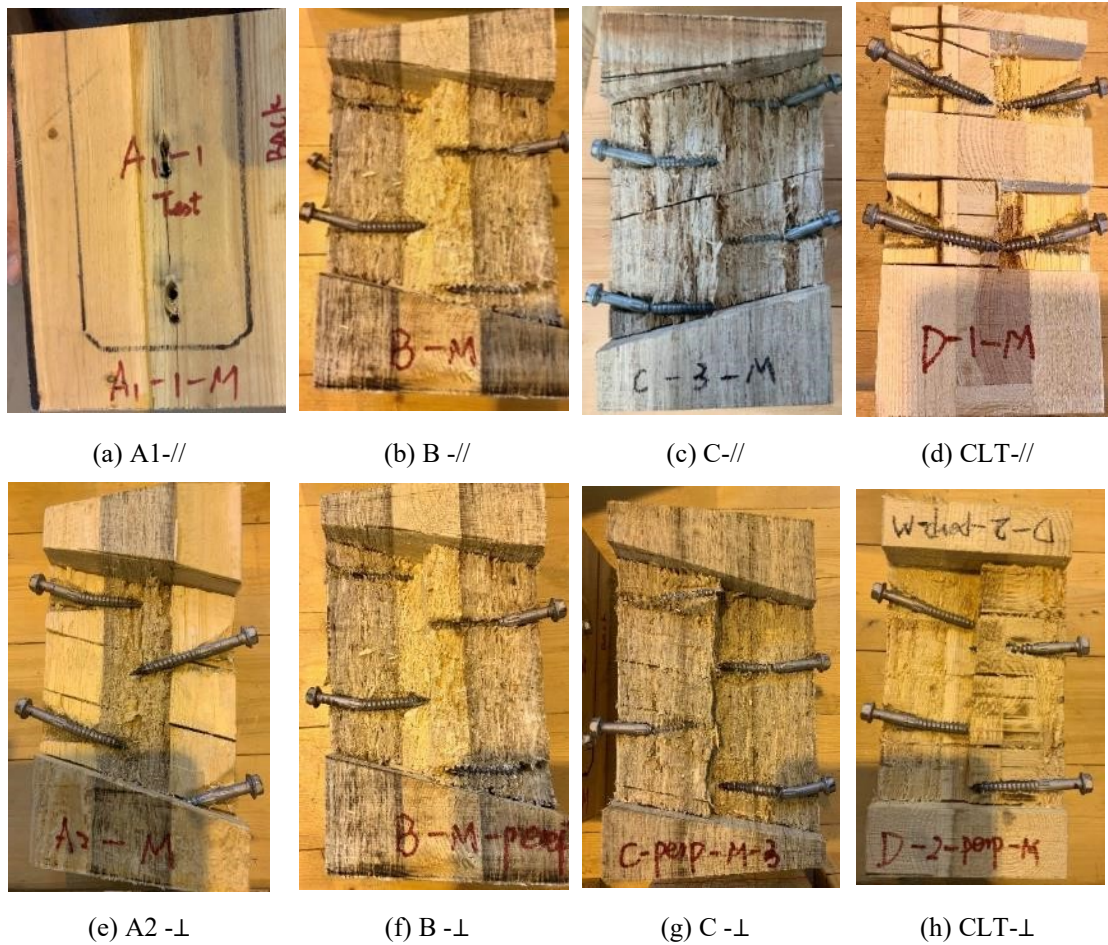
Figure 3.10 Typical failure modes under monotonic loading

3.3.2 Cyclic tests

Figure 3.11 depicts the hysteresis loops for all the test groups. It can be noted that the responses are relatively uniform for specimens A1, A2, and CLT loaded perpendicular to the grain and specimen B loaded parallel to the grain, while the other groups exhibited more variable responses among replicates. As can be seen from Figure 3.11 (a) to (d) and Table 3.5, load-displacement responses and mechanical properties for specimens A1 and A2 are quite similar. This indicates that the grain orientation of the core LSL layer may not have a significant influence on the overall performance of the connections.
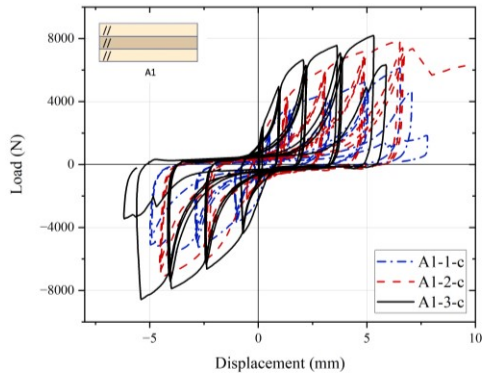
(a) A1-//
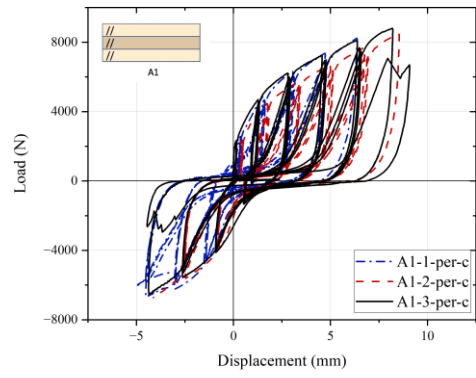
(b) A1-⊥
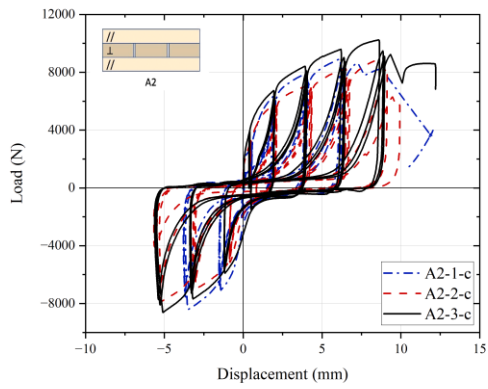
(c) A2-//
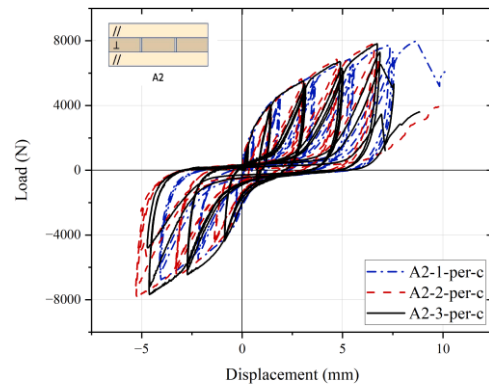
(d) A2-⊥
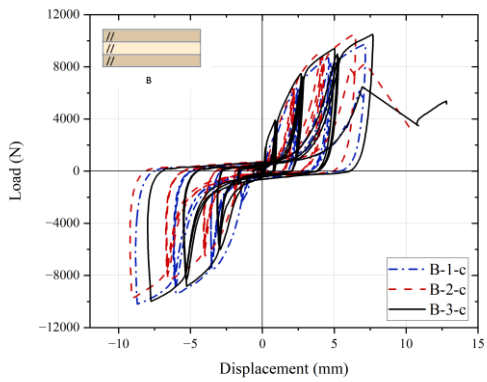
(e) B-//
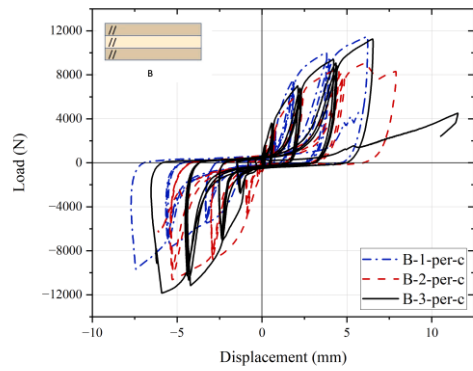
(f) B-⊥
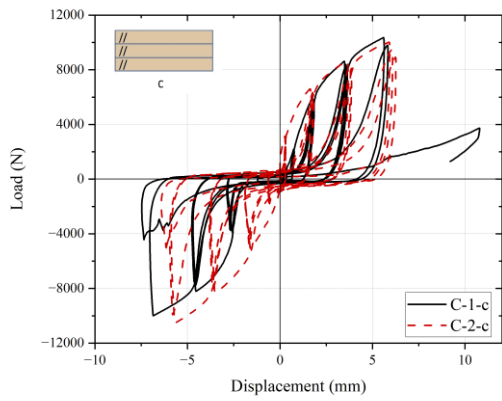
(g) C-//
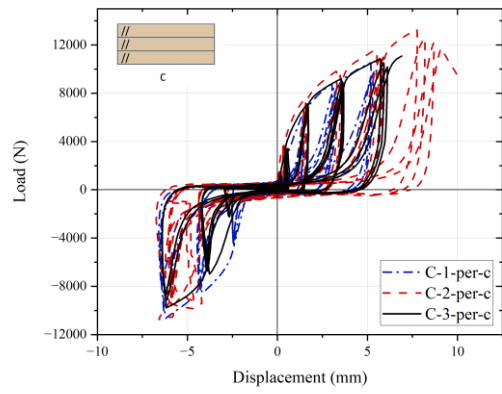
(h) C-⊥
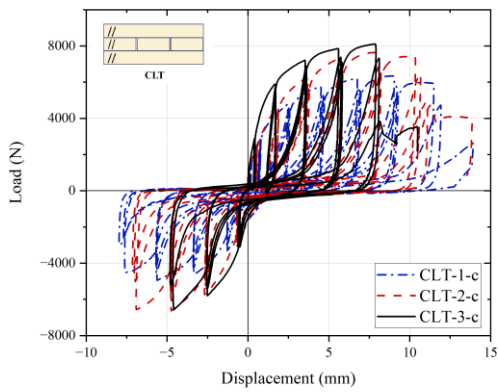
(i) CLT-//
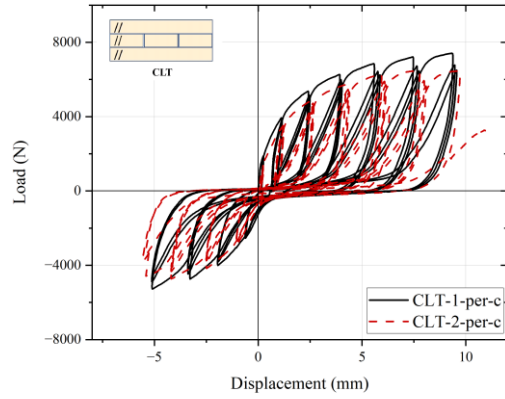
(j) CLT-⊥

Figure 3.11 Hysteresis loops from cyclic tests

Figures 3.12 to 3.21 present the envelope curves for all test specimens. Also superimposed on each figure are the load-displacement curves of the corresponding specimens under monotonic loading.
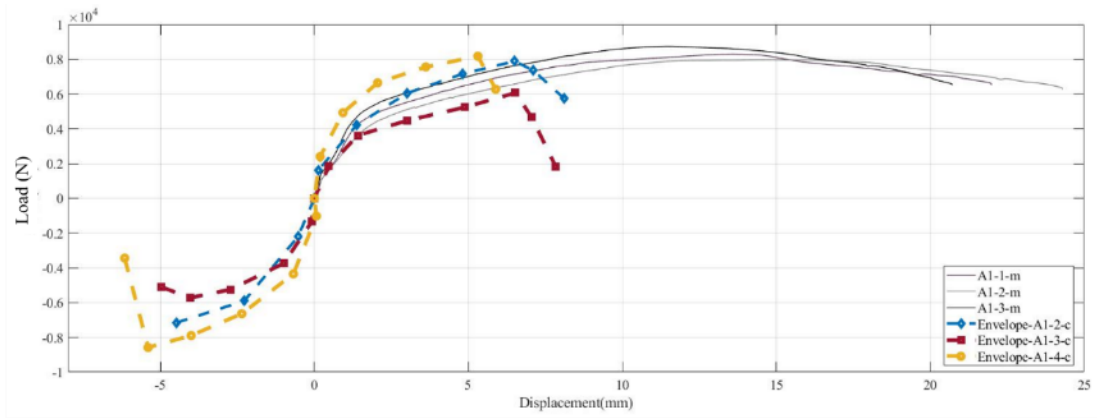
Figure 3.12 Comparison between envelope curves under cyclic loading and monotonic curves: A1-//
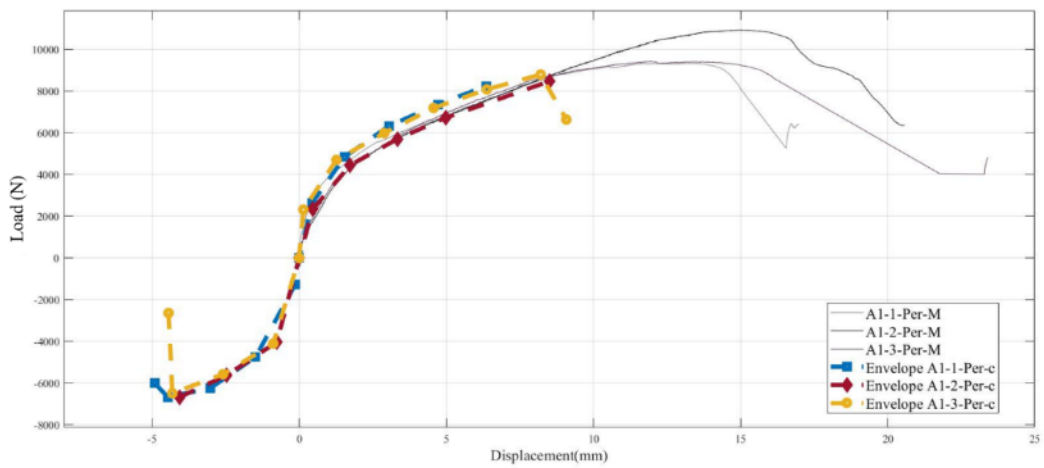
Figure 3.13 Comparison between envelope curves under cyclic loading and monotonic curves: A1-⊥
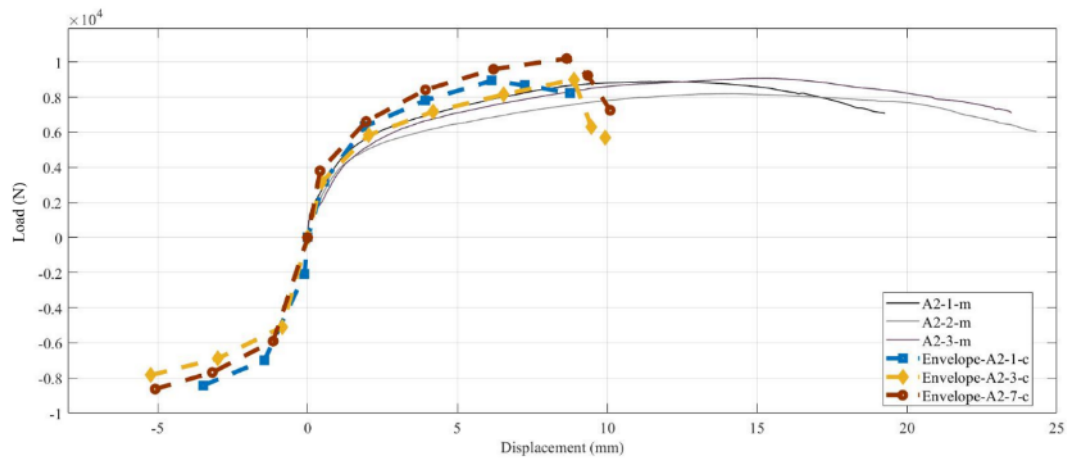
Figure 3.14 Comparison between envelope curves under cyclic loading and
monotonic curves: A2-//
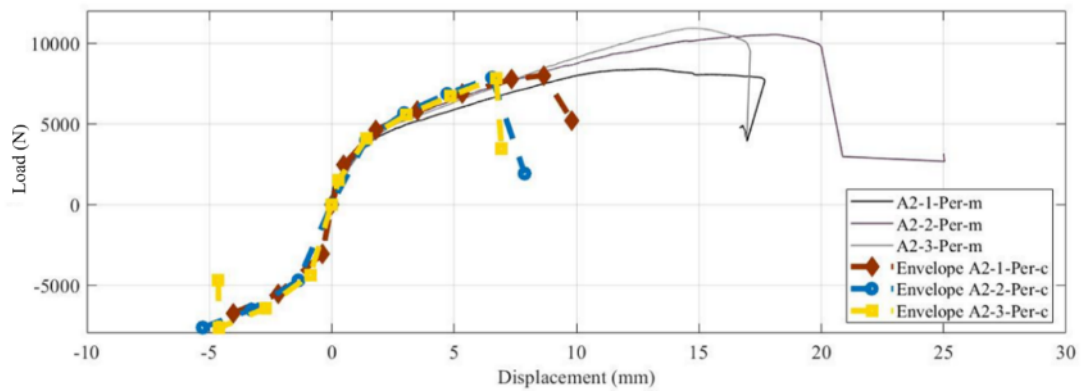
Figure 3.15 Comparison between envelope curves under cyclic loading and
monotonic curves: A2-⊥
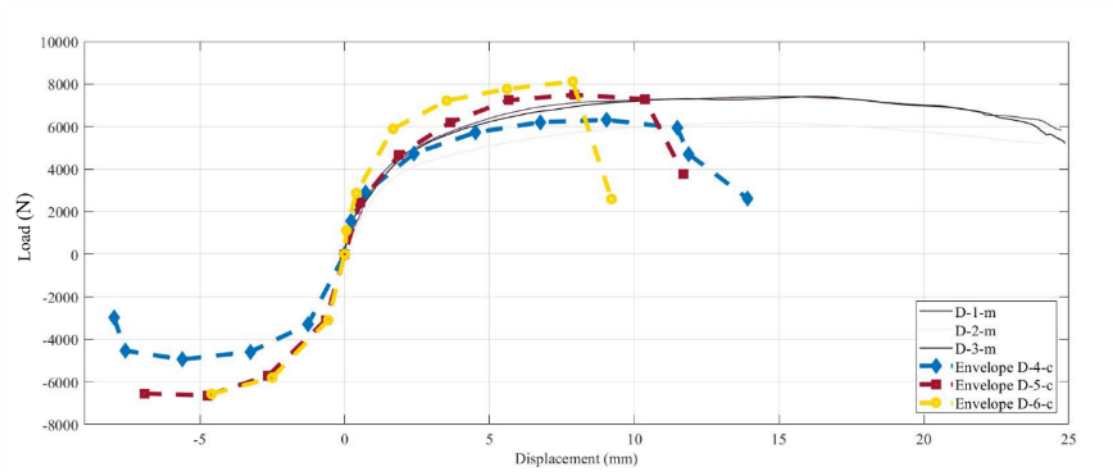
Figure 3.16 Comparison between envelope curves under cyclic loading and monotonic curves: CLT-//
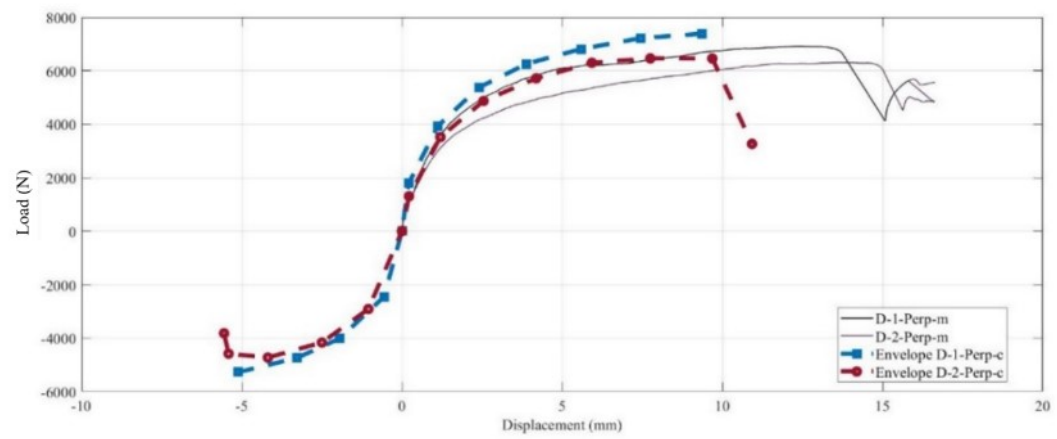
Figure 3.17 Comparison between envelope curves under cyclic loading and monotonic curves: CLT-⊥
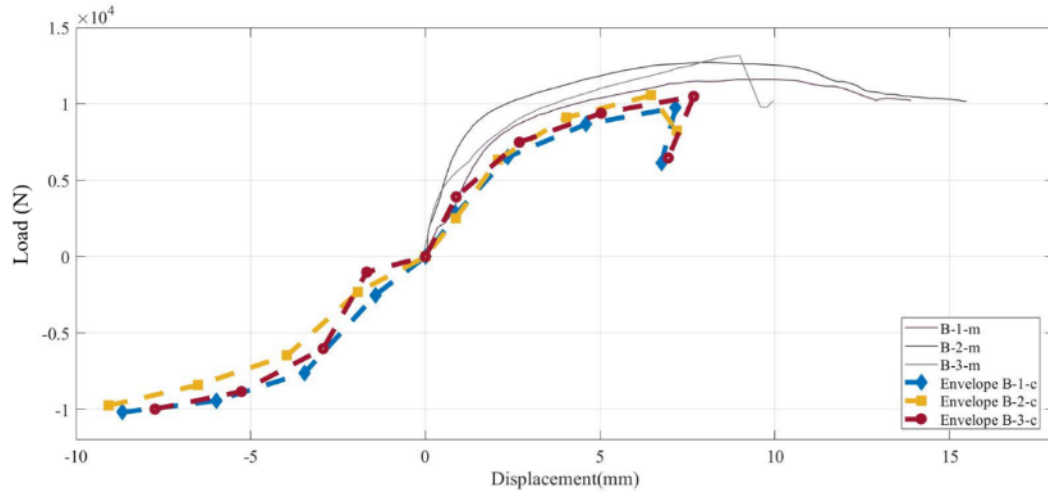
Figure 3.18 Comparison between envelope curves under cyclic loading and
monotonic curves: B-//
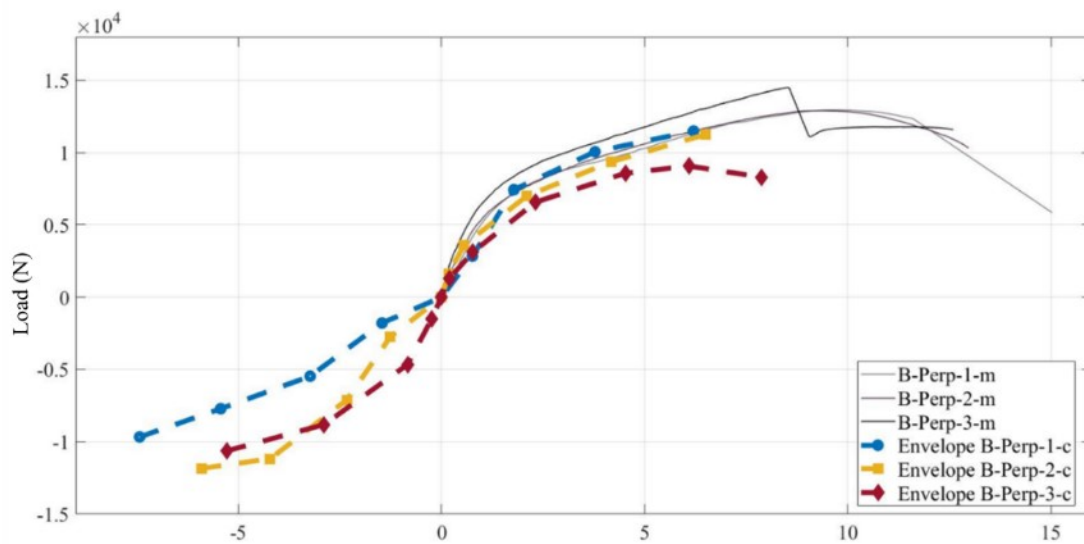
Figure 3.19 Comparison between envelope curves under cyclic loading and
monotonic curves: B-⊥
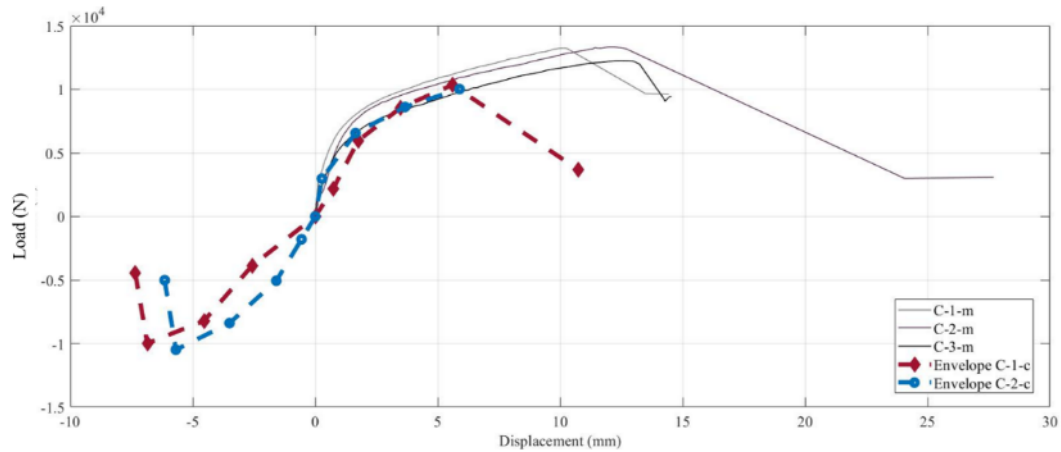
Figure 3.20 Comparison between envelope curves under cyclic loading and monotonic curves: C-//
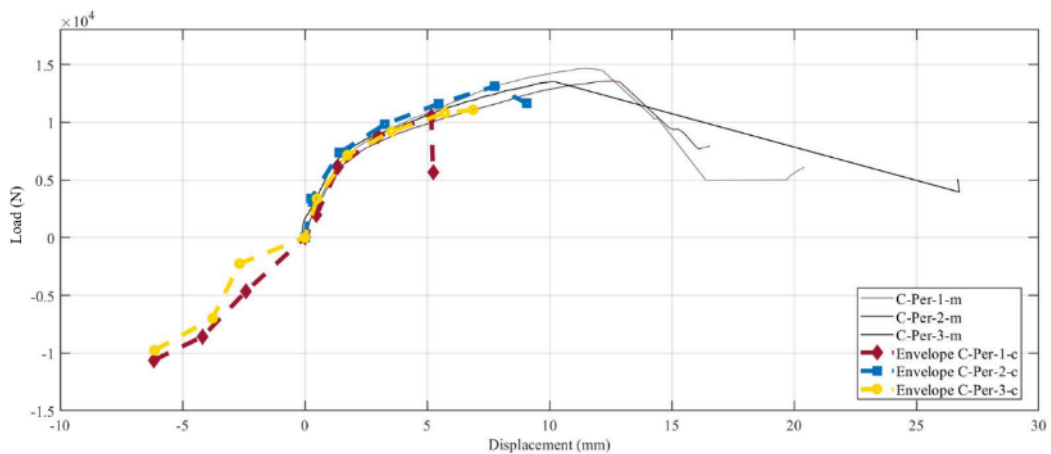
Figure 3.21 Comparison between envelope curves under cyclic loading and monotonic curves: C-⊥

It can be noted from Figures 3.12 to 3.21 that, except for specimens B and C, the peak load reached in the positive (tension) direction in general was higher than that in the negative direction (compression). This may be due to partial withdrawal occurring in the positive direction resulting in a weakened joint when the applied load was reversed in compression. Nevertheless, specimens B and C obtained comparable strengths in both positive and negative directions. This provides additional evidence that CLP with LSL as face layers tend to have higher withdrawal capacity, aligning with the fact that density

has a noticeable influence on withdrawal values. This is consistent with the finding that the withdrawal capacity of hybrid layups is largely influenced by the properties of the face layer (Mahdavifar et al., 2018).

Table 3.5. Summary of cyclic load test results

Specimen ID	K_e (kN/mm)	P_{yield} (kN)	Δ_{yield} (mm)	P_{peak} (kN)	Δ_u (mm)	E_d (kJ)	$\mu = \Delta_u /\Delta_{yield}$
A1-//-c	3.81	6.80	3.45	8.00	6.35	707.88	2.31
	(3.6 - 4.0)	(6.6 - 7.0)	(2.7 - 4.6)	(6.7 - 8.2)	(5.9 - 7.1)	(670.8 - 744.9)	(2.2 - 2.4)
A2-//-c	4.20	7.98	4.30	9.39	8.74	1048.66	2.08
	(3.8 - 4.4)	(7.6 - 8.5)	(3.4 - 5.0)	(9.0 - 10.3)	(8.3 - 9.0)	(852.2 - 1348.8)	(1.8 - 2.5)
B-//-c	4.11	8.63	3.98	10.22	7.44	1013.25	1.87
	(4.1 - 4.8)	(8.6 - 8.9)	(3.9 - 4.1)	(9.7 - 10.6)	(7.2 - 7.7)	(982.2 - 1030.6)	(1.8 - 1.9)
C-//-c	4.98	8.65	3.74	10.19	6.04	754.52	1.62
	(4.9 - 5.0)	(8.5 - 8.8)	(3.6 - 4.0)	(10.0 - 10.5)	(5.8 - 6.3)	(650.4 - 878.6)	(1.5 - 1.8)
CLT-//-c	3.57	6.25	3.54	7.36	10.44	910.00	2.42
	(2.7 - 4.6)	(5.4 - 6.9)	(3.0 - 4.0)	(6.3 - 8.1)	(9.2 - 11.5)	(724.6 - 1100.8)	(2.2 - 2.6)
A1-⊥-c	3.92	7.05	3.0	8.50	8.00	658.97	2.59
	(3.3 - 4.5)	(6.9 - 7.5)	(2.9 - 3.1)	(8.2 - 8.8)	(6.4 - 9.1)	(618.8 - 735.1)	(2.2 - 3.1)
A2-⊥-c	3.22	6.65	4.73	7.89	8.80	713.28	1.78
	(2.8 - 3.4)	(6.6 - 6.8)	(4.4 - 5.1)	(7.8 - 8.0)	(7.5 - 10.1)	(702.8 - 722.1)	(1.7 - 2.0)
B-⊥-c	4.56	8.99	3.83	10.58	6.88	762.28	1.67
	(3.9 - 6.1)	(7.8 - 9.6)	(3.3 - 4.3)	(9.1 - 11.4)	(6.2 - 7.9)	(714.3 - 822.2)	(1.6 - 1.8)
C-⊥-c	6.61	10.34	4.50	11.62	6.20	939.49	1.76
	(6.2 - 7.0)	(9.4 - 11.3)	(3.9 - 5.1)	(10.5 - 13.2)	(5.5 - 6.9)	(800.7 - 1120.9)	(1.7 - 1.8)
CLT-⊥-c	3.70	5.91	4.02	6.95	9.62	735.82	2.42
	(3.3 - 4.1)	(5.5 - 6.3)	(3.7 - 4.4)	(6.5 - 7.4)	(9.6 - 9.7)	(708.1 - 763.6)	(2.2 - 2.7)

Note: Values in brackets are range of the measured values.

The ultimate displacements under cyclic load are significantly smaller than those under monotonic load for the same specimen group. This phenomenon was also observed by Gavric et al. (2012) in wood-to-wood connections. Furthermore, specimen A2 and CLT

exhibit higher strengths under cyclic load than those under monotonic load. The cyclic test results are summarised in Table 3.5. The EEEP curve analysis was performed in the same manner as the monotonic test data. The strengths and yield loads of CLP and traditional CLT ranged from 6.95 kN to 10.22kN and 5.91kN to 8.65kN, respectively. The displacements at yield and failure ranged from 3.45 mm to 4.73 mm and 6.04 mm to 10.44 mm, respectively. Additionally, lower ductility was obtained in cyclic tests compared to monotonic test. This also indicated that the connection subjected to cyclic loads would be more brittle. This observation was also made in previous research on a novel CLT connection using STS with double inclination by Hossain et al. (2016). This could be due to low cyclic fatigue of the self-tapping screws under reversed cyclic load that could lead to premature fracture of the screws before a plastic hinge can be formed.

Figure 3.22 presents the typical failure of STS connection in CLP and CLT under cyclic loads. Evidence of fastener yielding can be observed. As shown in Figure 3.22, all the plastic hinges are formed in the face layer irrespective of layup combinations. A slight embedding of STS head was also observed. Moreover, the position of the plastic hinge always occurred at the intersection of the grip part and thread part of STS due to the stress concentration caused by the sudden change in the cross section.

(a) A1-//   (b) A2-//   (c) B-//

(d) B-⊥   (e) C-⊥   (f) CLT-//
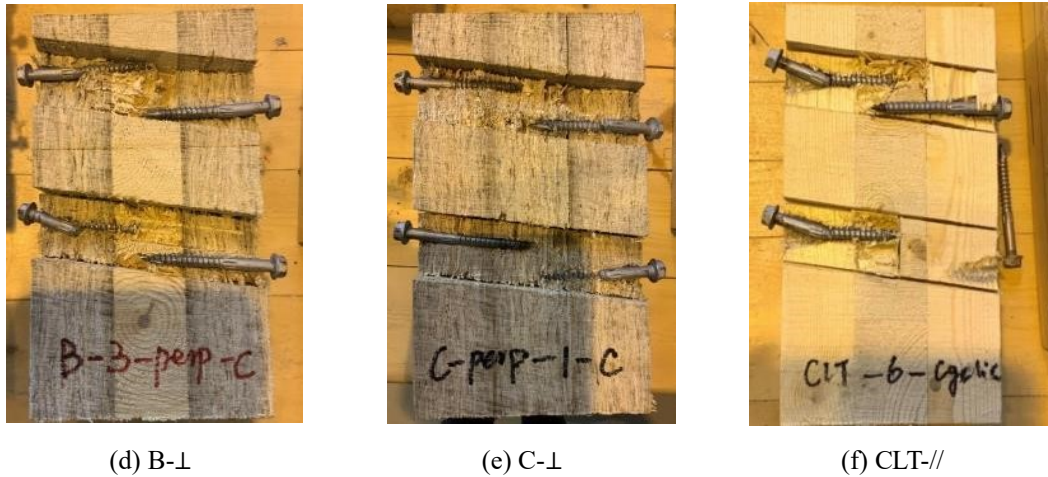
Figure 3.22 Typical failure modes under cyclic loads

Mahdavifar (2018) concluded that the core layer of hybrid CLT panels had no significant effect on yield modes or connection strength due to the plastic hinge not being located in the core layer. However, in this study although the formation of plastic hinges did not engage the core layer and only formed in the face layer with similar face-layer thicknesses, the difference in lateral strength and stiffness values between group A (high-density LSL substituting for lumber as a core layer) and CLT proved that the core layer still has an influence on the performance of fastener.

In comparison with the wood-to-wood connection tested by Gavric et al. (2015), the steel-to-wood CLP connections tested in this study were observed to be stiffer and have brittle failures (breakage of screws), even though the screws used had a smaller diameter.

Crushing of the wood member loaded in parallel and perpendicular to grain by STS is illustrated in Figure 3.23. Wood crushing was localised mainly in the vicinity of the screw head, approximately the size of the diameter of the screw when loaded in parallel to grain direction, whereas, the width of the damaged area was larger in the perpendicular direction.
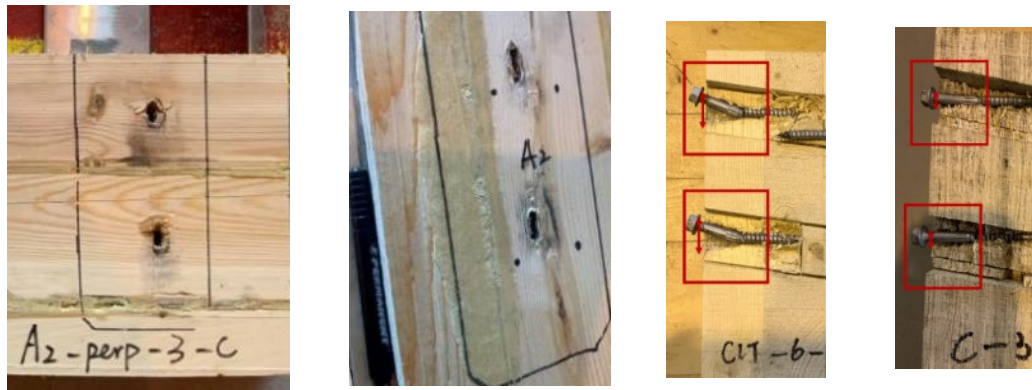
| (a) A2-⊥ | (b) A2-// | (c) CLT-// | (d) C-// |

Figure 3.23 Wood crushing

From Figure 3.23 (c) and (d), it can be observed that the considerable embedment of the STS head into the first layer of wood members, especially in the wood crushing area of lumber as the faces were larger than CLP with the LSL as the face layer. This observation matched well with the relative ductile behaviour of A1, A2, and traditional CLT specimens.

3.4 Analytical models

CLP consists of LSL and lumber resulting in variation in density profile over the thickness, which may cause STS to be embedded in layers of changing density. However, EYM in CSA O86 (2019) was developed based on the homogenous wood member. Therefore, it is necessary to investigate the fastener performance when embedded in a hybrid layup. In this study, the predicted lateral load resistance of individual STS was calculated using EYM equations given in CSA O86 (2019) and compared with the test results reported in this chapter.

One of the most important material properties that govern the lateral strength of timber connections is the embedment strength of the wood material. With regards to the embedment strength of CLP, currently, there is no guidance for designers to follow. As a first step in the evaluation of the applicability of CSA O86 EYM equations in CLP

connection, three embedment equations were evaluated. It is noteworthy to mention that the diameter of the screws in this case is relatively small, at 6.35 mm, and the embedment strength perpendicular to the grain may not differ from that which is parallel to the grain. As a result, embedment strength perpendicular to the grain was simply assumed to be equal to the values parallel to grain, which has been recommended by NDS (2018) and later adopted by Mahdavifar et al. (2018).

As stated above, three embedment strength equations were evaluated. The first one is the embedment strength, f_2, presented in CSA O86 (2019), as shown in Eq (3.2). Due to the cross section of CLT is not homogeneous, a modification factor $J_x = 0.9$ is recommended for the parallel direction in order to account for CLT features such as unglued edges and gaps:

$$f_2 = 50G(1 - 0.01d_F)J_x \tag{3.2}$$

where: G is specific gravity, d_F is the diameter of the fastener and J_x is the modification factor (0.9 for CLT and 1.0 in all other cases).

The second equation is the empirical embedment strength equation for threaded STS proposed by Khan et al. (2021) based on Bejtka model(2005), as described by Eq (3.3):

$$f_{h,\alpha} = \frac{0.436 \cdot \rho^{0.739} \cdot d^{-0.136}}{2.6 \cdot \cos^2\alpha + \sin^2\alpha} \tag{3.3}$$

where: ρ is the density in kg/m³, d is the diameter of the fastener in mm and α is the insertion angle.

The last equation was proposed by Khan et al. (2021), who found that there was minimal difference in capacity between threaded and non-threaded fasteners. The Khan equation is shown in Eq (3.4):

$$f_{h,\alpha} = \frac{0.206 \cdot \rho^{0.860} \cdot d^{-0.078}}{2.89 \cdot \cos^2\alpha + \sin^2\alpha} \tag{3.4}$$

The reason for selecting Eq (3.3) and Eq (3.4) was because they were both derived for threaded fasteners (Khan et al., 2021). Moreover, the three-layer LSL can be ideally treated as a homogenised panel, which was formed by three LSL single-layer panels in the same orientations with similar mechanical properties. In this thesis, the average density values of lumber and LSL were assigned to be 470 kg/m^3 and 661 kg/m^3 , respectively, based on a previous study (Zhou et al., 2018).

CSA O86 (2019) introduces EYM as a general basis to calculate the unit lateral resistance of fasteners, which consists of six equations for six failure mechanisms, as shown in Table 3.6 and in Chapter 2. Based on the material properties provided in Table 3.6 and the embedment strength provided by Eq (3.2), the unfactored unit lateral yielding resistance for conventional CLT was 4.78 kN/screw (mode f of the yield model) and 5.79 kN/screw (mode f) for three-layer LSL. Similarly, using embedment strength based on Eq (3.3) and Eq (3.4), the unfactored unit lateral yielding resistances were 6.20 kN/screw and 6.52 kN/screw (mode f of the yield model) for conventional CLT as well as 7.02 kN/screw and 7.51 kN/screw (mode f) for three-layer LSL, respectively. The detailed calculation procedures can be found in Appendix I.

Table 3.6 Properties of the connections

Parameter	Value
Diameter (d_F) [mm]	6.35
Length [mm]	63.5
Steel Thickness (t_1) [mm]	3
Effective Length (t_2) [mm]	53.5
Specific Gravity (Lumber)	0.42
Specific Gravity (LSL)	0.5
Density (lumber) [kg/m^3]	470
Density (LSL) [kg/m^3]	661
K_{sp}	3
$\emptyset_{steel}$	0.8
$\emptyset_{wood}$	0.8
f_u [N/mm^2]	537
f_y [N/mm^2]	1130.7
J_x(LSL)	1
J_x(CLT)	0.9
Insertion angle (α)	90°

The predicted lateral strengths of STS connection made of CLT and three-layer LSL (layup C) can represent the minimum and maximum of the entire testing group. Then, it can be deduced that the lateral strengths of the remaining groups made by CLP should lie between the maximum (three-layer LSL) and minimum (CLT).

Table 3.7 to Table 3.9 provide a comparison of lateral strengths acquired from experiments and analytical calculations, with the prediction based on CSA O86 yield equations and embedment strengths defined by Eq (3.2), (3.3), and (3.4), respectively.

Table 3.7 Comparison between predicted (Eq (3.2)) and experimental lateral strengths

Group	Test_m [kN]	Test_c [kN]	Prediction [kN]	Ratio_m	Ratio_c
CLT- //-m	7.00	7.36	4.78	1.46	1.54
CLT-⊥-m	6.53	6.95	4.78	1.37	1.45
C-//-m	12.95	10.19	5.79	2.24	1.76
C-⊥-m	13.92	11.62	5.79	2.40	2.01

Notes: "Test_m" represents the lateral strength of the individual screw under monotonic loading; "Test_c" represents the lateral strength of the individual screw under cyclic loading. "Ratio_m" is the ratio of "Test_m" over "Prediction'; and "Ratio_c" is the ratio of "Test_c" over "Prediction".

Table 3.8 Comparison between predicted (Eq (3.3)) and experimental lateral strengths

Group	Test_m [kN]	Test_c [kN]	Prediction [kN]	Ratio_m	Ratio_c
CLT- //-m	7.00	7.36	6.20	1.13	1.19
CLT-⊥-m	6.53	6.95	6.20	1.05	1.12
C-//-m	12.95	10.19	7.02	1.84	1.45
C-⊥-m	13.92	11.62	7.02	1.98	1.66

Notes: "Test_m" represents the lateral strength of the individual screw under monotonic loading; "Test_c" represents the lateral strength of the individual screw under cyclic loading. "Ratio_m" is the ratio of "Test_m" over "Prediction'; and "Ratio_c" is the ratio of "Test_c" over "Prediction".

Table 3.9 Comparison between predicted (Eq (3.4)) and experimental lateral strengths

Group	Test_m [kN]	Test_c [kN]	Prediction [kN]	Ratio_m	Ratio_c
CLT- //-m	7.00	7.36	6.52	1.07	1.13
CLT-⊥-m	6.53	6.95	6.52	1.00	1.07
C-//-m	12.95	10.19	7.52	1.72	1.36
C-⊥-m	13.92	11.62	7.52	1.85	1.55

Notes: "Test_m" represents the lateral strength of the individual screw under monotonic loading; "Test_c" represents the lateral strength of the individual screw under cyclic loading. "Ratio_m" is the ratio of "Test_m" over "Prediction'; and "Ratio_c" is the ratio of "Test_c" over "Prediction".

The lateral strengths of both LSL and CLT connections measured by tests were generally higher than those calculated by yield equations in CSA O86. The ratios for monotonic tests ranged from 1.37 to 2.40, 1.05 to 1.98, and 1.00 to 1.85 for Eq (3.2), as well as Eq (3.3) and Eq (3.4), respectively. Conversely, the ratios for cyclic tests varied from 1.45 to 2.01, 1.12 to 1.66, and 1.07 to 1.55 for Eq (3.2), Eq (3.3) and Eq (3.4), respectively. In general, Eq (3.4) provided the highest lateral resistances and closest predictions to test values among the three approaches of calculating embedment strength.

It can be observed that none of the methods provided accurate embedment strengths for calculating the lateral capacity of three-layer LSL with ratios of 1.72–2.40 under monotonic loads, and 1.36–2.01 under cyclic load. Analytical predictions became closer to the experimental results when Eq (3.4) was used to estimate embedment strength.

In general, the test results indicated that yield equations in CSA O86 are reasonably conservative. However, the yield equations always predicted mode f (yielding and bending of the screw at both the wood and steel members) to be the governing failure mode for both three-ply CLT and LSL. The predictions for failure mode can be considered as having a good agreement with the experiments. Since the steel side plate thickness was only 3 mm, it was difficult to form a plastic hinge in the steel plate and the failure of the screw in the steel plate was not obvious, whereas the failure that occurred in wood members matched well with the predicted yield mode. Moreover, the model did not take the variation of wood material properties (density) into account, thus it was reasonable to notice that there existed a discrepancy between predictions and test results.

Additionally, past studies (Khan et al., 2021) indicated that embedment properties were significantly influenced by insertion angles, in this study, all of specimens were ideally regarded as at a 90 degree insertion. However operating errors were unavoidable, which can also lead to variations.

The difference between measured and calculated lateral resistance using Eq (3.4) varied from 7% to 72% in the parallel direction and from 0.1% to 85% in the perpendicular direction under monotonic loads. However, the discrepancy between cyclic test results and predictions was relatively small, ranging from 13% to 36% in the parallel direction, and from 7% to 55% in the perpendicular direction due to the majority of cyclic tests having ultimate strength lower than the corresponding monotonic test strength. Furthermore, it is worth noting that the embedment strength of the LSL differs from sawn lumber (Hwang et al., 2002). Hence, it was necessary to explore and further develop embedment properties for LSL.

Lastly, a comparison was carried out between predictions using Eq (3.4) and test results for the different layups of CLP. In order to obtain a more accurate prediction for hybrid layups of CLP, a simplified approach was employed to address the changing densities over the thickness of CLP, using the mean density (ρ_m) for the layered panels with different densities, as presented in Eq (3.5) (EN 1995-1-1 2004):

$$\rho_m = \sqrt{\rho_{m,1}\rho_{m,2}} \qquad (3.5)$$

where ρ_m is the mean density, $\rho_{m,1}$ and $\rho_{m,2}$ are the respective densities of the two layer materials in CLP.

The mean density and corresponding embedment strength for the specimen groups are shown in Table 3.10. The calculated embedment strengths are comparable to those of a previous study (Murty et al., 2007), which discovered that the average embedment strength of small tube (6.4, 9.5, and 12.7mm outside diameters) connections for LSL is 50 MPa (COV = 8.2%) and spruce is 34 MPa (COV = 10.3%).

Table 3.10 Mean density and embedment strength of CLP

Layup	Mean density $[\frac{kg}{m^3}]$	Embedment strength [MPa]
A1	526.6	39.1
A2	526.6	39.1
B	590.0	43.1
C	661.0	47.5
CLT(D)	470.0	35.4
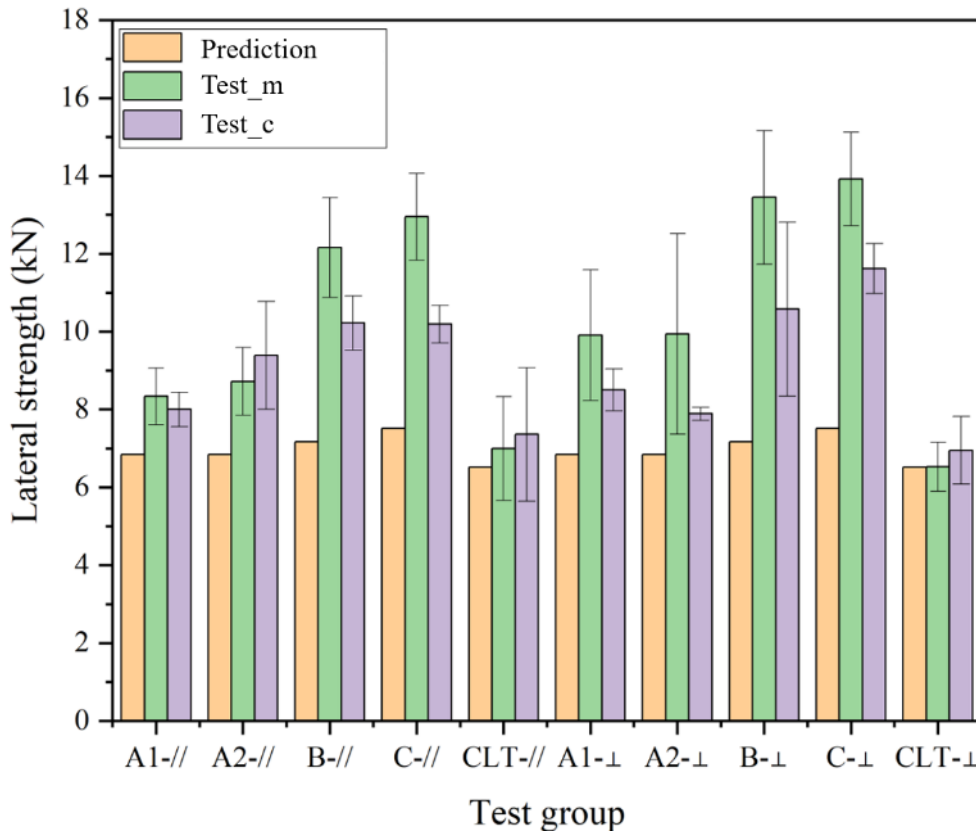
Figure 3.24 Comparison of lateral strength between measured and calculated per STS (error bar for standard error of measured values)

Figure 3.24 illustrates the difference between the predicted lateral resistance (using Eq (3.4)) and measured counterparts for CLP. The discrepancy between the experimental results and estimated lateral strength of connections ranged from 7.4% to 72.2% (A1:

21.9% lower; A2:27.5% lower; B: 69.6% lower; C: 72.2% lower; CLT: 7.4% lower) when STS placed parallel to the plane, and varied from 0.1% to 87.6% (A1: 44.8% lower; A2:45.3% lower; B: 87.6% lower; C: 85.1% lower; CLT: 0.1% lower) when STS placed perpendicular to the plane under monotonic loads. In general the predictions showed a better agreement with cyclic test results, ranging from 12.9% to 42.5% when STS was loaded parallel to face layer of the panel and from 6.6% to 54.5% when STS was loaded perpendicular to the faces of the panel.

There is no doubt that the predicted values of the CLT connections agree more closely with the test values among all the testing groups. For connection specimens A1 and A2, the calculated lateral strength and test strength had a good general correspondence. Furthermore, the calculated strengths for specimens B and C tended to be less precise and were conservative in nature.

3.5 Summary

Through the experimental investigation, the performance of STS connection in CLP under lateral loading was characterised. Different layer orientations and layups were included to assess the connection behaviour. It can be concluded that the diverse CLP layups resulted in significant differences in properties.

In this study, there was a noticeable influence of the density of the face layer on connection strength and stiffness. As surface layer density increases the lateral resistance and stiffness of the connection also increase. Generally, this type of STS (SDS25300) connection exhibited a low-ductility behaviour irrespective of monotonic or cyclic tests.

The experimental-analytical comparison was carried out to validate the applicability of yield models in CSA O86 (2019) for CLP connections. Three embedment equations were selected to estimate the embedment strength of CLP. Through comparison, it is noted that the embedment strength of STS in CLP was largely underestimated by Eq (3.3)(CSA O86 2019), especially for three-layer LSL panels. Eq (3.4) presented the closest

approximation. However, using the embedment strength calculated by Eq (3.4) it was found that the calculated lateral strengths of STS in CLP using the CSA O86 EYM were generally conservative. It is recommended that the actual embedment strengths of different CLP layups be measured by testing if CLP is to be accepted in structural applications.

Chapter 4 Performance of CLP shear walls

4.1 Introduction

In order to obtain a deeper understanding of the structural performance of shear walls built with multi-layer composite laminated panels (CLP), shear wall tests were carried out. In this study, four CLP layups were considered. For each CLP layup, one monotonic test and one reversed cyclic test were performed. One cyclic test was performed on CLT shear wall, which was used as a reference. The connections in the shear walls contained the same details as those tested in Chapter 3. In this chapter, a summary of test specimens and set-up is introduced, followed by test method and procedures. A summary of the test results is presented by giving the mechanical properties, namely, the lateral strength P_{peak}; yield strength P_{yield} ; stiffness K_e; ductility ratio μ; and dissipated energy E_d for all specimens. Finally, the predicted CLP shear wall capacity and deflection based on screw joint results in chapter 3 are compared with experimental results.

4.2 Test specimens

In terms of CLP shear wall experimental program, three-layer CLP panels were fabricated at InnoTech Alberta. The lumber material was SPF No. 2 or better grade lumber. In total, 21 panels with different layer arrangements were manufactured. These CLP panels were cut after the shear wall tests to provide the members for connection tests described in Chapter 3. Figure 4.1 illustrates the different layer orientations and detailed information of the CLP panels. The final dimensions of the panels were approximately 107 mm × 1232 mm × 2464 mm after pressing and trimming.
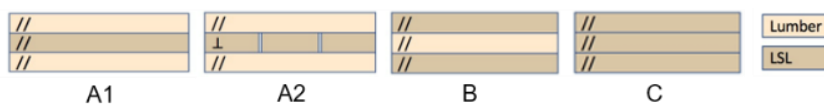
Figure 4.1 Illustration of CLP layups

Figure 4.2. depicts the connection types used in this shear wall test, including Simpson

Strong-Tie® steel brackets (Bracket AE116: 90 × 48 × 116 mm), hold-down (HDU8: 422.5 × 90 × 35 mm), and steel plate (HRS416Z: 406 × 82.5 × 3 mm). One fastener type was used in all connections (SDS screws: 6.35 × 63.5mm). Table 4.1 describes all of the wall configurations tested.

| (a) | (b) | (c) | (d) |
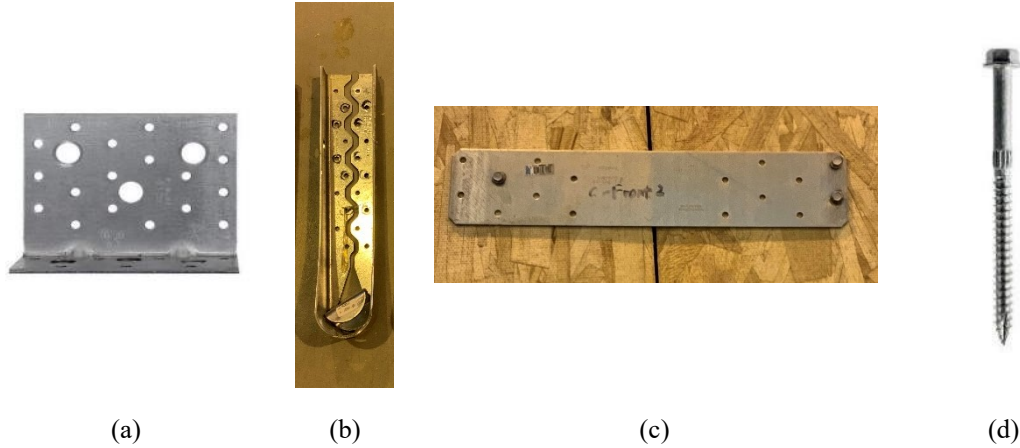
Figure 4.2 Connection hardware used in the fabrication of shear wall specimens: (a) angle bracket; (b) hold-down; (c) steel plate; and (d) SDS screw (courtesy of Simpson Strong-Tie®)

Table 4.1 CLP shear wall test matrix

Wall ID	No. of screws in brackets (each)	No. of screws in hold-down (each)	No. of vertical joints	No. of screws in each vertical joint	Target kinematic behaviour	Loading type
CLPA1-m	6	9	10	4	Single	Monotonic
CLPA1-c	6	9	10	4	Single	Cyclic
CLPA2-m	6	12	6	4	Coupled	Monotonic
CLPA2-c	6	12	6	4	Coupled	Cyclic
CLPB-m	6	9	6	3	Coupled	Monotonic
CLPB-c	6	9	6	3	Coupled	Cyclic
CLPC-m	6	9	6	4	Coupled	Monotonic
CLPC-c	6	6	6	6	Single	Cyclic
CLTD-c	6	9	6	3	Coupled	Cyclic

Note: The wall ID is corresponding to the panel layup. For instance, CLPA1 is layup A1 of CLP.

4.3 Test set-up

The CLP walls were anchored to a steel foundation with hold-downs and base shear connections. As the rollers had horizontal translational and rotational degrees of freedom, four 7 mm diameter rollers were placed at the bottom of the panel in order to ensure the movement of the panel was not restricted and also to prevent friction. A C-shaped channel was attached to the load cell and the actuator, transferring lateral load through the pin joints to the CLP shear walls. The C-shaped channel was connected to the top of the CLP panel by using two evenly spaced 25.4 mm (1″) bolts. It should be noted that lateral supports were used in all the tests to prevent the out-of-plane movement of the wall by using parallel rigid bars and wooden blocks between the guides and specimen. Figure 4.3 shows the full test set-up of the CLP shear wall tests.
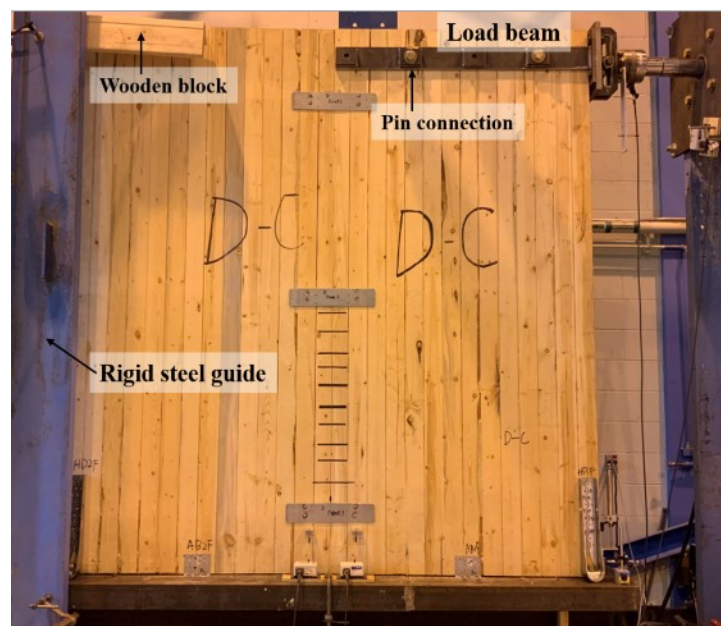
Figure 4.3 Shear wall test setup

After a wall specimen was fastened to the test frame, six linear variable differential transformers (LVDTs) were installed, which were then used to measure the various deformation components of the shear wall specimen (see Figure 4.4 and Table 4.2).
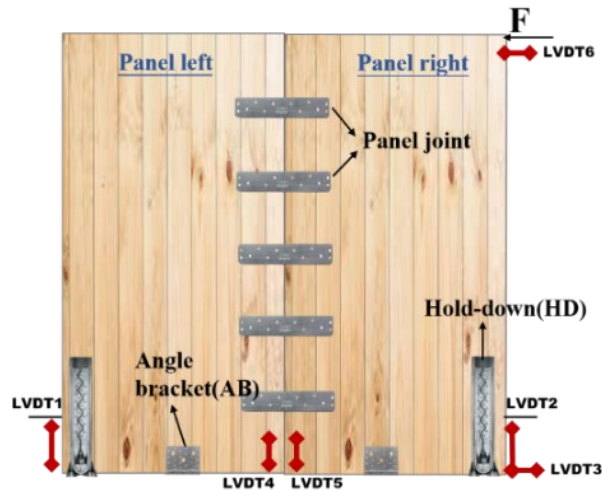
Figure 4.4 The shear wall sketch with measurement instrumentation

Table 4.2 Deformation component measured by LVDT

LVDT number	Measurement description
LVDT1	Bottom left corner uplift (negative)
LVDT2	Bottom right corner uplift (positive)
LVDT3	Sliding
LVDT4	Central panel uplift (positive)
LVDT5	Central panel uplift (negative)
LVDT6	Top horizontal displacement

The rocking of a shear wall was measured using LVDT1 and LVDT2, and a sliding deformation of the wall was recorded by LVDT3. Additionally, LVDT4 and LVDT5 were used to measure the vertical displacements of the centre line of the entire wall (the point of inter-panel connection of two panels) in order to verify the kinematic wall behaviours. LVDT6 was used to record the top horizontal displacement of the shear wall.

Each shear wall specimen was assembled with two 1.2 m wide by 2.4 m tall CLP or CLT panels of the same type side by side, resulting in an aspect ratio of 2:1 for coupled panel kinematic behaviour and 1:1 for single wall behaviour. In terms of Single-wall behaviour

(SW), a total number of ten steel plates with five on each side, were used to connect the two A1 panels together. The A1 wall panels were designed as a single-wall element with stiff and rigid panel-to-panel joints (see Figure 4.5 (a)). Conversely, A2, B, and C wall panels were all designed as Coupled-panel behaviour (CP), i.e., the two independent side-by-side panels had their own rotational centres. The panels were connected by three steel plates on each face (six in total) (see Figure 4.5 (b)). In this case, the panel-to-panel joints were designed to yield before the hold-down connections. Furthermore, the connection layout of each shear wall was designed to be symmetrical on the front and back faces.
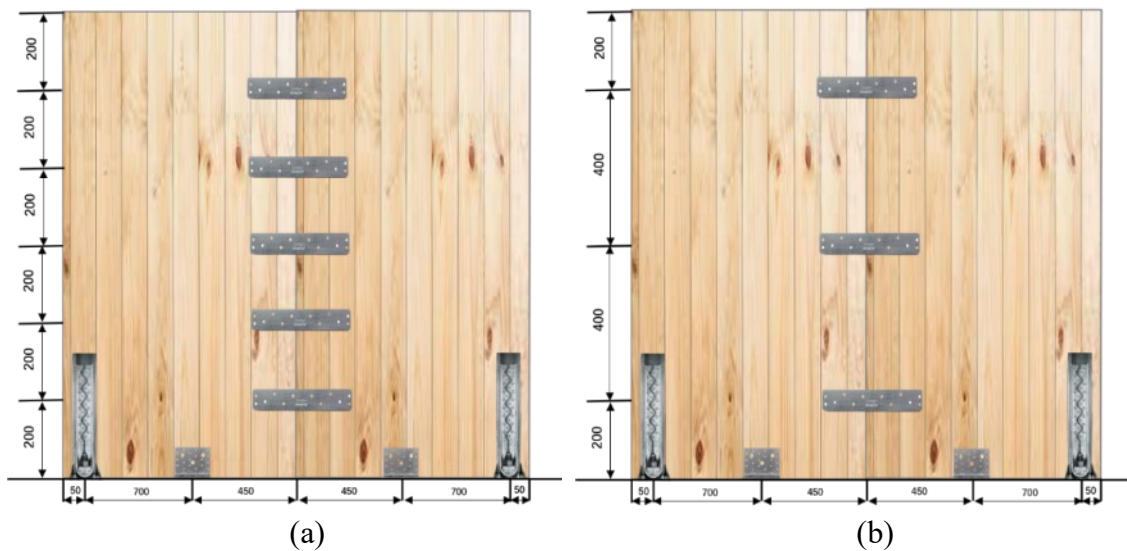
Figure 4.5 Shear wall layout: (a) Single wall behaviour (SW); (b) Coupled-panel behaviour (CP) (dimensions in mm)

It should be noted that wall CLPC did not fail under monotonic load as the test was stopped when the applied load reached the capacity of the test frame. As a result, the connections in the reversed cyclic load test of CLPC were modified by reducing the number of screws in the panel-to-panel and hold-down connections, so that failure could be achieved. In order to change CLPC from couple-panel to single-wall behaviour under cyclic loading, the number of screws in hold-down was reduced from 9 to 6 and 6 screws in each panel-to-panel connection to design the single-wall (SW) behaviour.

4.4 Test method and procedure

Monotonic and reversed cyclic displacement-controlled loading protocols were used in the test program. The specimens under monotonic loading were loaded at a rate of 0.2mm/s. The tests were stopped when the load dropped by more than 20% of the peak load. Monotonic load tests had to be carried out first before the cyclic tests since a reference displacement was required in the generation of reversed cyclic loading protocol. The reference displacement is defined by the post-peak displacement at 80% of the maximum load in the monotonic tests. The reversed cyclic loading protocol was based on ASTM E2126 (ASTM 2019) Method B, which employs a displacement-controlled loading procedure that consists of cycles grouped into phases of incrementally increasing displacement levels. The loading schedule consists of two displacement patterns in order to generate sufficient data in the elastic and inelastic analysis. The first displacement pattern consists of five reversed cycles with amplitudes of 1.25%, 2.5%, 5%, 7.5%, and 10% of the corresponding reference displacement of each type CLP. In the second part of the protocol, 20%, 40%, 60%, 80%, and 100% of the reference displacement is successively applied to the specimen and each amplitude phase consists of three full cycles (see Figure 4.6). Table 4.3 shows the loading cycles, loading rate and corresponding amplitudes applied for each of the two parts. The loading rate is required to be between 1 mm/s and 63.5 mm/s. However, since the hydraulic actuator in the laboratory cannot perform at such a fast-loading rate the loading rate was adjusted as tabulated in Table 4.3. All the tests were performed without applying any vertical load.
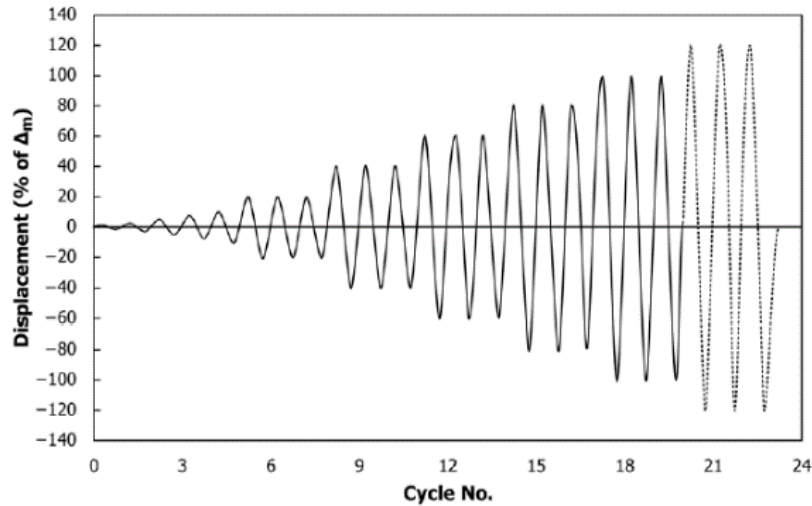
Figure 4.6 Displacement-controlled loading procedure of ASTM E2126 (ASTM 2019)

Table 4.3 Sequence of amplitudes for the reversed cyclic protocol

Pattern	Step	No. of cycles	Cycle no.	Amplitude (%)	Loading rate [mm/s]
	1	1	1	1.25	0.16
	2	1	2	2.5	0.16
	3	1	3	5	0.16
1	4	1	4	7.5	0.16
	5	1	5	10	0.16
	6	3	6–9	20	0.67
	7	3	10–12	40	0.67
	8	3	13–15	60	0.67
2	9	3	16–18	80	0.67
	10	3	19–21	100	0.67

4.5 Test results

4.5.1 Monotonic tests

The load-displacement curves of the test specimens under monotonic loading are shown in Figure 4.7. According to ASTM E2126 (ASTM 2019), equivalent energy elastic-plastic (EEEP) curves can be generated based on load-displacement curves of the monotonic tests, then the mechanical properties, namely, the lateral strength P_{peak}, yield strength P_{yield}, stiffness K_e, ductility ratio μ and dissipated energy E_d can be obtained.

67

The results are presented in Table 4.4.
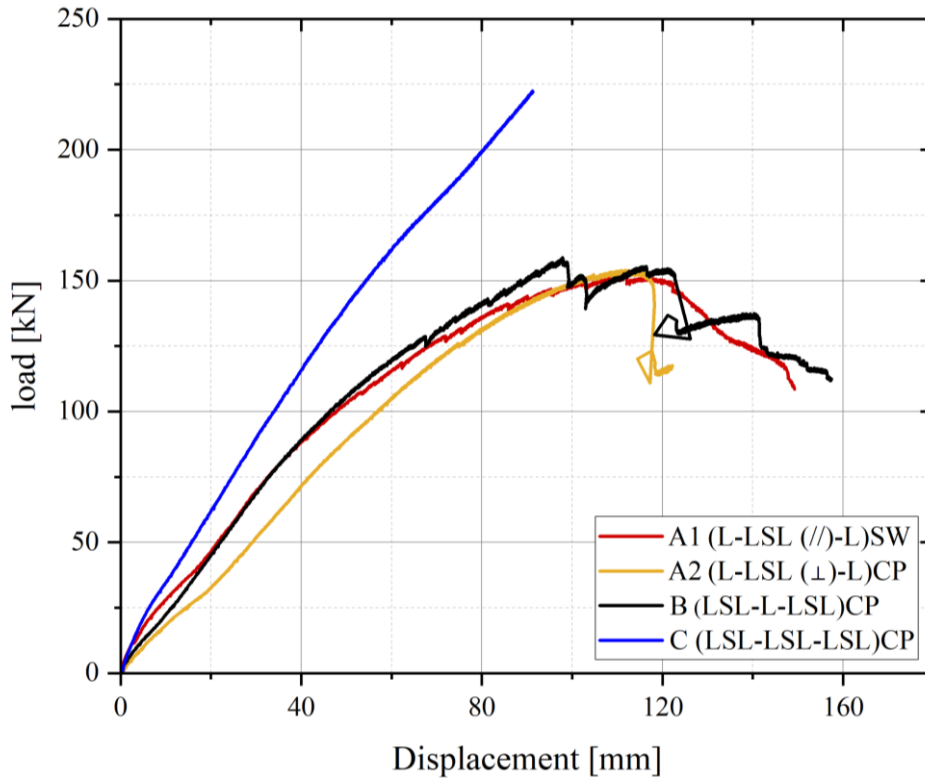
Figure 4.7 Load-displacement curves under monotonic loading (Note: Loading of wall CLPC was stopped at 222 kN before failure occurred.)

Table 4.4 Test results of CLP shear wall tests under monotonic loading

Wall ID	K_e	P_{yield}	Δ_{yield}	P_{peak}	Δ_{peak}	Δ_u	E_d	$\mu = \Delta_u / \Delta_{yield}$
	(kN/mm)	(kN)	(mm)	(kN)	(mm)	(mm)	(kJ)	
CLPA1-m	2.32	98.62	52.32	151.73	111.51	142.53	11.96	2.72
CLPA2-m	1.78	104.71	69.21	154.00	118.06	122.19	10.97	1.76
CLPB-m	2.39	80.28	57.25	158.89	91.1	157.77	12.12	2.75
CLPC-m	2.89	-	-	222.48*	95.59*	-	-	-

Due to the limitation of the frame capacity in the laboratory, the monotonic test of wall CLPC (three-layer LSL) stopped before the specimen failed, at about 95 mm displacement and a load of 222 kN. The average monotonic ductility ratio was 2.5, indicating low ductility according to Smith (2006). The ductility ratio found in these

monotonic tests is smaller than those presented in the literature (e.g. Gavric et al., 2015c) for CLT shear walls with nailed connections. These low shear wall ductility ratios are a direct result of the corresponding low ductile behaviour of the STS connections, as was discussed in Chapter 3.

It can be seen from Figure 4.7 that wall CLPC had the highest stiffness and would have considerably higher strength compared with the other three specimens even though fewer screws were used in the hold-down and panel joints. The superior performance was obviously due to the fact that wall CLPC is three layers of LSL which has a much higher density than SPF lumber. Wall CLPA1 and CLPA2 have the same layup; only the orientation of the core layer was different. However, CLPA1 (2.3 kN/mm) exhibited 30% higher stiffness in comparison with CLPA2 (1.78 kN/mm). Such a difference was mainly due to the presence of additional panel-to-panel joints which enhanced the lateral strength and initial stiffness of the overall wall performance of CLPA1, although the hold-down in wall CLPA2 was designed to be stronger and stiffer, indicating that the design of panel joints has a greater influence in a coupled-panel wall. Furthermore, based on the joint test results, the orientation of the core layer has a negligible influence on the overall wall performance.

Among the CLP walls that were designed to behave as the couple-panel behaviour (CLPA2-m, CLPB-m, CLPC-m), the initial stiffness of CLPB was 34% larger than that of CLPA2 and the ultimate displacement and ductility ratio of wall CLPB were 29% and 56% greater than those of CLPA2, even using fewer screws in the entire wall layout. This phenomenon was consistent with joint test results that specimen B is almost twice as stiff as specimens A1 and A2. A sudden drop of load of specimen A2 can be observed in Figure 4.7 after reaching the peak load due to the withdrawal of the screws in the hold-down followed by tear out of the base shear connections.

Besides, it is further verified that the performance of shear walls built by rigid panels is primarily dependent on the connection systems. This is demonstrated by the fact that

connection with layup B has less ductile behaviour compared with connection specimens with layup A1 and A2, but the ductility of shear wall CLPB-m is comparable or better than CLPA1-m and CLPA2-m.

The typical failure modes of CLP shear walls under monotonic loading are displayed in Figure 4.8 and summarised in Table 4.5. The evident failures of the connectors, are shown in Figure 4.8 (a) and (b). Brittle failures occurred at the base shear connections in the form of shear tear-out (when subjected to excessive tensile loads), as shown in Figure 4.8 (c), which may lead to the full potential of the strength of base shear connections not being reached. Furthermore, according to the failure shapes of the base shear connection and hold-down, bi-axial behaviours to resist both vertical (uplift) and horizontal (shear) loads can be confirmed. Over the past few years, a number of research studies have shown that angle brackets used as base shear connections are subjected to bi-directional loading (Liu, 2019; Masroor et al., 2020; D'Arenzo et al., 2021). Based on this study it can be observed that hold-down connections also can exhibit bi-directional behaviour, especially the unique shape of the hold-down used in this study.

(a) Screws withdrawal; deformation of hold-down.

(b) Deformation of the angle bracket.

(c) Shear out failure.

(d) Wood crushing.

(e) Wood splitting around base shear connections and panel edge tear out.

(f) Wood splitting around panel joint.

Figure 4.8 Typical failure modes under monotonic loading in shear wall connections

Table 4.5 Summary of failure modes under monotonic loading

Wall ID	Failure modes
CLPA1-m	Wood crushing at the right corner of hold down; wood splitting at the base shear connections, plastic deformation of the base shear connection, and the hold-down
CLPA2-m	Wood splitting around the base shear connections and panel edge tear-out
CLPB-m	Screws pull out, hold-down (right corner) deformed
CLPC-m	No failure mode observed

4.5.2 Cyclic tests

Table 4.6 summarises the test results of shear wall tests under cyclic loading in the two directions. In comparison with Table 4.4, it can be observed that all of the mechanical properties of CLP shear walls had a remarkable decrease, except the stiffness of CLPA2.

71

Table 4.6 Summary of test results of shear wall tests under cyclic loading

Wall ID	$K_e(+)$	$K_e(-)$	$P_{peak}(+)$	$P_{peak}(-)$	$\Delta_{ult}(+)$	$\Delta_{ult}(-)$
	(kN/mm)	(kN/mm)	(kN)	(kN)	(mm)	(mm)
CLPA1-c	1.81	1.90	129.18	126.17	99.59	100.1
CLPA2-c	1.78	1.73	121.77	70.92	79.85	79.53
CLPB-c	1.92	1.98	114.31	85.65	60.14	58.19
CLPC-c	2.38	2.26	149.33	116.32	80.03	80.01
CLT-c	1.49	1.65	100.66	53.77	79.97	77.53

The hysteresis loops obtained from cyclic tests are displayed in Figure 4.9 to Figure 4.13, along with envelope curves, and the monotonic curves. Additionally, to compare the envelope curve in both positive and negative directions, the envelope curve in the negative direction was turned 180 degrees around the origin, as shown in the following figures.

Figure 4.9 Comparison between hysteresis loops and monotonic curves of wall CLPA1

Figure 4.10 Comparison between hysteresis loops and monotonic curves of wall
CLPA2

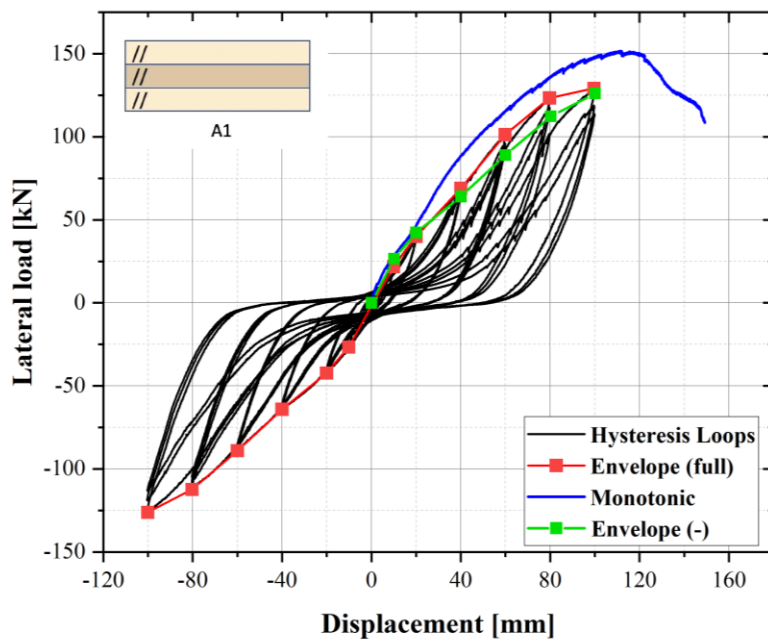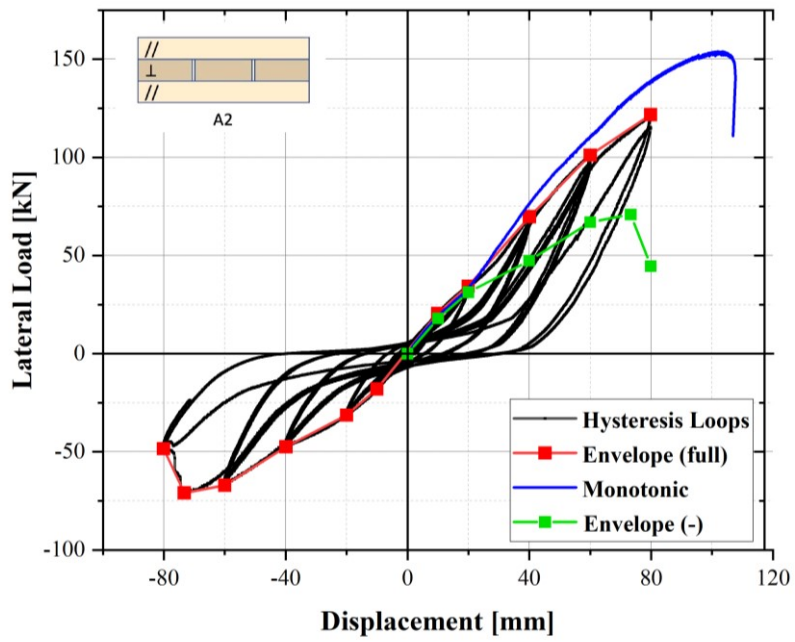Figure 4.11 Comparison between hysteresis loops and monotonic curves of wall
CLPB

Figure 4.12 Comparison between hysteresis loops and monotonic curves of wall
CLPC

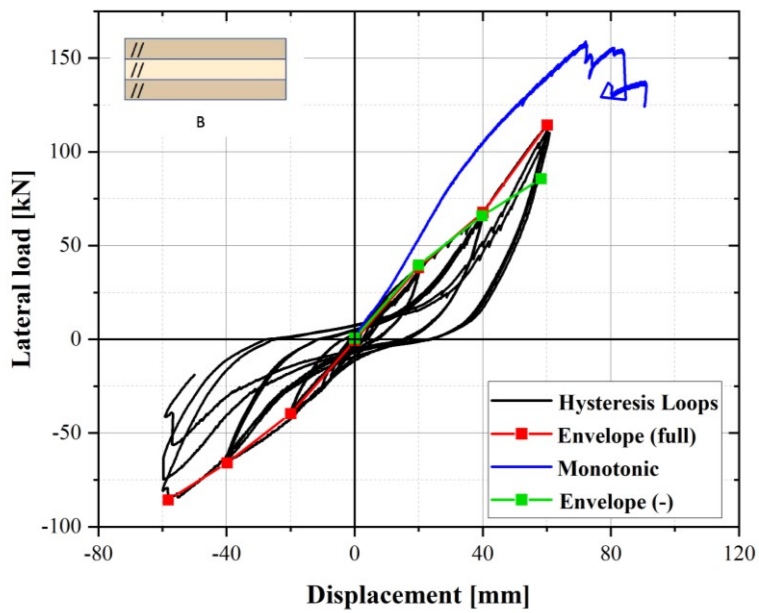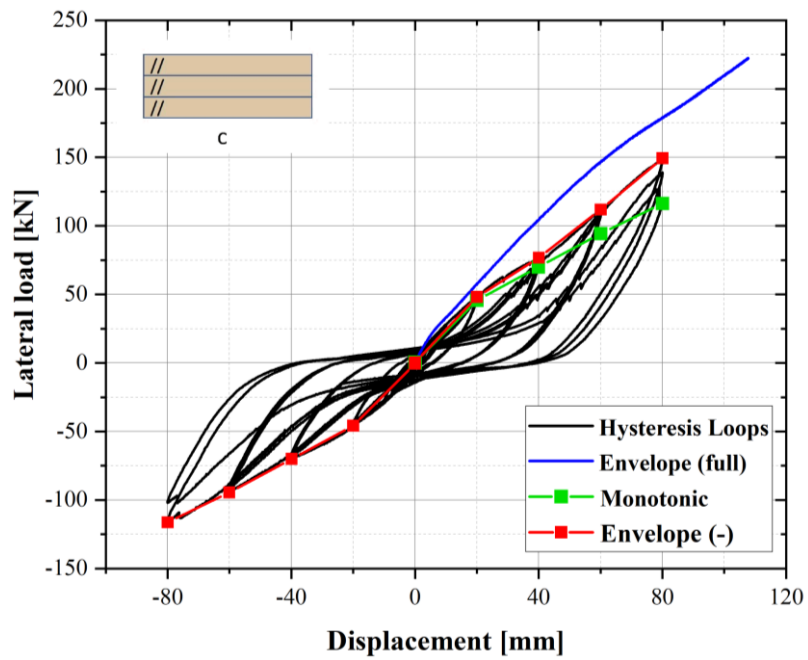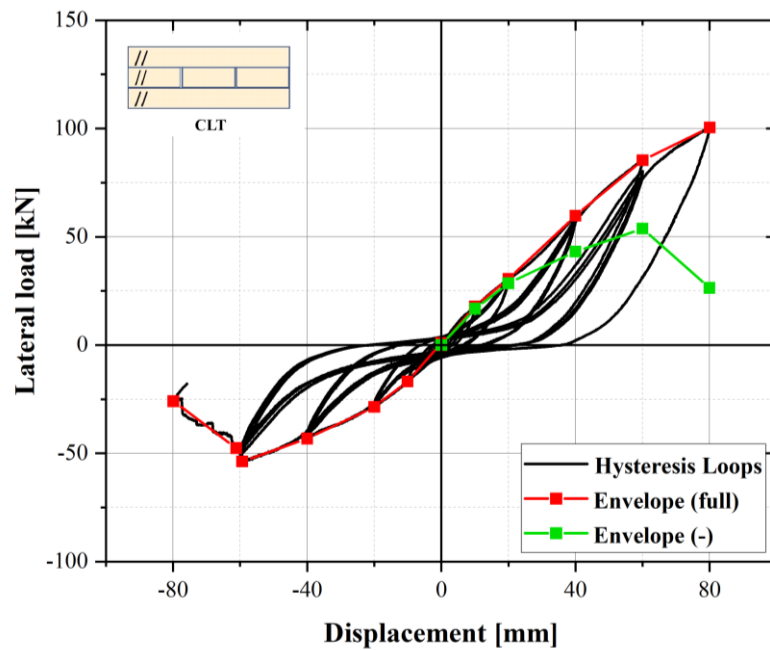

Figure 4.13 Hysteresis loops and envelope curves for traditional CLT

From the above load-displacement response figures, it is clear to see the differences
between the monotonic and reversed cyclic result. The peak loads from monotonic tests

were greater than the corresponding values for the cyclic tests, which was also observed by Popovski (2010). Peak loads from cyclic tests were reduced by 17.4%, 26.5%, 38.9%, and 48.9%, respectively, compared to corresponding monotonic values. Furthermore, the ultimate displacements obtained from monotonic tests were also greater than corresponding values obtained from cyclic tests, which was consistent with joint test results.

With regards to initial stiffness, there is a slight reduction (20%) when compared to monotonic test results. The most difference was for wall CLPC, with a 35% loss in stiffness under cyclic loads, which can be explained by different connection details between the monotonic and cyclic tests. In order to reach the failure limit state of wall CLPC under cyclic loading, the total number of screws in connection systems of the wall under cyclic tests was reduced. Furthermore, it can be observed from Figure 4.9 to Figure 4.13 that CLPA1, CLPA2, and CLT walls showed progressively decreased stiffness values before reaching ultimate load, whereas a slight increase can be observed for wall CLPB and CLPC at displacements of 40 mm to 60 mm. This phenomenon further proves that the utilisation of LSL in the face layer in place of lumber did make a difference.

In addition, all of the load-displacement responses displayed fairly symmetrical load-deflection responses. CLPA2 and CLT walls appear to show some asymmetric response characteristics. However, a closer examination of the load-deflection responses would indicate that these walls display apparent asymmetric load-deflection loops because they failed in one direction before they were able to reach the same displacement level in the opposite direction. Had these specimens been able to reach the same displacement level in the opposite direction, the load-deflection responses would appear more symmetrical, as can be observed in the other 3 walls. It should be noted that several previous studies (Popovski, 2010; Dires et al., 2022) also observed the unsymmetrical lateral force-deformation curves for cyclic tests, and low-cycle fatigue might be one of the reasons.

The dominant failure mode observed in the cyclic loading test was the screw yielding

followed by the withdrawal of screws, as shown in Figure 4.14 and Table 4.7.

a) Deformation of steel plates of panel joint connections

b) Wood splitting (Hold-down)

c) Kinematic wall behaviour (SW)

d) Kinematic wall behaviour (CP)

Figure 4.14 Typical failure modes of shear walls under cyclic loading

Unlike any other wall specimens, failure in CLPC-c wall occurred when the lateral load was applied in the positive direction (push). Withdrawal of screws occurred on the left wall. Compared to monotonic tests, more wood splitting was noticed on specimens with lumber as face layers in the hold-down.

Table 4.7 Summary of failure modes of shear walls under cyclic loading

Wall ID	Failure modes
CLPA1-c	Screws pull-out at the top panel joint and shear off at the right corner of the hold-down, wood splitting occurred around the outmost hold-down.
CLPA2-c	Screws pull-out at the top panel joint, wood crushing at the hold-downs, wood splitting at the hold-downs and base shear connections, panel edge tear out.
CLPB-c	Screws pull-out at the top panel joint.
CLPC-c	Screws pull-out at the top panel joint and right corner hold-down.
CLT-c	Screws pull-out at the top panel joint, wood splitting around all connectors (base shear connections, hold-downs, and steel plates).

As can be observed from Figure 4.15, although CLPA1 and CLPC walls were designed to behave as a monolithic wall, the negative values measured by LVDT5 proved that each wall segment rotated independently with its self-centering point. Furthermore, the negative measurement revealed there was a compression zone in the wall panels due to the bearing of the panels with the foundation. It is suggested that analytical models should take the lever arm coefficient (Casagrande et al., 2016) and effective width (Lukacs et al., 2019) into account to reach a closer prediction. A lever arm coefficient was used to account for the reduction in the length of the panel from the panel edge to the hold-down, while the effective width is the length of the panel in the "tensile zone", due to the centre of rotation not being located at the corner of the wall panel. Additionally, the bottom uplift displacement measured by LVDT2 and LVDT4 showed comparable load-displacement responses, with the exception of the wall CLPA1. This is of interest because theoretically the panel segment rotations should be different since the right panel uplift was primarily resisted by the hold-down whereas the left panel uplift was mainly resisted by base shear connections. The almost identical uplift displacements captured by the two bottom LVDTs help to verify the assumption that the deflections at the top of each wall segment are equal.

(a) CLPA1

(b) CLPA2

78
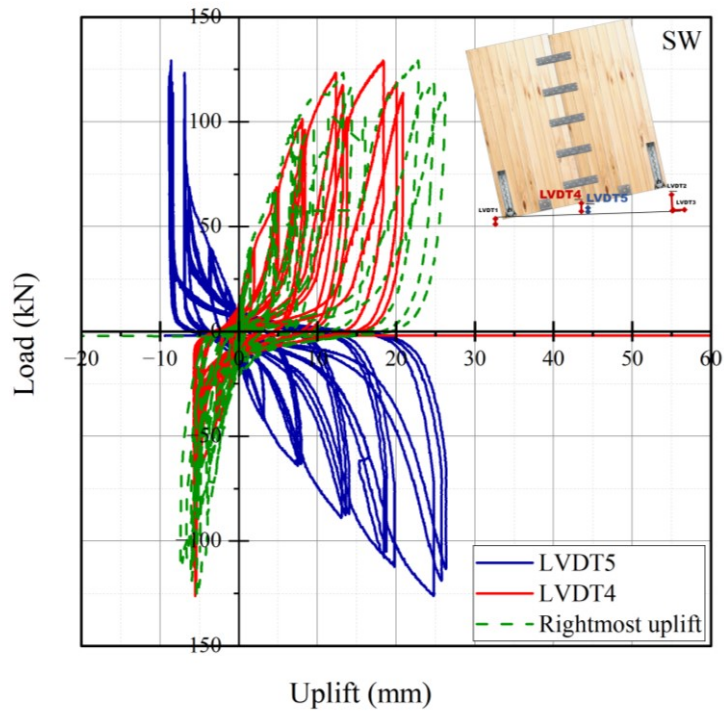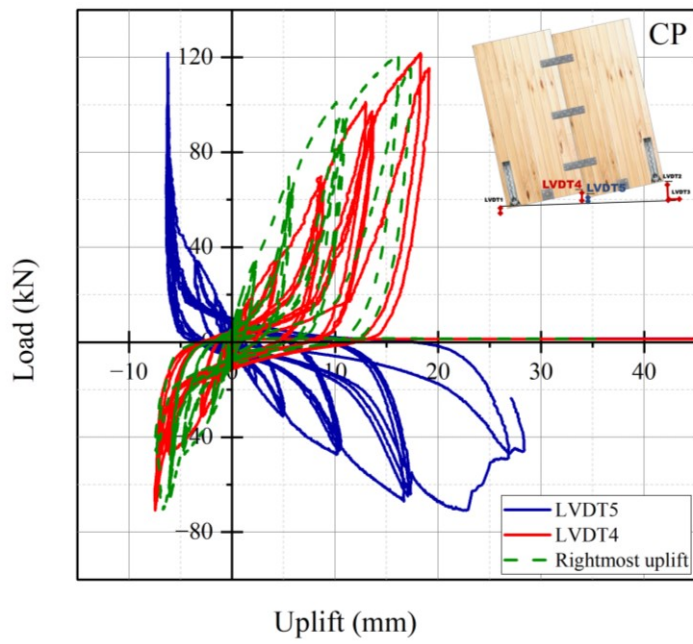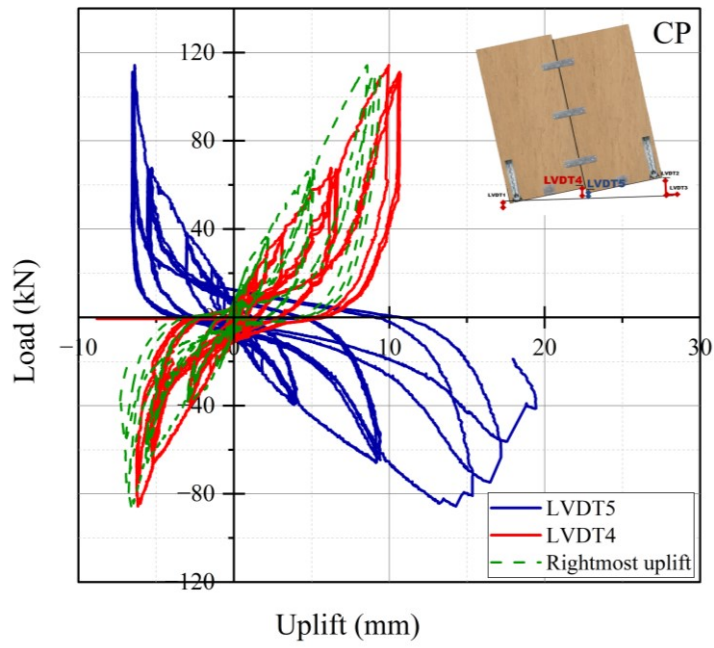
(c) CLPB
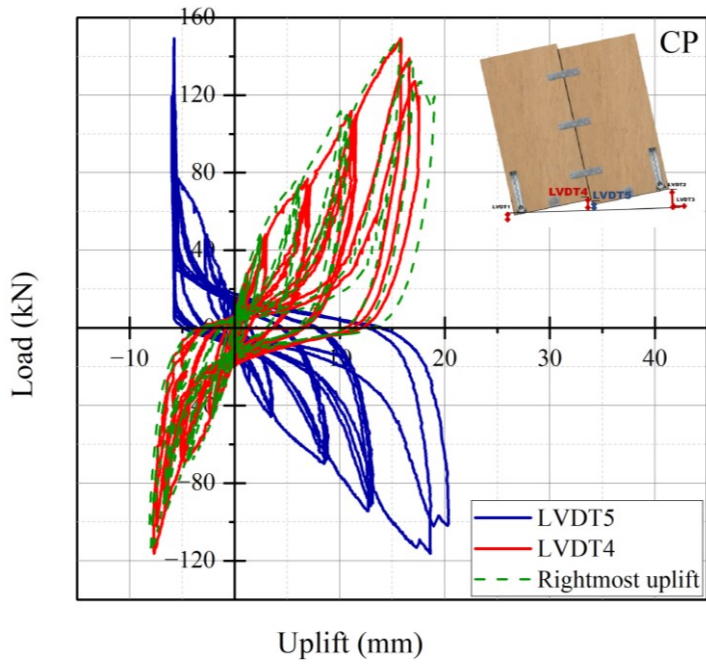
(d) CLPC
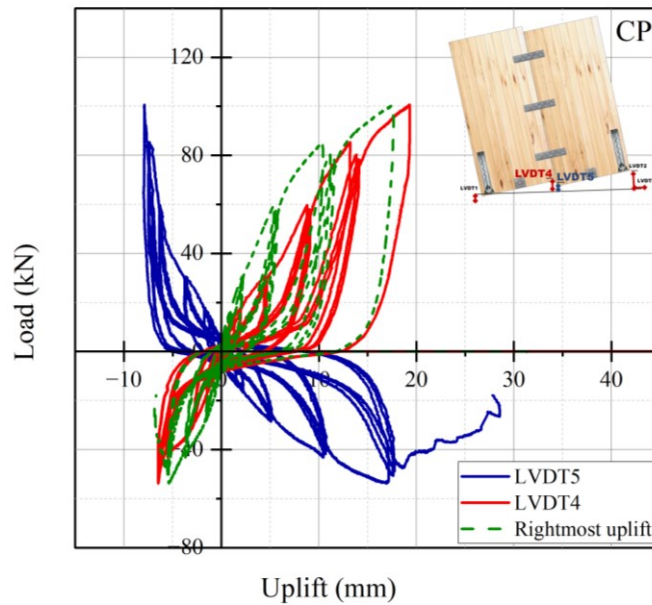
(e) CLT(D)

Figure 4.15 Uplift displacements of wall panels

4.6 Experimental-analytical comparison

4.6.1 Lateral resistance of CLP shear walls

In this section, the applicability of using current analytical models for CLT shear walls to CLP shear walls is evaluated. The lateral strengths of tested CLP shear walls were predicted using models developed by Shahnewaz et al. (2018) and CLP connection properties obtained in Chapter 3. The reasons for selecting this model are summarized below: (a) the analytical model provides equations for both SW and CP kinematic behaviours; (b) the model considers both the sliding and rocking contribution of the base shear connection with shear-uplift interaction; (c) it is practical to use this closed-form model to predict the lateral strength of shear walls without iterative procedures. Shahnewaz et al. (2018) proposed analytical models to estimate the in-plane lateral resistance of CLT shear walls subjected to three types of kinematic wall behaviours, namely sliding only, rocking only and combined sliding-rocking. Since the combined sliding-rocking behaviour was observed to be more reflective of the behaviour observed in shear walls tested in this study (Shahnewaz et al., 2019), only the model for combined

80

sliding-rocking was used in this thesis, as shown in Eq (4.1). The resistances of the shear wall due to overturning forces are calculated based on the moment equilibrium about the right corner of the wall and the unknown reaction force, R_1, can be determined by the vertical force equilibrium for the left panel. The lateral strength of the shear wall is reached when the yield strength of the hold-down in the left panel was reached. Figure 4.16 illustrates the distribution of reaction forces in the connections of a coupled wall based on the analytical model.
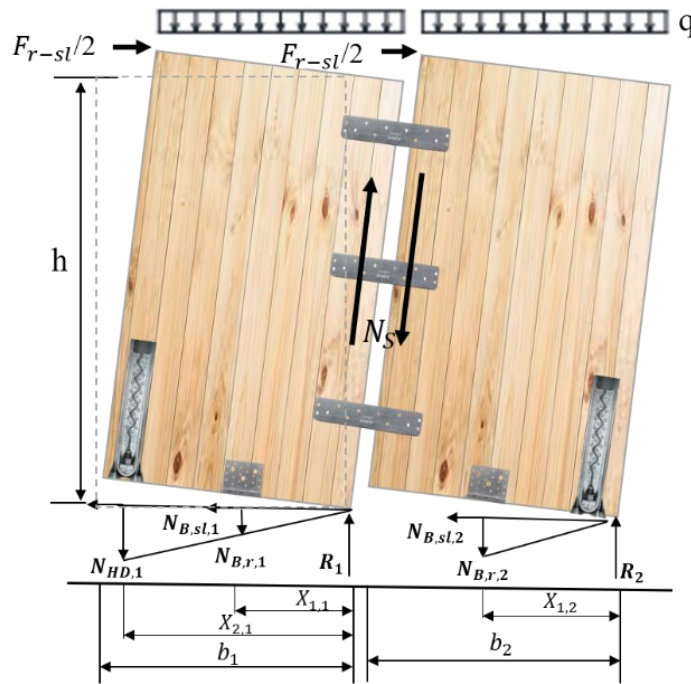
Figure 4.16 Force diagram of a coupled shear wall

$$F_{r-sl} = \frac{1}{h}\left[N_{HD}x_1 + \frac{N_{B,r}}{b_1}\left(\sum_{i=1}^{n_{B,1}} x_i{}^2\right) + \frac{N_{B,r}}{b_2}\left(\sum_{i=1}^{n_{B,2}} x_i{}^2\right) + q\frac{b^2}{2} - qb_1b_2 \right.$$
$$\left. + N_S b_2 \right]$$

(4.1)

where: F_{r-sl} = lateral resistance (kN); N_{HD} = resistance of hold-down (kN); $N_{B,sl}$ = sliding resistance of base shear connection (kN); $N_{B,r}$ = rocking resistance of base shear connection; N_S = resistance of panel joint (kN); X_i = distance from connection to edge

(rotation centre) (m); $n_{B,i}$ = number of brackets in panel i, h = height of the CLT panel (m); b_i = width of the panel segment (m); b = width of the entire wall (m); q = vertical load (kN/m).

In this study, the strength of the each connection was assumed to be equal to the sum of the strengths of the individual screws in the connection. Specifically, N_{HD} and $N_{B,r}$ were estimated by the sum of the total screw strength loaded parallel to grain, whereas N_S was estimated by the sum of total screw strength loaded perpendicular to grain.

The predicted lateral shear wall strengths using Eq (4.1) and the measured values are shown in Table 4.8. The experimental/predict strength ratios reveal that this model generally overestimates the shear wall capacity even considering the combined rocking-sliding behaviour.

Table 4.8 Comparison between analytical and experimental values of resistance of tested shear walls

Wall ID	$F_{r-sl,exp}$[kN]		$F_{r-sl,p}$[kN]		$Ratio = \dfrac{F_{r-sl,exp}}{F_{r-sl,p}}$	
	Monotonic (F_{ult,exp_m})	Cyclic (F_{ult,exp_c})	Monotonic (F_{p_m})	Cyclic (F_{p_c})	Monotonic (R_m)	Cyclic (R_c)
CLPA1	151.73	129.18	229.88	203.15	0.66	0.64
CLPA2	154.00	121.77	192.00	171.57	0.80	0.71
CLPB	158.89	114.31	201.30	155.37	0.79	0.74
CLPC	222.48*	149.33	232.27	204.84	--	0.73
CLT	-	100.66	-	107.09	-	0.94

Note: * testing of wall CLPC was stopped before failure occurred. $F_{r-sl,exp}$ denotes the experimental strength; $F_{r-sl,p}$ denotes the predicted strength.

The differences between analytical and exprimental strength values for monotonic tests

of CLPA1, CLPA2, and CLPB are about 34%, 20%, and 21%, respectively. It is should be noted that the ultimate strength of wall CLPC under monotonic loading should be higher due to the limitation of the testing frame capacity, so there is no comparison for that wall under monotonic loading. Also, the differences between analytical and exprimental strength values for cyclic tests of CLPA1, CLPA2, CLPB and CLPC are about 36%, 29%, 26%, and 27%, respectively. Only the CLT shear wall exhibits a closer approximation (6% overestimation), which shows the validity of the proposed model for predicting the lateral resistance of shear wall built with traditional CLT panels.

The general overestimation of strength by the Shahnewaz model may be explained by the fact that the connection failure modes in shear wall were more brittle than those observed in the connection tests. These include premature wood splitting in the hold-down connection and the low cyclic fatigue of the screws in the shear wall cyclic tests. Besides, it is known that the inherent lateral resistance of the connection should be greater than the sum of fastener resistances. However, the shear-out failure of base shear connections observed, as shown in Figure 4.8 (c), suggests that the base shear connection yielded before the yielding of screws. This shear-out failure was not observed in the connection test. Another reason could be due to the group effect of connection design strength. The predicted strength of shear walls may be overestimated based on the sum of individual STS resistance without taking group effect into account. Furthermore, the coupled effect of shear and uplift resistance of base shear connections may also lead to weakened shear resistance. This is because the connection may have been severely damaged by the tension loads regardless of monotonic loads or cyclic loads (Liu et al., 2019).

It is suggested that analytical models that ignore the vertical contribution of base shear connections are not recommended, even the coupled effect may weaken the strength in the primary direction of the connector (i.e., uplift resistance of hold-downs and shear resistance of base shear connections).

4.6.2 Deflections of CLP shear walls

A common design approach for CLT shear walls is to assume that the horizontal stiffness of the base connections governs the sliding mechanism, whereas the vertical stiffness of anchoring systems (hold-down) as well as the geometry of the wall panels govern the rocking mechanism. Additionally, the aspect ratio is a significant factor to influence the wall kinematic behaviour. Generally, when the shear wall has a high width-to-height ratio, the dominant behaviour will be sliding, whereas rocking will be dominant if the shear wall has a large height-to-width ratio.

In order to better understand the in-plane deformability of the entire CLP shear wall, predominant deformability components that contribute to the total wall deflection were analysed. Based on previous evaluations of CLT shear wall tests, it was found that rocking δ_r, sliding δ_{sl} and in-plane panel deformation (shear δ_s and bending δ_b) were the components that contribute to the total lateral displacement, as illustrated in Figure 4.17. The same principle could be also applied to CLP shear walls. Therefore, the total displacement of the shear wall can be expressed by Eq (4.2) (Gavric et al., (2015c)):

$$\delta_{total} = \delta_b + \delta_s + \delta_{sl} + \delta_r \tag{4.2}$$

| | | | |
| (a) | (b) | (c) | (d) |
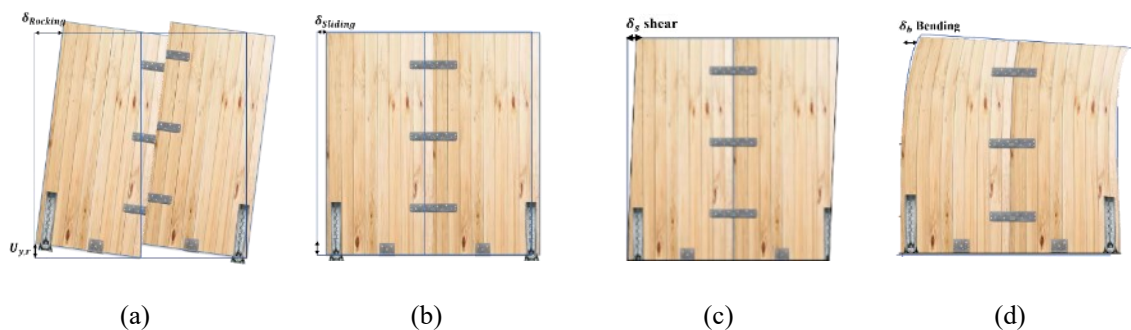
Figure 4.17 Deflection components: (a) rocking; (b) sliding; (c) shear; (d) bending

For the cases of coupled-panel behaviour, the total deflection can be calculated as the sum of the deflection of each wall segment, since each panel rocks independently, and

as mentioned before, although wall CLPA1 was designed to behave as a single wall, the bottom negative uplift displacements measured by the LVDTs between adjacent panels indicated that the panel segments still rocked independently.

The analytical equations of the deflection components are presented in Eq (4.3) to Eq (4.9). Firstly, due to the high in-plane stiffness, the mass timber panel generally behaves elastically, the bending deformation of the panel can be calculated by Eq (4.3):

$$\delta_b = \frac{Fh^3}{3EI_{eff}} \tag{4.3}$$

where EI_{eff} is the effective bending stiffness [N· mm^2] of the panels.

It is noted to mention that since currently there are no standards or methods for determining the in-plane shear properties of full-size CLP panels, k method (composite theory) provided by Blass et al. (2014) was applied to CLP with some adjustments to estimate the effective bending stiffness (EI_{eff}) of CLP, as described in Eq (4.4), Eq (4.5), and Eq (4.6). The detailed calculation procedure can be found in Appendix II.

$$k_4 = \frac{E_{90}}{E_0} + \left(1 - \frac{E_{90}}{E_0}\right) \times \frac{a_{m-2} - a_{m-4} + \cdots\cdots \pm a_1}{a_m} \tag{4.4}$$

where E_0 is the modulus of elasticity (MOE) parallel to the grain and E_{90} is the modulus of elasticity (MOE) perpendicular to the grain of the laminate. a_m is the total thickness of the panel [mm].

$$E_{I,eff,(A)} = E_{0,lumber}I * k_4 \tag{4.5}$$

$$E_{I,eff(B)} = E_{0,LSL}I * k_4 \tag{4.6}$$

where $I = t \times \frac{b^3}{12}$ moment of inertia [mm^4], t is the thickness of each layer [mm], b is the width of the panel [mm], $E_{I,eff,(A)}$ is the effective bending stiffness of layup A1 and

A2, $E_{I,eff,(B)}$ is the effective bending stiffness of layup B.

The shear deflection, δ_s, can be expressed by Eq (4.7):

$$\delta_s = \frac{1.2Fh}{(GA)_{eff}} = \frac{1.2Fh}{G_0 A_{eff}} \tag{4.7}$$

For CLP cases, the effective shear stiffness [N] was adjusted and calculated based on the assumption that only the parallel layers contribute to resisting the shear deformation, as described in Eq (4.8).

$$\delta_s = \frac{1.2Fh}{G_{0,LSL} A_{eff,LSL} + G_{0,lumber} A_{eff,lumber}} \tag{4.8}$$

where: shear modulus of lumber and LSL, $G_{0,lumber}$ and $G_{0,LSL}$ was assumed as 656 MPa and 462 MPa, respectively, based on a previous study (Zhou et al., 2018). A_{eff} is the effective cross-section of the panel accounting for the parallel layers only [mm^2].

The resistance to sliding was assumed to be provided by the base shear connections only, because the horizontal shear stiffness of the hold-down is relatively small compared with its uplift stiffness. Therefore, the sliding deflection, δ_{sl}, can be estimated with:

$$\delta_{sl} = \frac{F}{n_B k_B} \tag{4.9}$$

where n_B = number of base shear connections; k_B = stiffness of base shear connections.

The rocking contribution accounts for the majority of the lateral wall deflection. According to the analytical model by Shahnewaz et al. (2020), the rocking displacement on the top of the panel, δ_r, can be expressed as:

$$\delta_r = \left(\frac{Fh^2}{b_1^2} - \frac{qh}{2}\right) \times \frac{1}{k'_{HD}} \tag{4.10}$$

where k'_{HD} is the modified stiffness that considers both the hold-down and panel joint stiffnesses as presented in Eq (4.11):

$$k'_{HD} = k_{HD} + k_s \qquad (4.11)$$

where k_s is the stiffness of panel joints.

Due to rocking and sliding being the two main deformability components, experimental and analytical results are compared and presented in Table 4.9. The experimental horizontal deflection component of a panel due to the rocking motion was calculated by multiplying the measured uplift displacement (vertical) at the corresponding yield strength by the height-to-width ratio of the panel. The analytical results of sliding and rocking components were calculated based on Eq (4.9) and Eq (4.10), respectively.

Table 4.9 Comparison of predicted rocking and sliding deflections of shear walls under monotonic loading

Wall ID	Rocking δ_r [mm]		$\delta_{r,exp}/\delta_{r,eq}$	Sliding δ_{sl} [mm]		$\delta_{sl,exp}/\delta_{sl,eq}$	Load [kN]
	$\delta_{r,exp}$	$\delta_{r,eq}$		$\delta_{sl,exp}$	$\delta_{sl,eq}$		
CLPA1-m	17.4	12.8	1.4	2.3	1.6	1.4	95.3
CLPA2-m	28.2	9.1	3.1	3.6	2.6	1.4	105.9
CLPB-m	10.6	5.2	2.0	0.9	1.4	0.7	85.2
CLPC-m	22.5	7.1	3.2	2.3	2.5	0.9	155.2

Note: $\delta_{r,exp}$ means experimental rocking deflection; $\delta_{r,eq}$ means calculated rocking deflection; $\delta_{sl,exp}$ denotes experimental sliding deflection; $\delta_{sl,eq}$ denotes calculated rocking deflection; Load represents the load corresponding to these deflections.

It is obvious from Table 4.9 that the deflection due to rocking cannot be effectively predicted using the analytical model, especially the rocking deformation was largely underestimated. Wall CLPA1 was the only exception with a closer approximation on rocking behaviour, which can be explained by the design of the 'Single wall' connection layout. The underestimation of the rocking component can be explained by the following

two points: (1) Overestimation of stiffnesses of the connection by simply multiplying the stiffness value of an individual screw by the number of screws used in the connector; (2) Stiffness and capacity of hold-downs to resist uplift may decrease when subjected to the increasing lateral (horizontal) displacement. However, the difference between experimental and analytical sliding component varied from -30% to 40%. The reason for overestimation can be explained by the fact that the horizontal contribution of the hold-down was ignored, while the underestimation may be primarily caused by coupled effects weakening the shear resistance of the base connection.

The linear load-displacement responses based on elastic models are compared with test results, as presented in Figure 4.18.
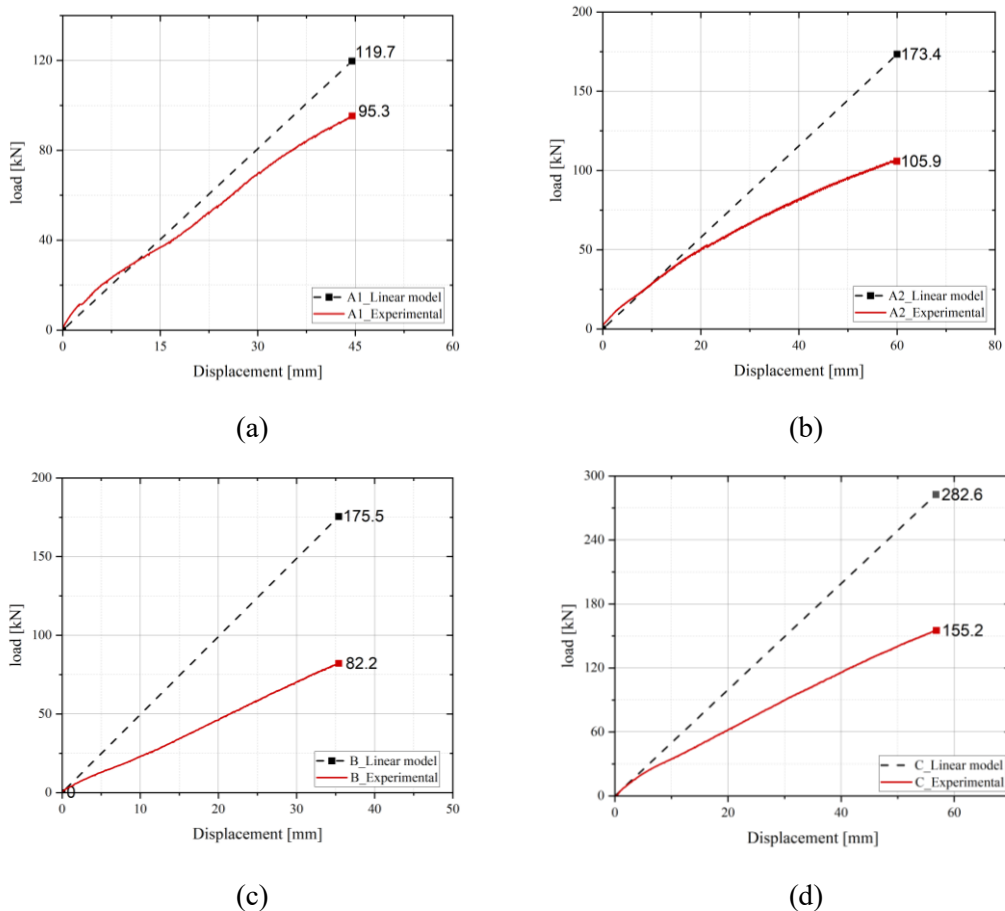

(a)

(b)

(c)

(d)

Figure 4.18 Comparison of monotonic test results with calculated load-displacement curves (elastic)

As can be seen from Figure 4.18, the deflection model cannot accurately predict the elastic behaviour for CLP shear walls, with the possible exception of wall CLPA1, since the predicted response is generally significantly stiffer than the test results. The main reason might be explained by the overestimated stiffness of the hold-down employed in the linear model, which highly limits the contribution of rocking.

Generally, a better agreement between predicted and measured responses for wall CLPA1 was observed, the reason might be that wall CLPA1 was designed as a single wall with relatively stiff inter-panel joints, which may indicate that the contribution of the hold-down in 'single-wall' kinematic motion might be less significant, whereas the inter-panel joints may contribute more to the overall wall behaviour. A few researchers (Tomasi and Smith, 2015b; Pozza et al., 2018) have noted that the stiffness and capacity of hold-downs and angle brackets are generally overestimated, whereas the panel-to-panel connection can be more reliable measured or predicted. This is a common issue with connections in CLT shear walls and it is necessary to further explore the relationship between the strengths of these connections and the sum of the strengths of single fasteners.

Due to the lack of distinct yield points in the cyclic tests, the experimental results were analysed by taking the average values of envelop curves in the positive and negative directions at the displacement corresponding to 85% of the ultimate load. The analytical-experimental comparison is presented in Table 4.10. Note that the analytical model is based on monotonic loading but the input connection strengths were derived from connection tests under cyclic loading.

Table 4.10 Comparison of predicted rocking and sliding deflections under cyclic loading

Group	Rocking δ_r [mm]		$\delta_{r,exp}/\delta_{r,eq}$	Sliding δ_{sl} [mm]		$\delta_{sl,exp}/\delta_{sl,eq}$	Load [kN]
	$\delta_{r,exp}$	$\delta_{r,eq}$		$\delta_{sl,exp}$	$\delta_{sl,eq}$		
CLPA1-c	16.3	12.9	1.3	4.3	3.6	1.2	109.8
CLPA2-c	22.6	9.2	2.5	4.9	4.5	1.1	103.5
CLPB-c	16.3	9.6	1.7	2.7	2.9	0.9	97.2
CLPC-c	25.2	11.4	2.2	3.5	2.2	1.6	126.9
CLTD-c	20.2	10.7	1.9	3.8	3.2	1.2	85.6

Note: $\delta_{r,exp}$ means experimental rocking deflection; $\delta_{r,eq}$ means calculated rocking deflection; $\delta_{sl,exp}$ denotes experimental sliding deflection; $\delta_{sl,eq}$ denotes calculated rocking deflection; Load represents the load corresponding to these deflections.

The differences between analytical predictions and cyclic experimental results are still large but smaller than the differences under monotonic results, especially for the sliding component. The elastic load-displacement relationships are shown in Figure 4.19.

(a) CLPA1   (b) CLPA2

(c) CLPB

(d) CLPC

(a) CLT (D)
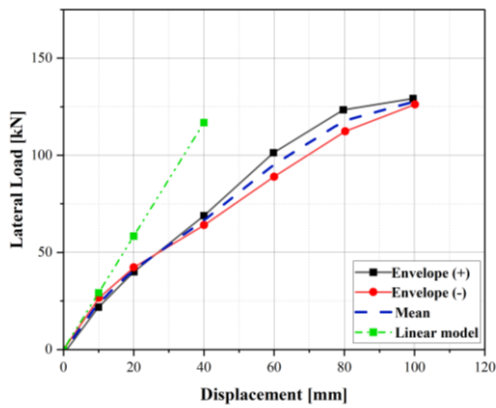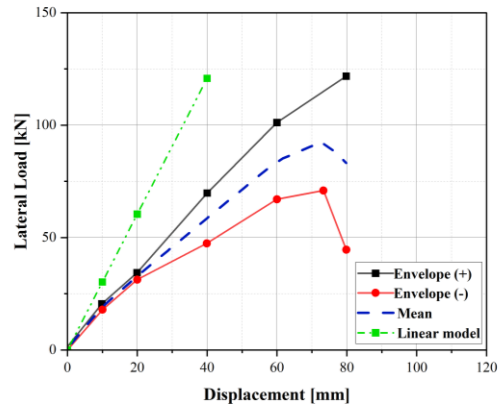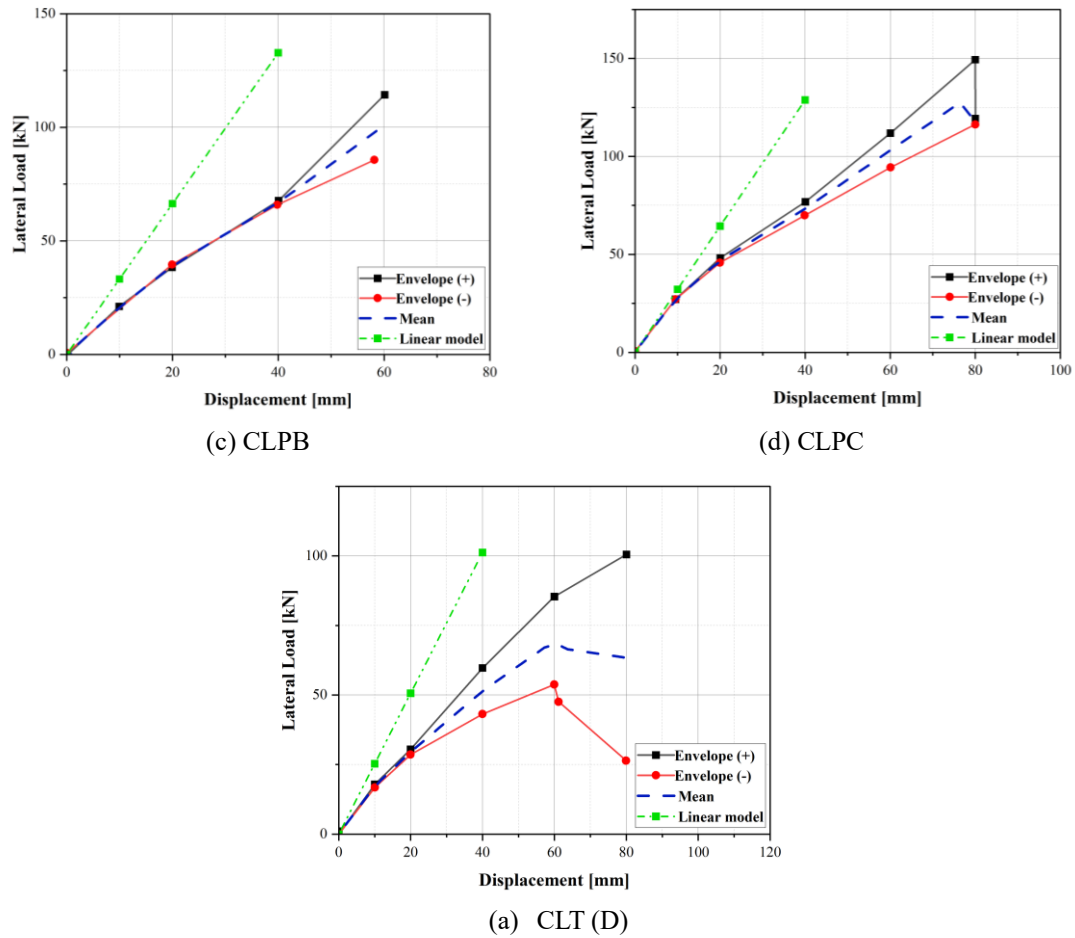
Figure 4.19 Comparison of cyclic test results with calculated load-displacement curves (elastic)

Figure 4.19 and Table 4.11 clearly display that the predicted elastic behaviour was reliable when walls were subjected to small lateral displacement up to about 10 mm, regardless of panel layups, which was also observed in monotonic tests (see Figure 4.18). This phenomenon is consistent with the past study performed by Pozza et al. (2018), who investigated axial capacity and stiffness of hold-downs (WHT540, Rothoblaas®). This could be explained by the fact that at higher load and displacement the axial elastic stiffness of the hold-down is likely reduced by the presence of shear load i.e. the axial-shear interaction of hold-down is relatively small when the hold-down displacement is less than 7.5 mm. Furthermore, similar to monotonic tests, CLPA1 and CLPC walls which were designed with stiffer panel-to-panel joints, exhibited better predictions compared to other walls.

Table 4.11 Comparison of experimental and analytical results at different displacement levels

	Displacement level [mm]	F_{eq} [kN]	F_{exp} [kN]	Ratio= F_{exp}/F_{eq} (%)
CLPA1	10	34.4	26.7	77.5
	20	68.8	42.3	61.5
	40	137.6	64.1	46.6
CLPA2	10	34.4	17.9	52.2
	20	68.8	31.3	45.5
	40	137.6	47.4	34.4
CLPB	10	33.2	23.4	70.5
	20	66.4	38.2	57.6
	40	132.8	67.7	51.0
CLPC	10	32.2	27.4	85.1
	20	64.4	48.1	74.8
	40	128.8	76.7	59.6
CLT	10	25.3	17.8	70.5
	20	50.6	30.5	60.3
	40	101.2	59.7	59.1

4.7 Summary

Several CLP shear wall configurations were investigated by means of monotonic and cyclic tests performed in accordance with ASTM E2126. The mechanical properties of each group were evaluated, including elastic stiffness, yield strength, peak load, and ductility ratio. Wall configurations included different types of panel layups and the number of screws used in anchoring systems, together with panel-to-panel connections. The test results confirmed that the connection layout is critical for the overall performance of CLP shear walls. The panel-to-panel connection plays a significant role in coupled-panel walls or even multi-panel walls, determining the kinematic wall behaviours. In fact, experimental evidence indicated that the use of stiffer panel-to-panel connections may be difficult to realise the single wall behaviour in practice, but did make

some difference to the entire wall behaviour.

The analytical models used to predict the elastic behaviour of CLP shear walls can generally provide an acceptable approximation in terms of the capacity of the shear walls. However, the deflection of CLP shear walls cannot be effectively estimated by simply using stiffness values obtained at the connection level tests. More specifically, the rocking behaviour was largely underestimated due to the overestimated stiffness of hold-downs. Meanwhile, the sliding deformation exhibited a relatively good match between predicted and measured responses. Through comparison, the results further verified the recommendations highlighted by Gavric (2015) that the tension and shear strength of screwed connection of hold-downs and angle brackets should not exceed the capacity of the steel net section. This would allow the full capacity of all the fasteners to be utilised in resisting the applied load. Therefore, it can be concluded that an appropriate capacity-based design of connections should be implemented for CLP shear walls to avoid brittle failures in order to achieve target capacity. In addition, the relationship between the sum of the fastener stiffness and the stiffness of the connection is complex, hence, more investigations are required.

Chapter 5 Conclusions and Recommendations for Future Work

5.1 Conclusions

This thesis focuses on the structural performance of shear walls built by 3-layer composite laminated panels (CLP). The structural performance of CLP shear walls was investigated with experimental and analytical methods. One of the key objectives was to evaluate the applicability of the current shear wall analytical models. Experimental investigations were conducted on the connections first. The connections with different layup combinations using the same screw patterns exhibited different strength and stiffness as well as load-displacement responses.

Connection behaviour

The following conclusions can be drawn in terms of self-tapping screw (STS) connections with CLP members:

The core layer of CLP did have a negligible effect on the lateral strength of the STS connections. As the density of the face layer increased, so did the lateral resistance and stiffness of connection. However, it is possible to be more precise by stating that the overall performance of connections is less significantly impacted by the orientation of the core layer made of the same type of material.

The European Yield Models can generally provide acceptable strength predictions for connection specimens with CLP that have lumber as the face laminates, whereas for specimens with structural composite lumber (SCL) made with high density species as faces the predictions are less accurate but conservative. Furthermore, the existing models for estimating the embedment strength of SCL and hybrid panel layups need to be developed.

Shear wall behaviour

Based on the studies on the connection behaviour of CLP members, full-scale CLP shear walls were designed and tested under both monotonic and cyclic loading. The following conclusions can be drawn from this study:

It was found that the resistance of coupled shear walls is governed by the panel-to-panel joints, the hold-down and base shear connections reaching their respective yield strength. In particular, the panel-to-panel joint between the adjacent panels is critical to determine the kinematic behaviour of the wall system.

As some unexpected brittle failures occurred in the connections in the shear wall tests, implementation of capacity-based design approach for CLP shear walls is necessary. The non-dissipative elements should be overdesigned to remain elastic.

The relatively lower contribution of rocking behaviour to lateral deflection of CLP shear walls was noticed in this study than previously reported for CLT shear walls, mainly due to the following reasons: (1) the stiffness of STS connections was higher than nail connections used in previous studies; (2) the self-centering ability of wall panels may be compromised without vertical loads applied in this study; (3) the full potential capacity of base shear connections was not reached due to the metal fracture of the brackets.

Evaluation of shear wall models

To verify the applicability of the current shear wall analytical models, a comparison was carried out between the experimental results and predictions. The analytical model considers the contribution of both primary and weak directions of base shear connections and hold-downs. The analytical models predict the load-carrying capacity of the CLP shear walls with acceptable accuracy. However, deflection predictions of the CLP shear wall in the elastic region were generally underestimated. Only the wall CLPA1 exhibited a relatively good match between the experimental and analytical results. Thus, it appears

that the existing model is suitable for evaluating the CLP shear walls with single-wall behaviour. In order to improve the accuracy of the analytical models, further research should be performed.

5.2 Recommendations for future work

More research is encouraged to further the understanding of the structural performance of shear walls built by multi-layer composite laminated panels. Due to project time limitations, a few topics could not be investigated in this thesis and should be the focus of future research, as listed below:

- While investigating the lateral strength of screwed CLP connections, the embedment strength plays a significant role. The embedment strength of LSL in different directions and the embedment strength in hybrid layup panels were not investigated.

- The results of STS connection tests presented in Chapter 3 were used to calculate the joint component properties (e.g., hold-down, base shear, and panel joints) in the CLP shear wall. The validity of this approach should be investigated further. Further, group effects of screwed CLP connections can be investigated in future work.

- Gravity load can contribute to resisting lateral load of the CLP shear wall performance. It was ignored in this preliminary study. However in practice gravity loads are often present. Hence, the effect of vertical load on CLP shear wall performance should be considered in future studies.

- The research investigated the applicability of proposed analytical models of CLT shear walls to CLP shear walls. One of the commonly accepted design principles for the kinematic behaviour of multi-panel shear walls is the sequence of yielding of hold-downs and inter-panel joints. The overstrength factor for associated cases should be further explored and defined to ensure the corresponding kinematic motion of the shear wall.

- As more recent research has highlighted the contribution of uplift resistance of base shear connections, as well as the bi-directional behaviour of hold-downs,

there is a need to improve the analytical models in order to achieve a closer approximation, especially the deflection of the shear wall was strongly influenced by the stiffness of connectors in current elastic analysis. The contribution of base shear connection strength and stiffness in rocking behaviour as well as the contribution of hold-down strength and stiffness in sliding behaviour should be further explored and defined.

Bibliography

APA—The Engineered Wood Association. (2019). *PS 2-10: Performance standard for wood-based structural-use panels*. APA, Tacoma, Washington. https://apawood-europe.org/wp-content/uploads/2013/10/PS-2-10.pdf

ASTM E2126-19. (2019). Standard test methods for cyclic (Reversed) load test for shear resistance of vertical elements of the lateral load resisting systems for buildings. ASTM International, West Conshohocken, PA, USA. https://www.astm.org/e2126-19.html

Augustin, M. (2008). *Timber structures - Handbook 1 of educational materials for designing and testing of timber structures: TEMTIS.* Leonardo da Vinci Pilot Project No. CZ/06/B/F/PP/168007. Ostrava, Czech Republic: VSB-Technical University of Ostrava.

AWC (American Wood Council) (2018). National Design Specification for wood construction. AWC, Washington, DC.

Brandner, R., Flatscher, G., Ringhofer, A., Schickhofer, G., and Thiel, A. (2016). Cross laminated timber (CLT): overview and development. *European Journal of Wood and Wood Products,* 74(3), 331-351.

Blass, H. J., and Bejtka, I. (2001). Screws with continuous threads in timber connections. In *RILEM Proceedings PRO, Joints in timber structures. 22*:193–202, Paris, France.

Casagrande, D., Rossi, S., Sartori, T., and Tomasi, R. (2016). Proposal of an analytical procedure and a simplified numerical model for elastic response of single-storey timber shear-walls. *Construction and Building Materials*, *102*, 1101–1112. https://doi.org/10.1016/j.conbuildmat.2014.12.114

Ceccotti, A. (2008). New technologies for construction of medium-rise buildings in seismic regions: the XLAM case. *Structural Engineering International, 18(2)*, 156-165.

D'Arenzo, G., Casagrande, D., Polastri, A., Fossetti, M., Fragiacomo, M., and Seim, W. (2021). CLT shear walls anchored with shear-tension angle brackets: Experimental tests and finite-element modeling. *Journal of Structural Engineering*, *147*(7). https://doi.org/10.1061/(asce)st.1943-541x.0003008

D'Arenzo, G., Rinaldin, G., Fossetti, M., and Fragiacomo, M. (2019). An innovative shear-tension angle bracket for Cross-Laminated Timber structures: Experimental

tests and numerical modelling. *Engineering Structures*, *197*, 109434. https://doi.org/10.1016/J.ENGSTRUCT.2019.109434

Dires, S., and Tannert, T. (2022). Performance of coupled CLT shear walls with internal perforated steel plates as vertical joints and hold-downs. *Construction and Building Materials*, *346*, 128389.

Fragiacomo, M. C., Dujic, B., and Sustersic, I. (2011). Elastic and ductile design of multi-storey crosslam massive wooden buildings under seismic actions. *Engineering Structures*, *33*(11), 3043–3053. https://doi.org/10.1016/j.engstruct.2011.05.020

Gavric, I., and Popovski, M. (2014). Design models for CLT shearwalls and assemblies based on connection properties. In *Proceedings of the INTER Conference*, Bath, UK.

Gavric, I., Fragiacomo, M., and Ceccotti, A. (2013). Capacity seismic design of X-LAM wall systems based on connection mechanical properties. In *Proceedings of the Meeting* (Vol. 46), Vancouver, Canada.

Gavric, I., Fragiacomo, M., and Ceccotti, A. (2015a). Cyclic behaviour of typical screwed connections for cross-laminated (CLT) structures. *European Journal of Wood and Wood Products*, *73*(2), 179–191. https://doi.org/10.1007/s00107-014-0877-6

Gavric, I., Fragiacomo, M., and Ceccotti, A. (2015b). Cyclic behaviour of typical metal connectors for cross-laminated (CLT) structures. *Materials and Structures/Materiaux et Constructions*, *48*(6), 1841–1857. https://doi.org/10.1617/s11527-014-0278-7

Gavric, I., Fragiacomo, M., and Ceccotti, A. (2015c). Cyclic Behavior of CLT Wall Systems: Experimental Tests and Analytical Prediction Models. *Journal of Structural Engineering*, *141*(11), 04015034. https://doi.org/10.1061/(asce)st.1943-541x.0001246

Hossain, A., Danzig, I., and Tannert, T. (2016). Cross-laminated timber shear connections with double-angled self-tapping screw assemblies. *Journal of Structural Engineering*, *142*(11), 04016099. https://doi.org/10.1061/(asce)st.1943-541x.0001572

Hwang, K., and Komatsu, K. (2002). Bearing properties of engineered wood products I: Effects of dowel diameter and loading direction. *Journal of Wood Science*, *48*(4), 295–301.

Johansen, K. W. (1949). Theory of timber connections. *International Association of Bridge and Structural Engineering*, *9*, 62-249.

Joyce, T., Ballerini, M., and Smith, I. (2011, August). Mechanical behaviour of in-plane shear connections between CLT wall panels. In *Proceedings of the CIB Working Commission W18–Timber Structures.* 44th meeting, Alghero, Italy.

Liu, J. (2019). *Coupling effects of CLT connections under bi-axial loading*. Doctoral dissertation, University of British Columbia.

Lukacs, I., Björnfot, A., and Tomasi, R. (2019). Strength and stiffness of cross-laminated timber (CLT) shear walls: State-of-the-art of analytical approaches. *Engineering Structures*, *178*, 136–147.

Khan, R., Niederwestberg, J., and Chui, Y. H. (2021). Influence of insertion angle, diameter and thread on embedment properties of self-tapping screws. *European Journal of Wood and Wood Products*, *79*(3), 707–718.

Ma, Y., Si, R., Musah, M., Dai, Q., Xie, X., Wang, X., and Ross, R. J. (2021). Mechanical property evaluation of hybrid mixed-species CLT panels with sugar maple and white spruce. *Journal of Materials in Civil Engineering*, *33*(7), 04021171.

Mahdavifar, V., Sinha, A., Barbosa, A. R., Muszynski, L., and Gupta, R. (2018). Lateral and withdrawal capacity of fasteners on hybrid Cross-Laminated Timber panels. *Journal of Materials in Civil Engineering*, *30*(9). https://doi.org/10.1061/(asce)mt.1943-5533.0002432

Masroor, M., Doudak, G., and Casagrande, D. (2022). Design of multi-panel CLT shear walls with bidirectional mechanical anchors following capacity-based design principle. *Journal of Performance of Constructed Facilities*, *36*(1), 04021113.

Murty, B., Smith, I., and Asiz, A. (2007). Wood and engineered wood product connections using small steel tube fasteners: Applicability of European yield model. *Journal of Materials in Civil Engineering*, *19*(11), 965–971.

NDS (National Design Specification). (2015). National design specification for wood construction. Washington, DC: American Forest and Paper Association.

Niederwestberg, J., Zhou, J., and Chui, Y. H. (2018). Mechanical properties of innovative, multi-layer composite laminated panels. *Buildings*, *8*(10). https://doi.org/10.3390/buildings8100142

Plesnik, T., Erochko, J., and Doudak, G. (2016). Nailed connection behavior in light-frame wood shear walls with an intermediate layer of insulation. *Journal of Structural Engineering*, *142*(7), 04016045.

Popovski, M., Schneider, J., and Schweinsteiger, M. (2010). Lateral load resistance of cross-laminated wood panels. In *World Conference on Timber Engineering* (Vol. 20, p. 24), Riva del Garda, Italy.

Popovski, M., and Gavric, I. (2016). Performance of a 2-Story CLT house subjected to lateral loads. *Journal of Structural Engineering*, *142*(4). https://doi.org/10.1061/(asce)st.1943-541x.0001315

Pozza, L., Ferracuti, B., Massari, M., and Savoia, M. (2018). Axial – Shear interaction on CLT hold-down connections – Experimental investigation. *Engineering Structures*, *160*, 95–110. https://doi.org/10.1016/j.engstruct.2018.01.021

SAE (Society of Automotive Engineers). (2014). Chemical compositions of SAE carbon steels. SAE J403-201406. Warrendale, PA: SAE International.

Shahnewaz, M., Popovski, M., and Tannert, T. (2019). Resistance of cross-laminated timber shear walls for platform-type construction. *Journal of Structural Engineering*, *145*(12), 04019149.

Shahnewaz, M., Popovski, M., and Tannert, T. (2020). Deflection of cross-laminated timber shear walls for platform-type construction. *Engineering Structures*, *221*. https://doi.org/10.1016/j.engstruct.2020.111091

Spasojevic, M. (2019). *Structural and hygrothermal performance of light wood-frame walls with insulated sheathing*. MSc thesis, University of Alberta.

EN 1995-1-1 (2004) Eurocode 5: Design of timber structures—part 1-1: general rules and rules for buildings. CEN, Brussels, Belgium.

Tomasi, R., and Smith, I. (2015). Experimental characterization of monotonic and cyclic loading responses of CLT panel-to-foundation angle bracket Connections. *Journal of Materials in Civil Engineering*, *27*(6). https://doi.org/10.1061/(asce)mt.1943-5533.0001144

Uibel, T., and Blaß, H. J. (2006). Load carrying capacity of joints with dowel type fasteners in solid wood panels. In *Proceedings. CIB-W18 Meeting*, Florence, Italy.

Wang, Q. (2009). *Relationship between fastening properties and load-deflection response of wood shear walls*. Doctoral dissertation, University of New Brunswick, Faculty of Forestry and Environmental Management.

Wang, Z., Gong, M., and Chui, Y. H. (2015). Mechanical properties of laminated strand lumber and hybrid cross-laminated timber. *Construction and Building Materials*, *101*, 622–627. https://doi.org/10.1016/j.conbuildmat.2015.10.035

Zhang, S., Daneshvar, H., and Chui, Y. H. (2021). Comparison of lateral load performance of light wood diaphragms built with sawn lumber and wood I-joists. *Journal of Materials in Civil Engineering*, *33*(1), 04020422.

Appendix I

Calculation procedures of the lateral Resistance of STS connection:

<div align="center">Table I.1 Properties of the connections</div>

Parameter	Value
Diameter (d_F) [mm]	6.35
Length [mm]	63.5
Steel Thickness (t_1) [mm]	3
Effective Length (t_2) [mm]	53.5
Specific Gravity (Lumber)	0.42
Specific Gravity (LSL)	0.5
Density (lumber) [kg/m^3]	470
Density (LSL) [kg/m^3]	661
K_{sp}	3
$\emptyset_{steel}$	0.8
$\emptyset_{wood}$	0.6
f_u [N/mm^2]	537
f_y [N/mm^2]	1130.7
J_x(LSL)	1
J_x(CLT)	0.9
Insertion angle (α)	90°

Lateral Resistance of the STS connection-CLT (based on CSA O86)

The embedded strength can be calculated as:

$$f_1 = K_{sp} \left(\frac{\emptyset_{steel}}{\emptyset_{wood}} \right) f_u = 3 \times \left(\frac{0.8}{0.6} \right) \times 537 = 2148 \text{ N/}mm^2$$

$$f_2 = 50G(1 - 0.01d_F)J_x = 50 \times 0.42(1 - 0.01 \times 6.35)J_x = 19.7\text{N/}mm^2$$

The unit lateral resistance, n_u:

(a) $f_1 d_F t_1 = 40.9 kN$

(b) $f_2 d_F t_2 = 7.6 kN$

(c) $f_1 d_F^2 \left(\sqrt{\dfrac{1}{6} \dfrac{f_2}{(f_1+f_2)} \dfrac{f_y}{f_1}} + \dfrac{1}{5} \dfrac{t_1}{d_F} \right) = 33.8 kN$

(d) $f_1 d_F^2 \left(\sqrt{\dfrac{1}{6} \dfrac{f_2}{(f_1+f_2)} \dfrac{f_y}{f_1}} + \dfrac{1}{5} \dfrac{t_2}{d_F} \right) = 167.4 kN$

(e) $f_1 d_F^2 \dfrac{1}{5} \left(\dfrac{t_1}{d_F} + \dfrac{f_2}{f_1} \dfrac{t_2}{d_F} \right) = 9.7 kN$

(f) $f_1 d_F^2 \sqrt{\dfrac{2}{3} \dfrac{f_2}{(f_1+f_2)} \dfrac{f_y}{f_1}} = 4.78 kN$

Therefore, the minimum unit lateral resistance of the connection, $n_u = 4.78 kN$.

Lateral Resistance of the STS connection-3-LSL

The embedded strength can be calculated as:

$f_1 = K_{sp} \left(\dfrac{\emptyset_{steel}}{\emptyset_{wood}} \right) f_u = 3 \times \left(\dfrac{0.8}{0.6} \right) \times 537 = 2148 \ N/mm^2$

$f_2 = 50G(1 - 0.01 d_F) J_x = 50 \times 0.5(1 - 0.01 \times 6.35) = 23.4 N/mm^2$

The unit lateral resistance, n_u(3-LSL):

(a) $f_1 d_F t_1 = 40.9 kN$

(b) $f_2 d_F t_2 = 8.9 kN$

(c) $f_1 d_F^2 \left(\sqrt{\dfrac{1}{6} \dfrac{f_2}{(f_1+f_2)} \dfrac{f_y}{f_1}} + \dfrac{1}{5} \dfrac{t_1}{d_F} \right) = 33.8 kN$

(d) $f_1 d_F^2 \left(\sqrt{\dfrac{1}{6} \dfrac{f_2}{(f_1+f_2)} \dfrac{f_y}{f_1}} + \dfrac{1}{5} \dfrac{t_2}{d_F} \right) = 167.7 kN$

(e) $f_1 d_F^2 \dfrac{1}{5} \left(\dfrac{t_1}{d_F} + \dfrac{f_2}{f_1} \dfrac{t_2}{d_F} \right) = 10.0 kN$

(f) $f_1 d_F^2 \sqrt{\dfrac{2}{3} \dfrac{f_2}{(f_1+f_2)} \dfrac{f_y}{f_1}} = 5.79 kN$

Therefore, the minimum unit lateral resistance, $n_u = 5.79 kN$.

Lateral Resistance of the STS connection-CLT (based on Eq 3.3 and CSA O86)

The embedded strength can be calculated as:

$$f_1 = K_{sp}\left(\frac{\varnothing_{steel}}{\varnothing_{wood}}\right)f_u = 3 \times \left(\frac{0.8}{0.6}\right) \times 537 = 2148 \text{ N}/mm^2$$

$$f_2 = \frac{0.206 \cdot \rho^{0.860} \cdot d^{-0.078}}{2.89 \cdot \cos^2\alpha + \sin^2\alpha} = 35.4 \text{ N}/mm^2$$

The unit lateral resistance, n_u:

(a) $f_1 d_F t_1 = 40.9 kN$

(b) $f_2 d_F t_2 = 12.0 kN$

(c) $f_1 d_F{}^2 \left(\sqrt{\frac{1}{6}\frac{f_2}{(f_1+f_2)}\frac{f_y}{f_1}} + \frac{1}{5}\frac{t_1}{d_F}\right) = 33.8 kN$

(d) $f_1 d_F{}^2 \left(\sqrt{\frac{1}{6}\frac{f_2}{(f_1+f_2)}\frac{f_y}{f_1}} + \frac{1}{5}\frac{t_2}{d_F}\right) = 149.2 kN$

(e) $f_1 d_F{}^2 \frac{1}{5}\left(\frac{t_1}{d_F} + \frac{f_2}{f_1}\frac{t_2}{d_F}\right) = 10.6 kN$

(f) $f_1 d_F{}^2 \sqrt{\frac{2}{3}\frac{f_2}{(f_1+f_2)}\frac{f_y}{f_1}} = 6.53 kN$

Therefore, the minimum unit lateral resistance of the connection, $n_u = 4.78 KN$.

Lateral Resistance of the STS connection- 3-LSL (based on Eq3.3 and CSA O86)

The embedded strength can be calculated as:

$$f_1 = K_{sp}\left(\frac{\varnothing_{steel}}{\varnothing_{wood}}\right)f_u = 3 \times \left(\frac{0.8}{0.6}\right) \times 537 = 2148 \text{ N}/mm^2$$

$$f_2 = \frac{0.206 \cdot \rho^{0.860} \cdot d^{-0.078}}{2.89 \cdot \cos^2\alpha + \sin^2\alpha} = 47.5 \text{ N}/mm^2$$

The unit lateral resistance, n_u:

(a) $f_1 d_F t_1 = 40.9 kN$

(b) $f_2 d_F t_2 = 16.1 kN$

(c) $f_1 d_F{}^2 \left(\sqrt{\frac{1}{6}\frac{f_2}{(f_1+f_2)}\frac{f_y}{f_1}} + \frac{1}{5}\frac{t_1}{d_F}\right) = 33.8 kN$

(d) $f_1 d_F{}^2 \left(\sqrt{\frac{1}{6}\frac{f_2}{(f_1+f_2)}\frac{f_y}{f_1}} + \frac{1}{5}\frac{t_2}{d_F}\right) = 149.7 kN$

(e) $f_1 d_F{}^2 \frac{1}{5}\left(\frac{t_1}{d_F} + \frac{f_2}{f_1}\frac{t_2}{d_F}\right) = 11.4kN$

(f) $f_1 d_F{}^2 \sqrt{\frac{2}{3}\frac{f_2}{(f_1+f_2)}\frac{f_y}{f_1}} = 7.56kN$

Therefore, the minimum unit lateral resistance, $n_u = 7.56kN$.

Appendix II

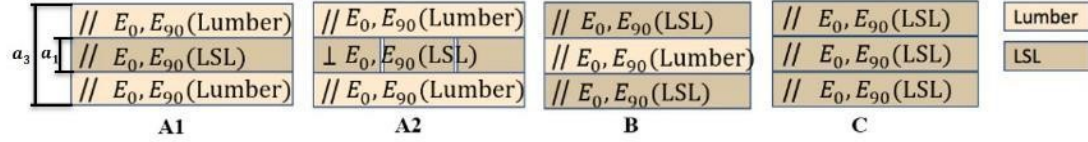## The Applicability of k method to 3-ply CLP panels

Figure II.1 CLP layups

Table II.1 Elastic properties of laminates in CLP assumed in design calculations

Material	$E_0(MPa)$	$E_{90}(MPa)$	$G_0(MPa)$
Lumber	11299	376	656
LSL	11240	1823	462

Note: E_0 and E_{90} are the MOE parallel to grain and perpendicular to grain, respectively.

For the layup A1, the composition factor was simiply assumed to be 1, as three layers are all in the parallel direction. And the utilization of LSL in the core layer may not bring a significant change to the bending stiffness. Then, the effective bending stiffness of A1 can be calculated as:

$$k_{4(A1)} = \frac{E_{0,LSL}}{E_{0,lumber}} + \left(1 - \frac{E_{0,LSL}}{E_{0,lumber}}\right) \times \frac{a_1}{a_3} = 0.997$$

$$E_{I,eff(A1)} = E_{0,lumber}I * 2 * k_4 = 11299 \times \frac{106.3 \times 1200^3}{12} \times 2 \times 1 = 3.45 \times 10^{14} \text{ N/mm}^2$$

For the layup A2, the composition factor was adjusted as:

$$k_{4(A2)} = \frac{E_{90,LSL}}{E_{0,lumber}} + \left(1 - \frac{E_{90,LSL}}{E_{0,lumber}}\right) \times \frac{a_1}{a_3} = 0.45$$

Then, the effective bending stiffness of A2 can be calculated as:

$$E_{I,eff(A2)} = E_{0,lumber}I * 2 * k_4 = 11299 \times \frac{106.3 \times 1200^3}{12} \times 2 \times 0.45 = 1.55 \times 10^{14} \text{ N/mm}^2$$

In terms of the layup B with LSL faces and a lumber core, the composition factor and the effective bending stiffness were determined as:

$$k_{4(B)} = \frac{E_{90,lumber}}{E_{0,LSL}} + \left(1 - \frac{E_{90,lumber}}{E_{0,LSL}}\right) \times \frac{a_1}{a_3} = \frac{11299}{11240} + \left(1 - \frac{11299}{11240}\right) \times \frac{35.1}{107.3}$$

$$= 1.005$$

$$E_{I,eff(B)} = E_{0,LSL}I * k_4 = 11240 \times \frac{107 \times 1200^3}{12} \times 2 \times 1.005 = 1.21 \times 10^{14} \text{ N/mm}^2$$

For the layup C, consised of entire LSL with the grain direction of all layers parallel compsition factor $k_{4(C)} = 1$

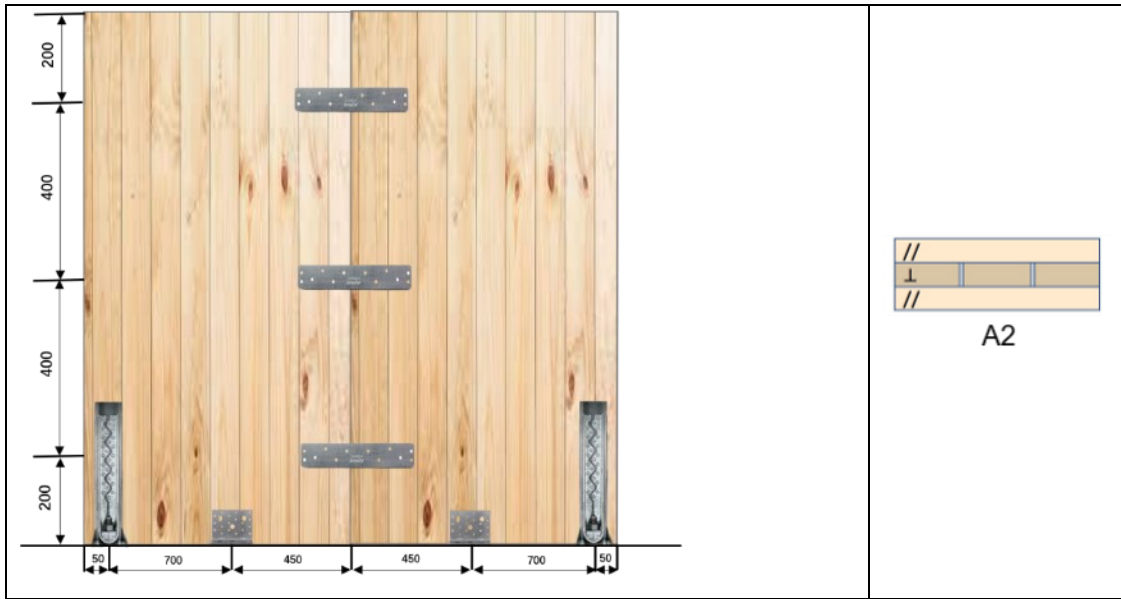**Shear wall test configurations and test results**
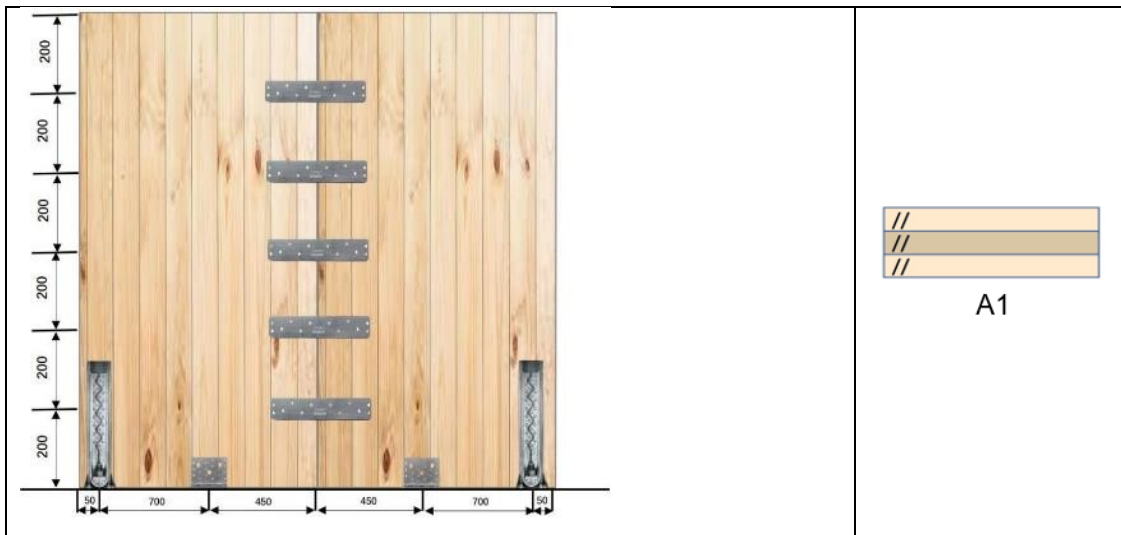
Figure II.2 Wall test configuration A1 (both monotonic and cyclic).

Table II.2 Connection layout in wall A1

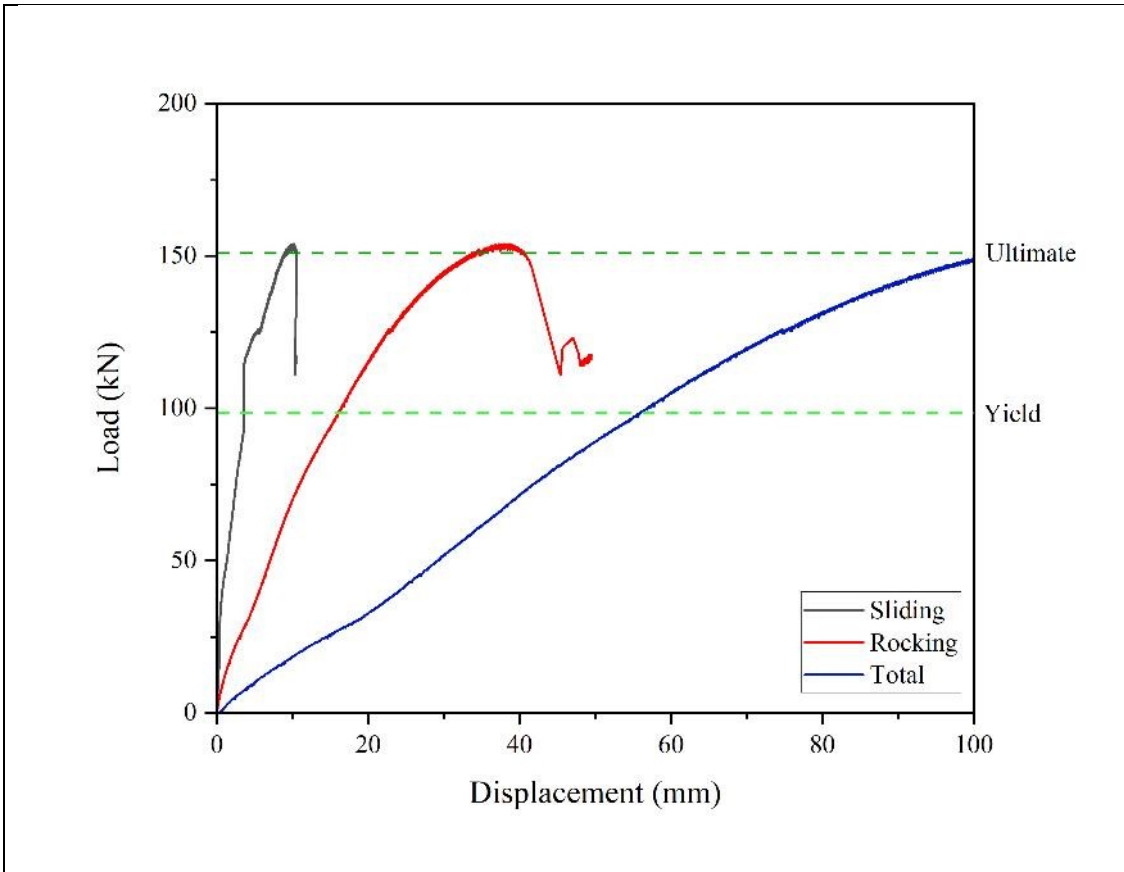| Connection layout	No. of connections	No. of screws
Hold-down	4	9
Base shear connection	4	6
Panel joint	10	4
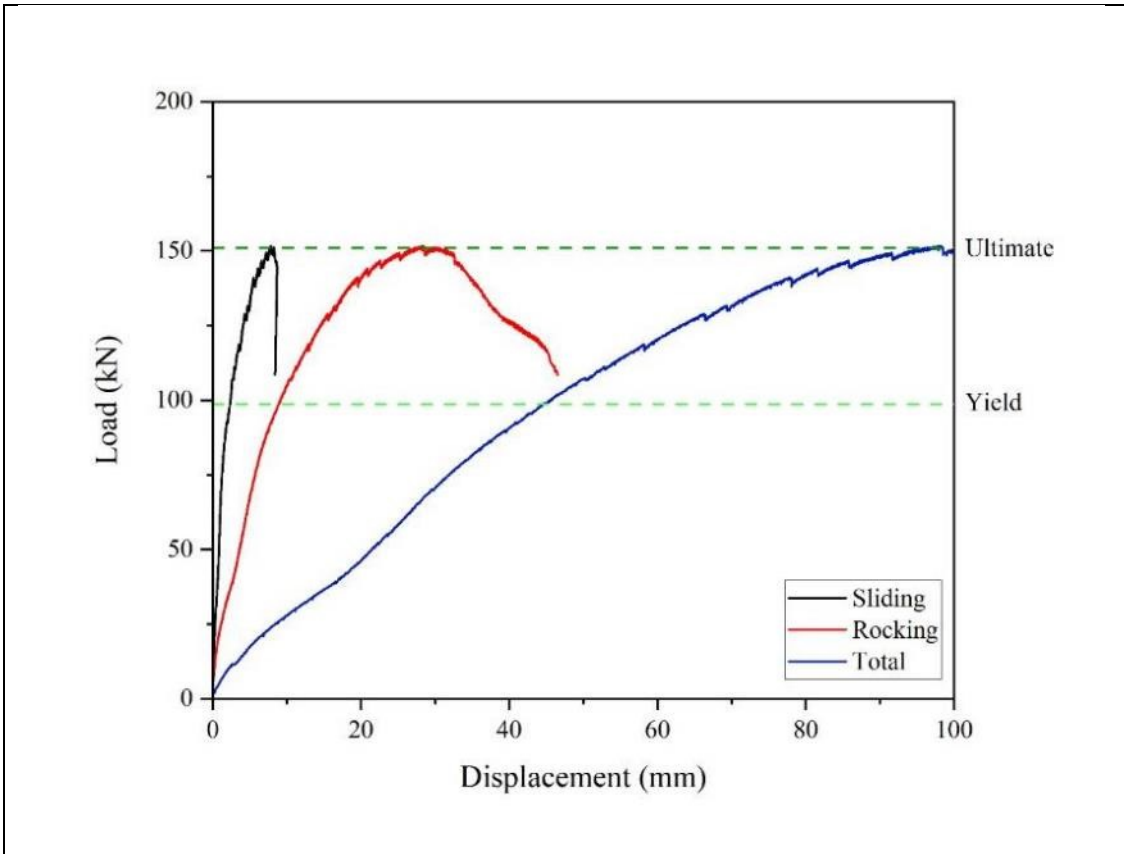
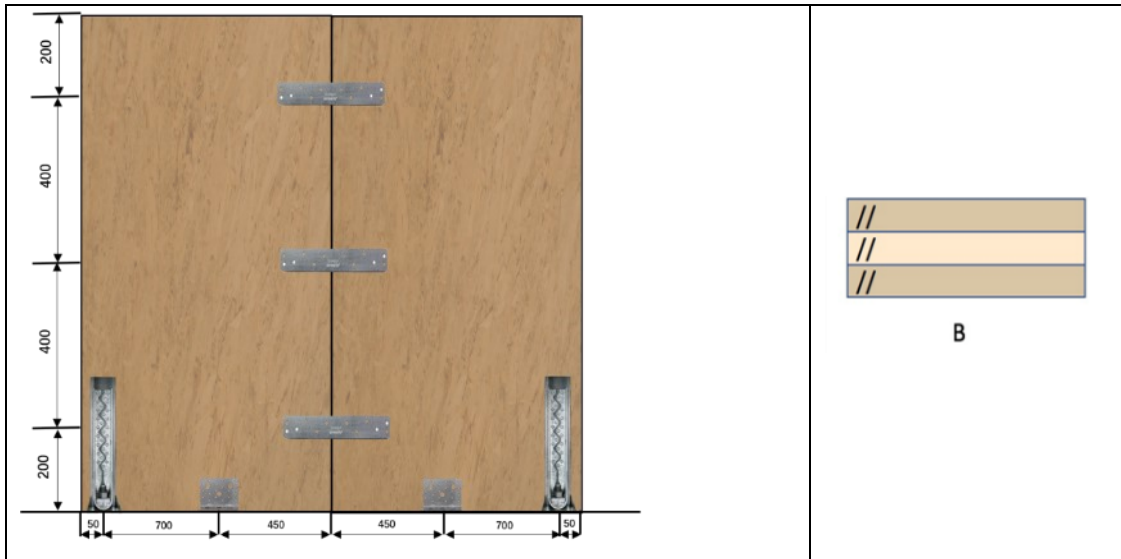Figure II.3 Load-displacement responses of wall A1 under monotonic loading.

Figure II.4 Wall test configuration A2 (both monotonic and cyclic).

Table II.3 Connection layout in wall A2

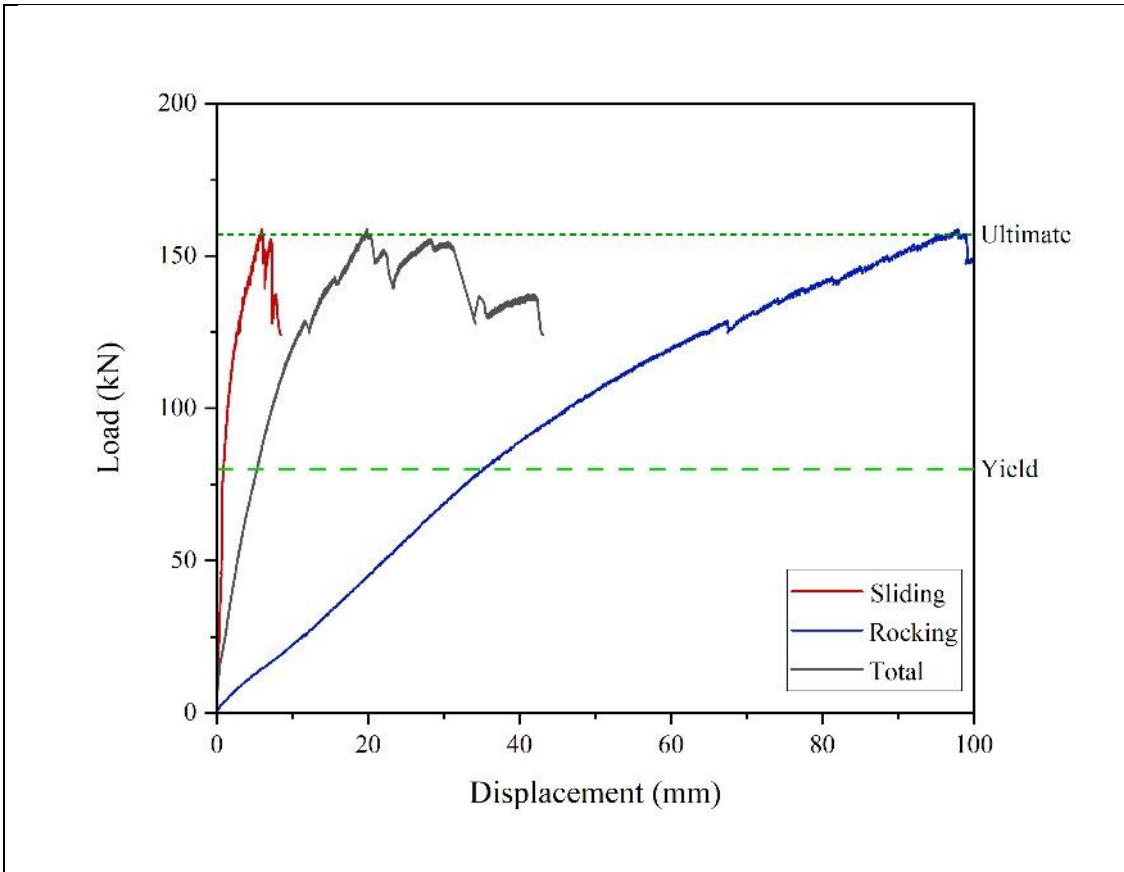| Connection layout	No. of connections	No. of screws
Hold-down	4	12
Base shear connection	4	6
Panel joint	6	4

Figure II.5 Load-displacement responses of wall A2 under monotonic loading.

Figure II.6 Wall test configuration B (both monotonic and cyclic).

Table II.4 Connection layout in wall B

Connection layout	No. of connections	No. of screws
Hold-down	4	9
Base shear connection	4	6
Panel joint	6	3

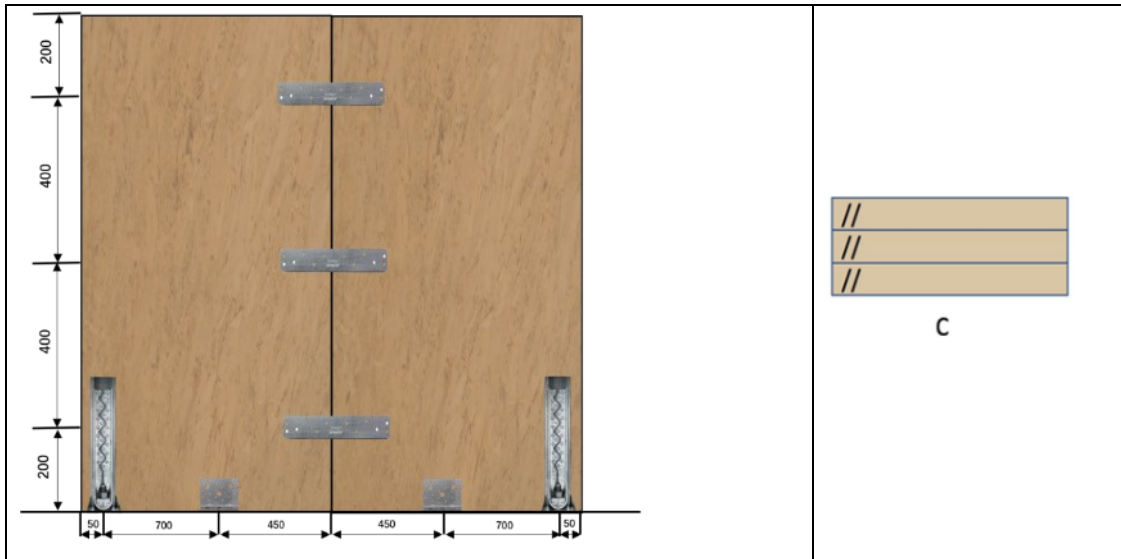Figure II.7 Load-displacement responses of wall B under monotonic loading.

Figure II.8 Wall test configuration C (monotonic).

Table II.5 Connection layout in wall C

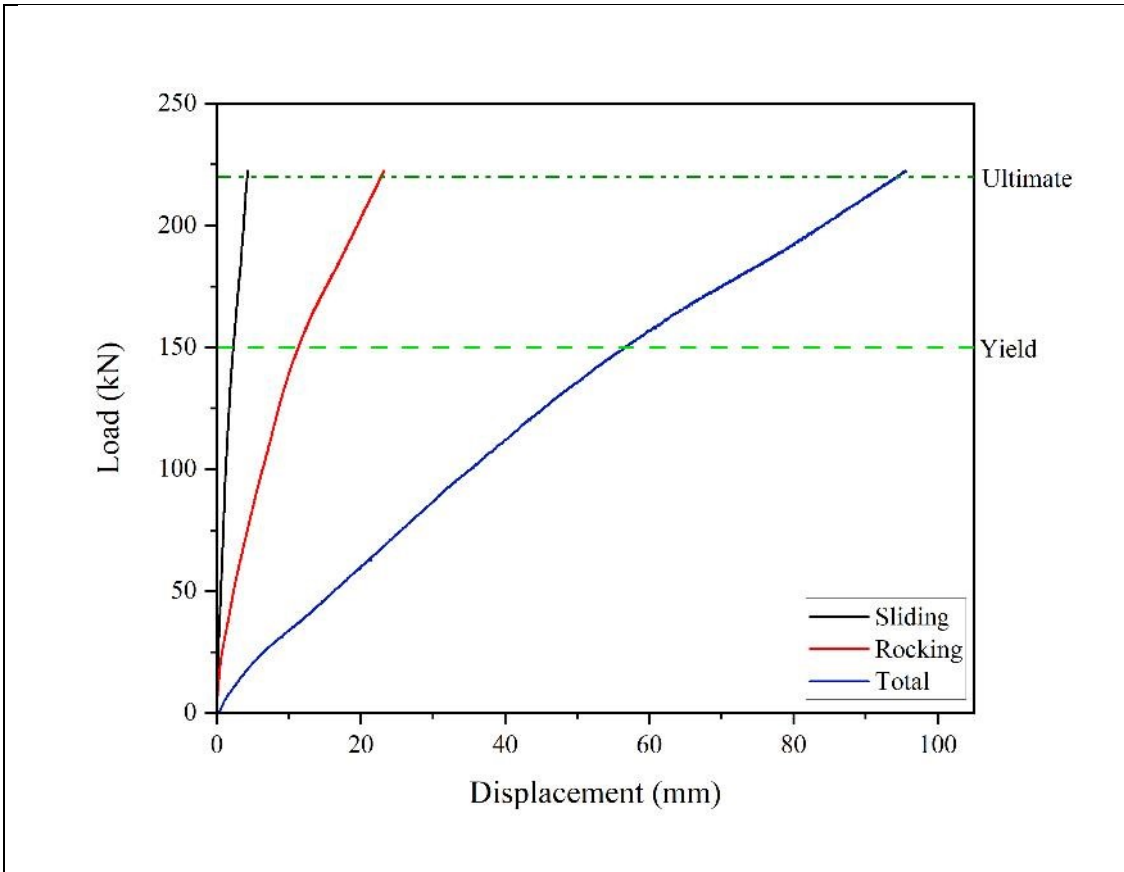| Connection layout	No. of connections	No. of screws
Hold-down	4	9
Base shear connection	4	6
Panel joint	6	4

Figure II.9 Load-displacement responses of wall C under monotonic loading.